INFORMATION TO USERS

This was produced from a copy of a document sent to us for microfilming. While the most advanced technological means to photograph and reproduce this document have been used, the quality is heavily dependent upon the quality of the material submitted.

The following explanation of techniques is provided to help you understand markings or notations which may appear on this reproduction.

1. The sign or "target" for pages apparently lacking from the document photographed is "Missing Page(s)". If it was possible to obtain the missing page(s) or section, they are spliced into the film along with adjacent pages. This may have necessitated cutting through an image and duplicating adjacent pages to assure you of complete continuity.

2. When an image on the film is obliterated with a round black mark it is an indication that the film inspector noticed either blurred copy because of movement during exposure, or duplicate copy. Unless we meant to delete copyrighted materials that should not have been filmed, you will find a good image of the page in the adjacent frame. If copyrighted materials were deleted you will find a target note listing the pages in the adjacent frame.

3. When a map, drawing or chart, etc., is part of the material being photographed the photographer has followed a definite method in "sectioning" the material. It is customary to begin filming at the upper left hand corner of a large sheet and to continue from left to right in equal sections with small overlaps. If necessary, sectioning is continued again—beginning below the first row and continuing on until complete.

4. For any illustrations that cannot be reproduced satisfactorily by xerography, photographic prints can be purchased at additional cost and tipped into your xerographic copy. Requests can be made to our Dissertations Customer Services Department.

5. Some pages in any document may have indistinct print. In all cases we have filmed the best available copy.

University
Microfilms
International

300 N. ZEEB RD., ANN ARBOR, MI 48106

GILES, CLYDE LEE

ULTRASOUND SPECTROSCOPY

The University of Arizona PH.D. 1981

PLEASE NOTE:

In all cases this material has been filmed in the best possible way from the available copy. Problems encountered with this document have been identified here with a check mark __✓__.

1. Glossy photographs or pages __✓__
2. Colored illustrations, paper or print _____
3. Photographs with dark background __✓__
4. Illustrations are poor copy _____
5. Pages with black marks, not original copy _____
6. Print shows through as there is text on both sides of page _____
7. Indistinct, broken or small print on several pages _____
8. Print exceeds margin requirements _____
9. Tightly bound copy with print lost in spine _____
10. Computer printout pages with indistinct print _____
11. Page(s) _____ lacking when material received, and not available from school or author.
12. Page(s) _____ seem to be missing in numbering only as text follows.
13. Two pages numbered _____. Text follows.
14. Curling and wrinkled pages _____
15. Other _____

ULTRASOUND SPECTROSCOPY

by

Clyde Lee Giles

A Dissertation Submitted to the Faculty of the

COMMITTEE ON OPTICAL SCIENCES (GRADUATE)

In Partial Fulfillment of the Requirements
For the Degree of

DOCTOR OF PHILOSOPHY

In the Graduate College

THE UNIVERSITY OF ARIZONA

1 9 8 1

THE UNIVERSITY OF ARIZONA
GRADUATE COLLEGE

As members of the Final Examination Committee, we certify that we have read the dissertation prepared by Clyde Lee Giles

entitled Ultrasound Spectroscopy

and recommend that it be accepted as fulfilling the dissertation requirement for the Degree of Doctor of Philosophy.

H. H. Barrett	8-12-80
	Date
W. Swindell	8-12-80
	Date
R R Mammone	8-12-80
	Date
	Date
	Date

Final approval and acceptance of this dissertation is contingent upon the candidate's submission of the final copy of the dissertation to the Graduate College.

I hereby certify that I have read this dissertation prepared under my direction and recommend that it be accepted as fulfilling the dissertation requirement.

H. H. Barrett	10-22-81
Dissertation Director	Date

STATEMENT BY AUTHOR

This dissertation has been submitted in partial fulfillment of requirements for an advanced degree at The University of Arizona and is deposited in the University Library to be made available to borrowers under rules of the Library.

Brief quotations from this dissertation are allowable without special permission, provided that accurate acknowledgment of source is made. Requests for permission for extended quotation from or reproduction of this manuscript in whole or in part may be granted by the head of the major department or the Dean of the Graduate College when in his judgment the proposed use of the material is in the interests of scholarship. In all other instances, however, permission must be obtained from the author.

SIGNED: 

ACKNOWLEDGEMENTS

I am immeasurably indebted to my dissertation advisor and mentor, Professor Harry Barrett. Not only did Professor Barrett introduce me to the dissertation problem, but he also provided the guidance, inspiration, patience and encouragement necessary to complete such a task. I feel privileged to have had the opportunity to have been one of Professor Barrett's students.

A special note of thanks goes to Dr. David Hecht of Itek Corporation who generously constructed the ultrasonic transducers. I am also very grateful to the following University of Arizona professors who provided both biological specimens and their time: Gene Gerner and Tim Bowden, Radiology, Health Sciences Center; Bryan Fuller, Biological Sciences; Howard White, Biochemistry; and Jim Cramer, Veterinary Science. I would like to express much appreciation to Professors Bob Shannon and Bill Swindell for their careful consideration of this dissertation and their valuable comments and suggestions.

For preparation of this manuscript, many thanks go to Dr. John Mergenthaler for the computer plots, to Paula Stark for the typing and corrections and to Norma Emptage for her readily-given support and advice.

To the Optical Sciences Center's students, faculty and staff, I wish to express my gratitude for providing me with a stimulating and pleasant atmosphere.

Finally, I would like to thank Joan Pomerlean and Mary Barnes whose support in the final moments meant much to this dissertation's completion.

TABLE OF CONTENTS

TABLE OF CONTENTS--Continued

LIST OF ILLUSTRATIONS

LIST OF ILLUSTRATIONS--Continued

LIST OF ILLUSTRATIONS--Continued

ABSTRACT

An ultrasound spectrometer was designed, constructed and used to measure the frequency dependence of forward-scattered ultrasound from biological specimens. A piezo-electric transducer was continuously tuned through the frequency range of 150 to 400 MHz, producing ultrasound of the same frequency. Pulse modulation of the input signal permitted a frequency resolution of 2 MHz. The received pulse was detected at various temporal positions of its amplitude, thereby allowing measurement of the interference of the scattered and unscattered ultrasound radiation. Because of system nonlinearities all received signals were calibrated with respect to the attenuation of ultrasound in water over the system frequency range. The attenuation of water over the frequency range of 150 to 400 MHz was consequently measured and the values agreed very well with figures given in the literature.

Forward-scattering experiments were performed with both physical objects and biological specimens. Sapphire spheres and plastic cylinders exhibited the expected Mie scattering resonant structure. Planar glass plates showed the commonly observed Fabry-Perot resonant structure. Measurement of the resonant frequencies agreed well with theoretically-predicted values.

The biological specimens consisted of various cell suspensions of densities on the order of 100 million cells per milliliter. Because of the high cell densities necessary for signal measurement, only signal attenuation was measured. No resonant structure was observed. Synchronized growth colonies of mouse leukemia cells were investigated at both the plateau and log stages of cell growth. The attenuation of melanoma cells was measured with and without melanin. Also, various lines of tumor cells were investigated. For all of these cell suspensions, the attenuation in dB/mm increased linearly with the logrithm of frequency. Though the slope of the attenuation-frequency curves varied from cell line to cell line, the variation for the same cells under different biological conditions was not appreciable. For all of the above cell lines, no attenuation fell out of the range of 5 to 55 dB/mm.

CHAPTER 1

INTRODUCTION

Every dissertation has a motif. The motif of this dissertation is its approach to the problem of acoustic[1] scattering from biological materials. Scattering theory has basically two formulations; the volume integral approach, which leads to the familiar Born approximation and Fourier transform of scattering sources, and the acoustic Mie approach which leads to the scattered wave rigorously represented as an infinite sum of partial waves. Ultrasonic scattering from tissue has always employed the former approach because of the large ratio of wavelength to particle size and the density of scatterers. However, the Mie scattering formalism has been very useful in chemistry, atmospheric physics, and astronomy in characterizing scattering sources. The Mie approach is to consider scattering from an individual particle, and then assume that the scattered wave from many particles is essentially the incoherent sum of the intensities of the scattered wave from each particle. The volume integral approach is to

---

1. Throughout this work, the terms acoustic and ultrasonic will be used interchangeably. Acoustic waves are sound waves. Ultrasonic waves are high frequency sound waves covering the frequency range of high kilohertz to gigahertz. Thus, ultrasound denotes a special frequency range of acoustic waves.

consider that the scattered wave is from an aggregate of particles or a continuous medium. The Mie method is particularly useful when the scattering wavelength is comparable to or less than the particle size. A major drawback of the Mie approach is that the scattered wave has solutions only for simply shaped objects. It is amazing, though, how many physical entities can be successfully modeled as spherical, cylindrical, etc. The scattering approach investigated in this work is that of the Mie theory. The reason is the success of the Mie theory in scattering characterization in other fields, and that, seemingly, no one else has used this approach.

To investigate experimentally biological media with the above in mind, the frequency of irradiation must be continuously scanned and the wavelength must be comparable to the size of the scattering particle. A frequency range of 100 to 500 MHz was initially decided upon but was, for experimental reasons, reduced to the range of 150 to 350 MHz. This yields an approximate wavelength scan of 10 to 4 microns in most biological specimens, which are ultrasonically very similar to water. This wavelength is on the order of cellular sizes and could induce resonant scattering from the cells. This resonant scattering is predicted by the Mie formulation. Such resonant scattering in the forward direction was seen for physical scattering objects,

such as sapphire spheres and not for biological scattering objects, such as cells. For biological specimens absorption values over the above frequency range were measured. No resonant structure for biological specimens was observed. The reasons are discussed in Chapter 6.

The remaining portion of this chapter is a discussion of the following chapters, what they are intended to be. Chapter 2 is a discussion of the background related to ultrasound spectroscopy and biological material investigation. The chapter is short. With the exception of ultrasound microscopy, there has been little done at these high megahertz frequencies. If the reader is unfamiliar with physics of acoustics, he should read Appendix A, possibly before Chapter 2, and definitely before Chapter 3. Appendix A is a brief description of the physical parameters and basic equations of acoustics.

In Chapter 3 the fundamental formulation of the scattering of a time-harmonic acoustic or scalar wave from a general scattering source is derived from Green's theorem. Both the volume and surface integral formulation are presented. Each is considered separately. The Mie theory for scattering from a fluid sphere is then derived from the surface integral representation. The final sections are concerned with scattering resonances, forward scattering, and the scattering of pulses.

Chapter 4 describes the experimental apparatus and the problems of experimentation. The experimental configuration is traced from the VHF source to the final detected signal. A sample-and-hold module shows how different temporal portions of the received pulsed can be separately recorded. The transducer system and the problems of system nonlinearity are discussed. There is a brief description of specimen preparation.

The measurements themselves are discussed in Chapter 5. The ultrasonic attenuation of water is measured from 150 to 400 MHz, and agrees well with values found in the literature. From the visual examination of the scattered pulses from Crofon fibers,[1] a geometrical scattering model emerges, which is shown to be derivable from the Mie scattering equations for large size parameters, derived in Appendix B. Data evaluated using this model reveal the ultrasound velocity of the scatterer. The agreement with other stated velocity values is good. This simple model must be extended to account for scattering from sapphire spheres, which are physically elastic rather than fluid. The scattering data from suspensions of latex spheres are suggestive of a possible resonance. Problems

---

1. Crofon fibers are flexible plastic optical fibers made by E. I. duPont de Nemours & Co. The core of the fiber is surrounded by a thin sheath of lower refractive index.

in forward-scattering from tissues is discussed. The forward-scattering data from various cell suspensions provide no resonances but attenuation curves over the previously mentioned frequency range. Attenuation curves from various cell suspensions are compared. The attenuation of suspensions of bovine blood cells is shown to agree well with hemoglobin solution attenuation values.

Chapter 6 covers conclusions and suggestions for further work. Many reasons are given for the lack of scattering resonances from the cell suspensions. For further work, more experimental investigation of cell suspensions is suggested. A numerical analysis of Mie scattering for cells modeled as fluid spheres is proposed.

CHAPTER 2

BACKGROUND

Ultrasound is a new and useful radiation modality in medicine and biology, and there exist many excellent books on the subject (Fry 1978; Wells 1977; and Hussey 1975). The reason is the inherent nature of biological material. Many biological media behave ultrasonically as a fluid through which ultrasound readily propagates, though not without some attenuation. There is considerable biological variation in density ρ, compressibility κ, and shape. Ultrasound is sensitive to all of these parameters. The speed c of an ultrasound wave is $(\rho\kappa)^{-\frac{1}{2}}$ and the reflection coefficients are functions of the characteristic impedance Z which equals ρc. (For further explanation of these quantities refer to Appendix A.) The wavelength of ultrasound in biological media can be millimeters to submicron depending on the frequency, thus providing a sensitive probe from tissue and organs to cells. For these reasons, interest in biomedical ultrasound has mushroomed in the past decade and ultrasound has become a common diagnostic tool in most hospitals.

Much of the interest in ultrasound in biology and medicine is in the low megahertz frequency range, i.e. 1 to

10 MHz. At these frequencies, ultrasound attenuation in biological media is small enough so that, within a safe irradiation level, a detectable signal occurs after the sound has entered into and been reflected from the tissues in the human body. This leads naturally to ultrasonic imaging of the variations in density and speed seen by the penetrating and reflected wave. The wavelength of the ultrasound in tissue at these frequencies is 1.5 to .15 mm, which is the approximate limit of the image resolution. A desire to increase resolution to the optical and suboptical range led to the development of the ultrasound microscope (Quate 1979; Kessler and Yuhas 1979.) With frequencies up to the low gigahertz regime, resolution can be on the order of microns or less. These instruments work only at specified frequencies because of detector design.

There have also been many measurements of the ultrasonic properties of tissues and suspensions of biological macromolecules (Dunn and O'Brien 1978.) An excellent compilation of tissue properties may be found in the article by Goss, Johnston and Dunn (1978). The vast majority of these measurements were made in the low megahertz range. The high megahertz range is dominated more by suspension than tissue measurements. As acoustic microscopy becomes more popular, the situation may change. The vast majority of these measurements were made at individual frequencies.

The concern in this dissertation is with ultrasound spectroscopy, a continuous sweep of ultrasonic frequency. There is some ultrasonic spectroscopy at the lower frequencies but none at the higher megahertz frequencies.

There are some very good reasons why high-frequency spectroscopy has not been investigated. Probably the most compelling is the greater absorption at the higher frequencies. For most soft tissue the absorption coefficient α increases rapidly with increasing frequency (Wells 1977), limiting high-frequency ultrasound to the investigation of thin specimens, as in microscopy, or to contact backscatter measurements. Another reason has been the lack of broad-band high-frequency transducers. This is no longer the case and high-frequency broad-band transducers are now available. The ones used in this experiment will be described in Chapter 5.

The remaining portion of this chapter will deal with the low-frequency spectroscopy work and high-frequency ultrasound investigations. The intent of these sections is to be representative of this work, and to show how these efforts differ from that of this dissertation. For further study, it is suggested that the reader consult some of the excellent references mentioned in each section.

Low Frequency Spectroscopy

Scattering of ultrasound from biological specimens in the low megahertz frequency regime has a particular theoretical model (Nicholas 1978). The scattering centers are very close together compared to the wavelength and often quite dense. This readily lends itself to volume scattering formulation in the Green's theorem approach (see Chapter 3). The scattering sources are the volume inhomogeneities of closely interwoven cells, tissue structure, blood vessels, etc. This theoretical scattering model is different from the one used in this dissertation. Some of these differences are discussed in Chapter 3. The purpose of both models is the same, ultrasound signatures of biological specimens.

Low-frequency spectroscopy is quite easy to perform with broad-band transducers. The reflected frequency spectrum is used to discriminate between different kinds of tissue and pathologies of the same tissue. Waag, Lerner and Gramiak (1976) used swept-frequency techniques over the range of 1 to 8.5 MHz to distinguish between normal and cirrhotic liver by comparing the scattered frequency spectrum over the range. With a broad-band pulse of 10 MHz, Lele, Mansfield, and Murphy (1976) investigated the frequency spectrum of the reflected echo using a spectrum analyzer. The frequency dependence of the attenuation

showed characteristic differences between normal and necrotic liver, muscle and kidney cortex. Hill (1976) showed in vivo spectral differences over a range of 1 to 3 MHz of the ultrasonic backscattering characteristics of fat, liver, and spleen. After measuring the slope of the frequency spectrum of the forward-scattered signal, O'Donnell and Miller (1979) were able to distinguish between normal and ischemic myocardium. Lizzi and Elbaum (1979), over the frequency range of 5 to 13 MHz, investigated the frequency spectrum of detached retinas and vitreous hemorrhages. The spectral reflectance of human lung in the frequency range of 1 to 10 MHz was considered by Rhyne (1979). The differences between a normal, healthy lung and one with severe chronic pulmonary disease were not easy to distinguish. If one considers the instantaneous power spectrum of a reflected B-scan pulse, then the literature is full of such clinical investigation (Jennings, Holasek and Purnell, 1979). Often, ultrasound spectroscopy is used in conjunction with other measurements. For example, Hill (1976) and Waag et al. (1979) also utilize angular scattering measurements in their tissue investigations. Billy and Quentin (1979) use a wide-band transducer with very short pulses to investigate the frequency spectrum of periodic surface structures such as mushrooms. In general, ultrasound spectroscopy in the low megahertz domain is often used, but described by other means.

High Frequency Spectroscopy

To the author's knowledge, there has been no ultrasound spectroscopy in the high megahertz range. All the work in this frequency range has been at specific frequencies. Until the acoustic microscope, most of the measurements have been with solutions of biological macromolecules. An excellent summary of this work is Dunn and O'Brien, Jr. (1978). Ultrasonic absorption of salmon sperm DNA in aqueous solution as a function of pH was measured up to 50.50 MHz by O'Brien, Jr., Christman and Dunn (1972). Even among this data, the author was only able to find high-frequency measurements for aqueous solutions of bovine hemoglobin. The measurements of the attenuation α/f^2 several discrete frequencies between 100 and 500 MHz by Edmonds (1962) and Edmonds et al. (1970), ranged around 4 to 6×10^{17} cm^{-1} sec^{+2}. For the last authors, crystalline hemoglobin was dissolved in solution.

For tissues, measurements of ultrasonic properties at these frequencies is also scarce. Acoustic microscopy's primary concern is with imaging. The article entitled "Comprehensive compilation of empirical ultrasonic properties of mammalian tissues" by Goss, Johnston and Dunn (1978) lists very few measurements at frequencies greater than 50 MHz. For beef blood, attenuation measurements at 50, 70, and 90 MHz yield 158, 241, and 327 (dB/cm)(cm^3/gm). For

human or mouse kidney, the scanning laser acoustic microscope for 96 and 222 MHz gives the attenuation values of 87±7.5 and 450±66 dB/cm. In over 600 different listings of tissue, many at different frequencies, only the above exist for frequencies greater than 50 MHz.

CHAPTER 3

ACOUSTIC SCATTERING THEORY

In order to understand the physical, measurable parameters that characterize the interaction of acoustic energy with biological media, the measurables themselves must be defined. This chapter develops the theory of scattering of acoustic waves by fluid particles. It is a summary of many works. The theory is scalar and is applicable to any scalar scattering phenomenon. The development starts with Green's theorem and proceeds to volume and surface scattering representations. The Mie theory for a spherical particle is extensively explained. Some explanation of approximations for various size parameters and the scattering of pulsed radiation is mentioned. It is strongly suggested that Appendix A be read before reading this chapter.

Scattering of a Plane Wave by a Scattering Region

Given some scattering source, what in general can be specified about the scattered wave? Define the incident pressure (scalar) wave as P_i and the scattered wave by P_s. Assume that the time dependence of both waves is harmonic, $e^{-i\omega t}$, where ω is the angular frequency. A common boundary condition for all scattering problems is

that far away from the scattering region, P_s approaches a wave diverging from a point source (in three dimensions) located in the scattering region. Also, the magnitude of P_s is proportional to P_i. Using the coordinate system of Fig. 3.1, the incident wave is $P_i = P_o e^{iKz}$ and satisfies the source-free Helmholtz wave equation $(\nabla^2 + K^2)P_i = 0$ where K is the wavenumber. The above conditions imply that at infinity

$$P_s \to P_o \Phi(\theta,\phi) \frac{e^{iKr}}{-iKr} \; ; \; r \to \infty \; , \tag{3.1}$$

a diverging spherical wave. In two dimensions, the form is slightly different (Morse and Ingard 1968). Figure 3.1 defines the spherical coordinates of P_s. The function $\Phi(\theta,\phi)$ is dimensionless and is called the scattering amplitude or angular-distribution factor. All scattering measurables are directly related to this function.

One important measurable quantity, the scattering cross-section σ_s, is defined as the total power scattered divided by the incident intensity I_i. From Appendix A, the instantaneous intensity I of a pressure field is $P\bar{u}$, where $\bar{u}$ is the instantaneous particle velocity (not to be confused with the wave velocity c). For both plane and spherical waves, the time-average intensity for a time-harmonic wave is $\frac{|P|^2}{\rho c}$, where ρ is the density of the medium. Thus,

$$\sigma_s = \frac{\oint \bar{I}\cdot d\bar{s}}{I_i} = \frac{\oint \frac{|P_s|^2}{\rho c} ds}{\frac{|P_i|^2}{\rho c}} = \frac{\oint |P_s|^2 ds}{|P_i|^2} . \quad (3.2)$$

Using the previous expressions for P_i and P_s, one has

$$\sigma_s = \oint \frac{1}{K^2} |\Phi(\theta,\phi)|^2 d\Omega \quad (3.3)$$

where $d\Omega$ is the solid angle the radiation is scattered into. The quantity $\frac{1}{K^2} |\Phi|^2$ gives the angular distribution of the

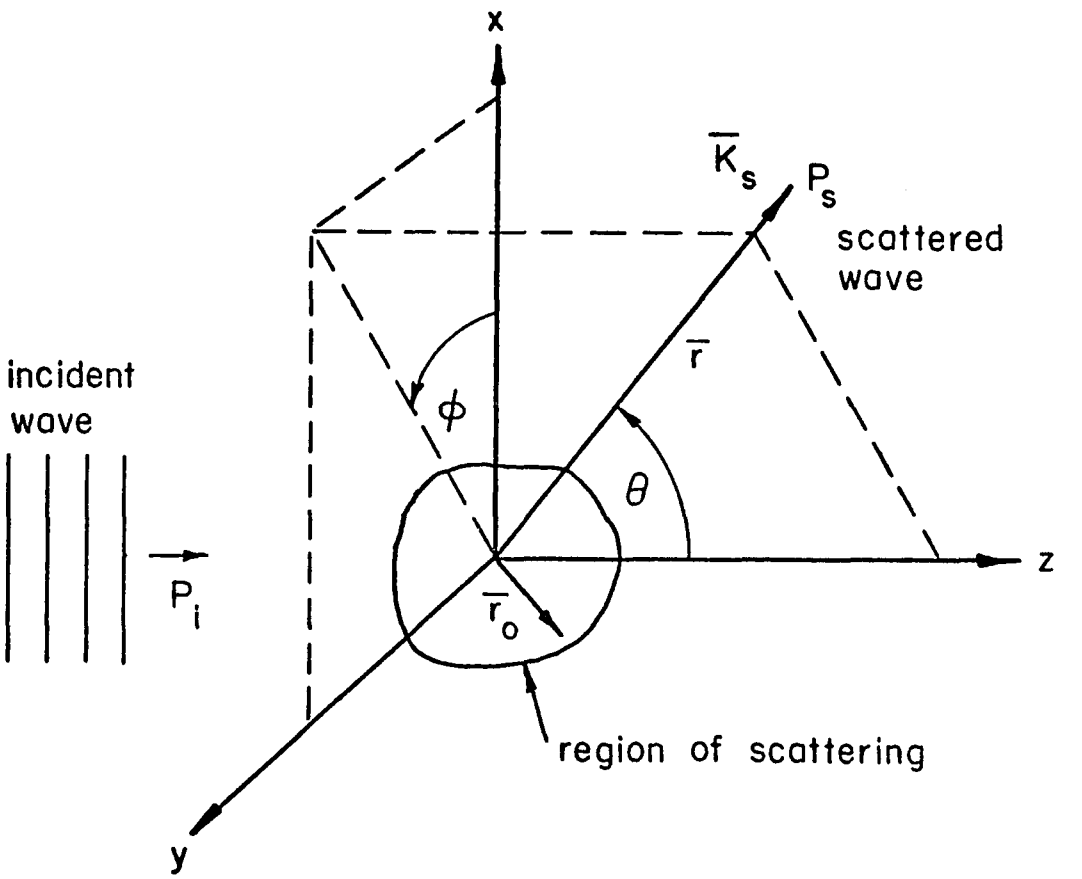

Fig. 3.1. Geometry of scattering region.

scattered radiation and is often referred to as the differential scattering cross-section $d\sigma/d\Omega$. It, as well as σ_s, has the dimensions of area/steradian.

Another viewpoint of the scattering process is to place a scattering medium between an incident plane wave and a detector. Less of the incident beam is now seen by the detector. This extinction of the incident beam by the scattering medium is due to the scattering of radiation out of the beam. If the medium also absorbs the incident radiation, further extinction occurs. Since this absorption occurs within the scattering medium, one may generalize the scattering cross-section to a surface integral over large r, as previously denoted, plus a surface integral around the scattering medium. This extinction or total cross-section σ_t may be represented as

$$\sigma_t = \sigma_s + \sigma_a \tag{3.4}$$

where σ_a is the absorption cross-section.

If the scattering medium is a particle, one may define efficiencies for the extinction, scattering and absorption cross-sections as such:

$$Q_t = \frac{\sigma_t}{A}, \tag{3.5}$$

$$Q_s = \frac{\sigma_s}{A}, \tag{3.6}$$

$$Q_a = \frac{\sigma_a}{A} \tag{3.7}$$

where A is the particle cross-sectional area projected onto a plane perpendicular to the incident beam. Efficiencies are dimensionless and can be greater than unity. The reason is that in the world of small particles, the interference of scattered waves allows more radiation to be scattered and absorbed than would be geometrically incident upon the particle.

To calculate σ_t, one must know either $\Phi(\theta,\phi)$ or the appropriate statistics of $\Phi(\theta,\phi)$. The following sections are primarily concerned with the derivation of Φ or Φ-related quantities.

Green's Theorem and the Scattering Integral

Green's theorem proves to be a powerful tool in the mathematical formulation of the scattering process. From the theorem, one may derive either scattering from boundaries or from inhomogeneities throughout a volume or, if necessary, both. For this treatment, the scattering region will be assumed of finite extent, so that, at infinity, the scattered wave has the form given earlier. Another assumption is that the incident and scattered wave is time-harmonic, i.e., varies as $e^{-i\omega t}$. Any other temporal function of the incident wave can be Fourier-synthesized from its respective frequency-space component.

Starting with Green's theorem, one has

$$\int_V \left[G(\bar{r},\bar{r}_o)\nabla_o^2 P(\bar{r}_o) - P(\bar{r}_o)\nabla_o^2 G(\bar{r},\bar{r}_o) \right] dV_o \qquad (3.8)$$

$$= \oint_S \left[G(\bar{r},\bar{r}_o)\nabla_o P(\bar{r}_o) - P(\bar{r},\bar{r}_o)\nabla_o G(\bar{r},\bar{r}_o) \right] \cdot d\bar{S}_o$$

where $\bar{r}$ is the radius vector pointing to the position at which one wishes to investigate the wave and $\bar{r}_o$ is the radius vector over which the surface and volume integration is performed. Since $P(\bar{r}_o)$ is a pressure wave, it satisfies the Helmholtz wave equation with an appropriate, known time-harmonic source.

$$\nabla_o^2 P(\bar{r}_o) + K^2 P(\bar{r}_o) = - f(\bar{r}_o) \qquad (3.9)$$

where $f\ e^{-i\omega t}$ is the source. The choice of such a source is contingent upon the assumption that the source would radiate at the same frequency as the incident wave. Using the assumptions of the previous section about the form of the scattered wave, on chooses a Green's function that represents radiation from a point source and is a solution, for the unbounded medium, of the equation (Morse and Ingard, 1968)

$$(\nabla_o^2 + K^2) G(\bar{r},\bar{r}_o) = - \delta(\bar{r}-\bar{r}_o), \qquad (3.10)$$

which is $G(\bar{r},\bar{r}_o) = \dfrac{e^{iKR}}{4\pi R}$ where $R = |\bar{r}-\bar{r}_o|$. Substituting

the previous wave equations into the Green's theorem, utilizing the delta function, one has

$$P(\bar{r}) = \int_V f(\bar{r}_o) G(\bar{r},\bar{r}_o)\, dV_o + \oint_S \left[G(\bar{r},\bar{r}_o) \nabla_o P(\bar{r}_o) - P_o(\bar{r}_o) \nabla_o G(\bar{r},\bar{r}_o) \right] \cdot d\bar{S}_o \tag{3.11}$$

which is an equation for the pressure wave within and on any surface bounding the region of interest, in terms of the volume integral of the source function f and of the surface integral of the boundary values of P and its gradient over the boundary surface. In other words, the total field at $\bar{r}$ is the summation of the fields due to the elementary sources plus waves reflected and/or refracted at the boundary. Equation 3.11 is the most general form for deriving the scattered wave within the previous assumptions and is also the starting equation for deriving radiation equations for various sources(Morse and Ingard 1968).

For the scattering problem, one assumes that the source of scattered radiation is the incident wave. Assume a plane wave incident and a surface of integration as shown in Fig. 3.2. Let the surface S_1 go to infinity. Over S_1, the pressure field is, due to linear superposition, a sum of the scattered field and incident field. Since the scattered field consists of outward going waves, then by

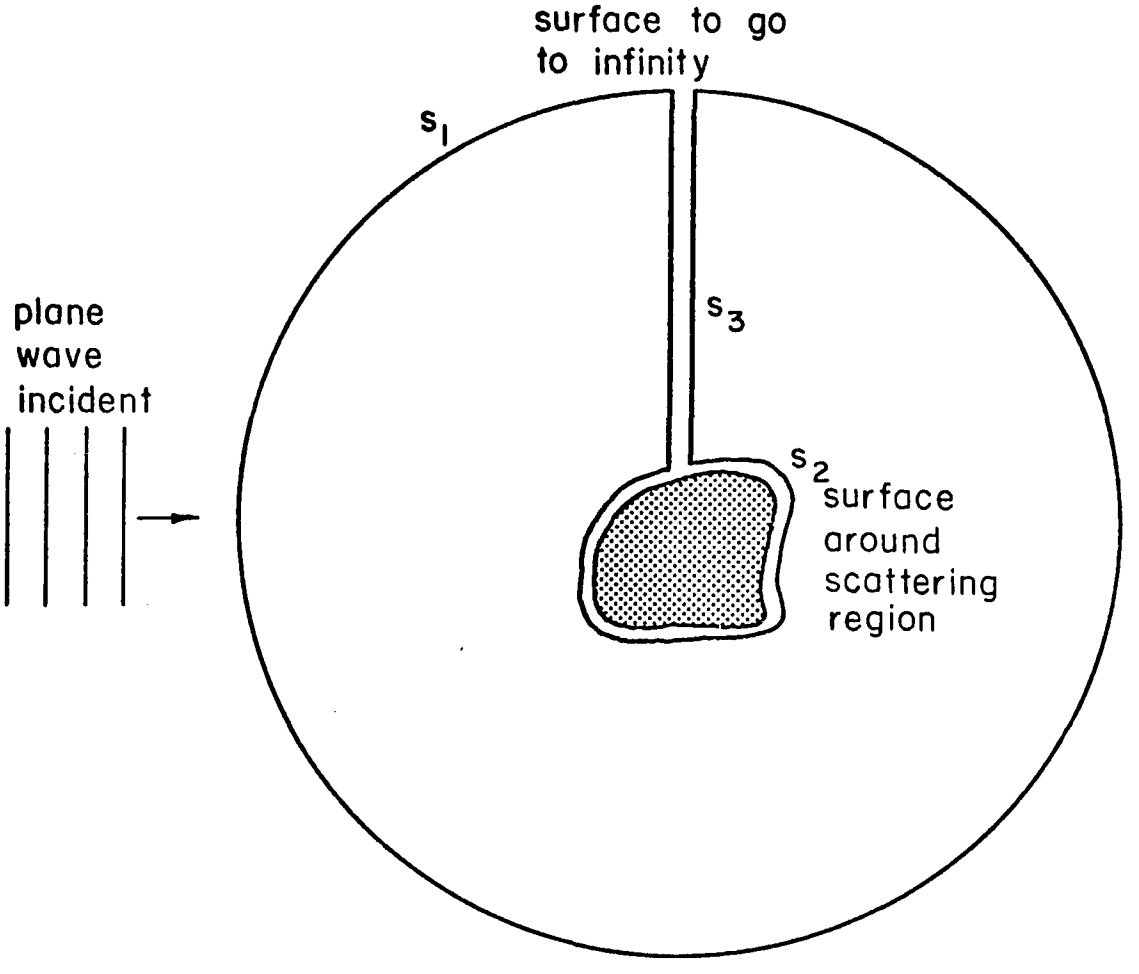

Fig. 3.2. Surface geometries for evaluation of scattering integral.

imposition of the Rayleigh-Sommerfeld radiation condition, (Goodman 1968) the surface integral of the scattered wave component must be zero. However, the incident wave is present at infinity and, in fact, the surface integral over the surface S_2 at infinity produces the incident wave

$P_i(\bar{r})$ (Morse and Ingard, 1968). Since the integral over S_3 is obviously zero, the scattering integral becomes

$$P(\bar{r}) = P_i(\bar{r}) + \int_R f(\bar{r}_o) G(\bar{r},\bar{r}_o)\, dV_o + \oint_{S_2} \left[G(\bar{r},\bar{r}_o) \nabla_o P(\bar{r}_o) - P(\bar{r}_o) \nabla_o G(\bar{r},\bar{r}_o) \right] \cdot d\bar{S}_o \tag{3.12}$$

where R is the region enclosed by surface S_2 and where the source f is nonzero. Representing the scattered wave $P_s(\bar{r})$ as

$$P_s(\bar{r}) = \int_R f(\bar{r}_o) G(\bar{r},\bar{r}_o)\, dV_o + \oint_{S_2} \left[G(\bar{r},\bar{r}_o) \nabla_o P(\bar{r}_o) - P(\bar{r}_o) \nabla_o G(\bar{r},\bar{r}_o) \right] \cdot dS_o \tag{3.13}$$

the total wave may be written as

$$P(\bar{r}) = P_i(\bar{r}) + P_S(\bar{r}) \ , \tag{3.14}$$

the sum of the incident and scattered waves.

Usually in scattering problems only one of the integral expressions in equation (3.13) is present. If there are no source terms, such as volume inhomogeneities, and all the scattering is from a physical discontinuity such as a sphere or slit, only the surface integral term

remains. If however, the boundary discontinuity is small and there are many sources, the surface integral is ignored and the volume integral remains. Obviously, with significant discontinuities and sources, both terms must remain. To my knowledge, there has been no general study that indicated a definite answer as to which integral should be considered. One distinction is that for scattering from surfaces or a particular particle, the surface integral may be solved explicitly whereas the volume integral is nearly always solved through approximations. As will be seen, the volume integral, through the Born approximation, leads to a most familiar integral expression, whereas the surface integral produces the rigorous Mie theory expressions.

Scattering from Sources and Approximations to the Scattered Wave

If the boundary discontinuities are small compared to volume inhomogeneities, one may consider only the volume integral as responsible for scattered wave. Thus, the total pressure wave equation becomes

$$P(\bar{r}) = P_o(\bar{r}) + \int_R f(\bar{r}_o) G(\bar{r},\bar{r}_o) dV_o \quad . \tag{3.15}$$

At large distances from the scattering region, $r >> a$, a the maximum distance of the scattering volume, the Green's

function takes the form

$$G(\bar{r},\bar{r}_o) \rightarrow \frac{1}{4\pi r} e^{(iKr - i\bar{K}_s\cdot\bar{r}_o)}$$

where $\bar{K}_s$ is the scattering vector with magnitude K and with direction of the radius vector $\bar{r}$ from the origin to the point of observation. Refer to Fig. 3.1 for clarification of coordinate systems. This far-field or Fraunhofer approximation now allows one to represent the pressure wave as

$$P(\bar{r}) = P_i(\bar{r}) + \frac{e^{iKr}}{4\pi r} F(\bar{K}_s) \qquad (3.16)$$

where $F(\bar{K}_s) = \int_\infty f(\bar{r}_o) e^{-i\bar{K}_s\cdot\bar{r}_o} dV_o$ is the Fourier transform or the source function. The limits of integration are easily extended to infinity if $f(\bar{r})$ includes its own boundaries.

Perhaps a more useful expression for the scattered wave emerges if P_i is assumed to be an incident plane wave of amplitude P_o. The total pressure wave then may be written as

$$P(\bar{r}) = P_o e^{i\bar{K}_i\cdot\bar{r}} + P_o \frac{e^{iKr}}{-iKr} \Phi(\bar{K}_s) \qquad (3.17)$$

where $\Phi(\bar{K}_s) = \frac{K}{4\pi P_o i} \int_\infty f(\bar{r}_o)\ e^{i\bar{K}_s\cdot\bar{r}_o} dV_o$ is the familiar dimensionless scattering amplitude defined previously. Both $\Phi(\bar{K}_s)$ and $F(\bar{K}_s)$ are measurables in any real scattering situation, since the scattered wave is often measured at a

considerable distance from the scattering region. The combination of the incident plane wave and the far-field approximation is a special one. For this case, one is assured that if the total wave is measured off axis, (where the axis is defined as the direction of the plane wave) the total wave is the scattered wave alone. In theory this is not correct, but in practice a plane wave is of large, but finite extent and most of its angular spectrum is in the forward direction. In the forward direction, any comparison of theory with experiment must take into consideration the incident plane wave.

The next phase in calculating the scattered wave or its Fourier transform is to determine $f(\bar{r})$. This is not easy, since, in many physical problems, $f(\bar{r})$ is a product of another function and the actual wave present, i.e., $f(\bar{r}) = S(\bar{r})P(\bar{r})$. Such a representation of $f(\bar{r})$ causes the expression for the scattered wave to be an integral equation, which is solved exactly only for a few special cases. The equation may be solved by variational methods, (Morse and Feshbach 1953), or by successive approximations. If, for the first approximation, the field $P(\bar{r})$ is replaced by the known incident field, then the scattered field in in equation (3.15) may be written as

$$P_s(\bar{r}) = \int_R P_i(\bar{r}_o) S(\bar{r}_o) G(\bar{r},\bar{r}_o) dV_o \quad . \tag{3.18}$$

If $P_s(\bar{r})$ turns out to be considerably less than that $P_i(\bar{r})$ throughout R, then this approximation, called the Born approximation, gives a satisfactory representation of the scattered wave. If this is not the case, successive higher-order terms may be added to the first-order term. As an example, let the first order term be called P_1, i.e., $P_1 = P_s$ in equation (3.18). Then the total wave field may be represented as

$$P(\bar{r}) = P_i(\bar{r}) + \sum_{n=1}^{\infty} P_n(\bar{r}) \quad \text{where}$$
$$P_{n+1}(\bar{r}) = \int_R P_n(\bar{r}_o) S(\bar{r}_o) G(\bar{r},\bar{r}_o) dV_o \ . \tag{3.19}$$

If the far-field or Fraunhofer approximation is also valid, and the incident wave is a plane wave $P_i = P_o e^{i\bar{K}_i \cdot \bar{r}}$, the Born approximation yields for the scattered wave

$$P_s(\bar{r}) = \frac{e^{iKr}}{-iKr} \Phi(\bar{K}_s - \bar{K}_i) \quad \text{where}$$
$$\Phi(\bar{K}_s - \bar{K}_i) = \frac{P_o}{4\pi i} \int_\infty S(\bar{r}_o) e^{-i\bar{r}_o \cdot (\bar{K}_s - \bar{K}_i)} dV_o \quad \text{where } K_i = K\hat{z} \ . \tag{3.20}$$

The scattering amplitude Φ is the Fourier transform of the more easily found source function $S(\bar{r}_o)$. For scattering in the forward direction $\bar{K}_s = \bar{K}_i$ and the scattered wave becomes proportional to the total integrated effect of the

source. Note that the total wave measured in the forward direction would be $P_i + P_s$, not just P_s. More will be said about this later in this chapter.

Mie Scattering Theory

In the previous section the effects of volume sources were considered greater than that of the boundary interface in the scattering process. This is a practical assumption in many cases since the surface integral problem is exactly solvable for only certain geometries of the scatterer. For a single simply-shaped particle, solutions to the scattered wave are widely available (Bowman, Senior and Uslenghi, 1969). A treatment of the surface integral approach for a single spherical particle will be the topic of this section. This analysis is meant to be instructive. It is not always necessary to go through the full machinery of the Green's surface integral in many cases (Rschevkin, 1963).

Recall equation (3.12) for the total pressure field. Since there are no source terms, the volume integral is zero and the total field may be expressed as

$$P(\bar{r}) = P_i(\bar{r}) + \oint_{S_2} \left[G(\bar{r},\bar{r}_o)\nabla_o P(\bar{r}_o) - P(\bar{r}_o)\nabla_o G(\bar{r},\bar{r}_o) \right] \cdot d\bar{S}_o \ . \tag{3.21}$$

The scattering particle is a sphere of radius a, and a pressure field can propagate inside the sphere. In this sense, the sphere is often termed acoustically nonrigid. Physical examples of such a sphere would be a fluid or any medium which propagates only longitudinal waves. The medium may or may not be absorbing. The surface integral over the surface of the sphere results in the equation

$$P_s(\bar{r}) = a^2 \int_0^{2\pi} d\phi_o \int_0^{\pi} d\theta_o \sin\theta_o \Big[P(r_o,\theta_o,\phi_o) \frac{\partial}{\partial r_o} G(r,\theta,\phi;r_o,\theta_o,\phi_o) - G(r,\theta,\phi;r_o,\theta_o,\phi_o) \frac{\partial}{\partial r_o} P(r_o,\theta_o,\phi_o) \Big]_{r_o=a} \tag{3.22}$$

where the spherical coordinates with subscript zero are those of the sphere, and the unsubscripted spherical coordinates are those of the scattered wave. See Fig. 3.1 for further clarification. The reversal in sign is due to the inward pointing surface integral. Refer to Fig. 3.2. For spherical symmetry the Green's function becomes in spherical coordinates

$$G(\bar{r},\bar{r}_o) = \frac{iK}{4\pi} h_o(K|\bar{r}-\bar{r}_o|)$$

$$= iK \sum_{\ell=0}^{\infty} \sum_{m=-\ell}^{\ell} Y^*_{\ell m}(\theta_o,\phi_o) Y_{\ell m}(\theta,\phi) j_\ell(Kr_o) h_\ell(Kr), \quad r > r_o \tag{3.23}$$

where the Y's are spherical harmonics, j's spherical Bessel functions and h's spherical Hankel functions. These functions are defined in (Jackson 1975). Also due to spherical symmetry, the pressure field may be represented in a spherical harmonic series

$$P(r,\phi,\phi) = \sum_{\ell m} Y_{\ell m}(\theta,\phi) q_{\ell m}(Kr), \quad K = \frac{\omega}{c} \tag{3.24}$$

where $q_{\ell m}$ is an appropriate combination of $j_\ell(Kr)$ and $h_\ell(Kr)$ and associated constants which fit the boundary conditions at $r = a$. If equation (3.24) is placed in equation (3.22), the scattered wave becomes

$$P_s(\vec{r}) = ia^2K^2 \int_0^{2\pi} d\phi_o \int_0^{\pi} d\theta_o \Bigg[\sin\theta_o \sum_{st} \sum_{\ell m} Y_{st}(\theta_o,\phi_o) Y^*_{\ell m}(\theta_o,\phi_o)$$

$$\times Y_{\ell m}(\theta,\phi) \cdot \Big(q_{st}(Ka) j'_\ell(Ka) - q'_{st}(Ka) j_\ell(Ka) \Big) h_\ell(Kr) \Bigg] \tag{3.25}$$

where the quantity $q'(\eta) \equiv \frac{dq}{d\eta}$. If the order of integration and summation is reversed and using the integral property

$$\int_0^{2\pi} d\phi_o \int_0^{\pi} d\theta_o \sin\theta_o \, Y^*_{\ell m}(\theta_o,\phi_o) Y_{st}(\theta_o,\phi_o) = \delta_{\ell s}\delta_{mt},$$

equation (3.25) reduces to

$$P_s(\bar{r}) = ia^2K^2 \sum_{\ell m} Y_{\ell m}(\theta,\phi) h_\ell(Kr) \Big[q_{\ell m}(Ka) j'_\ell(Ka) - q'_{\ell m}(Ka) j_\ell(Ka) \Big]. \quad (3.26)$$

As might have been expected, the equation for the scattered wave is also a spherical harmonic series with its bracketed constants still to be determined.

The first step in determining these constants is to find the relation between $q_{\ell m}(Ka)$ and its derivative $q'_{\ell m}(Ka)$, or equivalently the relation between P and $\frac{\partial P}{\partial r}$ at the surface of sphere. For a wave incident on the spherical surface, the acoustic properties of the material are such that the equation

$$\frac{\partial P}{\partial r} = - i\beta KP \quad (3.27)$$

holds at $r = a$, where the negative sign is due to the inward direction of the surface normal (see Fig. 3.2) and β is the specific acoustic admittance. This equation is derived in Appendix A. Since P is a spherical harmonic series, there can exist a different β for each of these terms. For example, from the definition of β, for the wave outside $r = a$, at the surface, the radial velocity component is

$$u_r = - \frac{1}{\rho c} \sum_{\ell m} Y_{\ell m} \beta_{\ell m} q_{\ell m} \quad (3.28)$$

where $u_r = -u \cdot \hat{n}$. Furthermore, generalizing equation (3.27), one sees that

$$q'_{\ell m}\Big|_{r=a} = -i\beta_{\ell m}\, q_{\ell m}\Big|_{r=a} \quad . \tag{3.29}$$

These acoustic admittances can be determined by the properties of the material inside $r = a$ [which is not part of the region over which the surface integral for the total field holds]. If one finds the acoustic admittances for the inside surface of the sphere, then the outside admittances are known, and, subsequently, the relation between $q_{\ell m}$ and $q'_{\ell m}$. Let the material of the sphere be such that its density is ρ_e and its pressure wave speed c_e. By symmetry, the wave for $r < a$ must also be a spherical harmonic series and, because the wave cannot go to infinity at $r = 0$, one must use j_ℓ rather than h_ℓ. Thus, the general expression for the pressure wave for $r < a$ would be

$$P = \sum_{\ell m} Y_{\ell m} A_{\ell m} j_\ell(K_e r) \tag{3.30}$$

where the $A_{\ell m}$'s are unknown constants and $K_e = \frac{\omega}{c_e}$.

To determine the admittance β_e, recall the definition of β_e. At the inside surface,

$$\bar{u} \cdot \hat{n} = \frac{\beta_e}{\rho_e c_e} P \quad \text{or} \quad u_r = -\frac{\beta_e}{\rho_e c_e} P \tag{3.31}$$

where $\bar{u}\cdot\hat{n} = -u_r$, the radial component of $\bar{u}$. But,

$$u_r = \frac{1}{i\omega\rho_e}\frac{\partial P}{\partial r}\bigg|_{r=a} = \frac{1}{i\rho_e c_e}\sum_{\ell m} Y_{\ell m} A_{\ell m} j'_\ell(K_e a)$$

$$= \frac{1}{i\rho_e c_e}\sum_{\ell m} Y_{\ell m} A_{\ell m} j_\ell(K_e a)\frac{j'_\ell(K_e a)}{j_\ell(K_e a)}$$

$$= -\frac{1}{\rho_e c_e}\sum_{\ell m} \beta_{e_\ell} Y_{\ell m} A_{\ell m} j_\ell(K_e r)\bigg|_{r=a}$$

where $\beta_{e_\ell} = i\frac{j'_\ell(K_e a)}{j_\ell(K_e a)}$. (3.32)

From equation (A20);

$$\frac{\rho_e c_e}{\beta_{e_\ell}} = \frac{\rho c}{\beta_\ell} . \tag{3.33}$$

Substituting equation (3.32) into equation (3.33), one finds the sought after relation between $q'_{\ell m}$ and $q_{\ell m}$:

$$\frac{q'_{\ell m}}{q_{\ell m}} = \frac{\rho c}{\rho_e c_e}\frac{j'_\ell(K_e a)}{j_\ell(K_e a)} = -i\beta_\ell . \tag{3.34}$$

Finally, the expression equation (3.25) for the scattered wave becomes

$$P_s(\bar{r}) = ia^2K^2\sum_{\ell m}[j'_\ell(Ka) + i\beta_\ell j_\ell(Ka)]q_{\ell m}(Ka)$$

$$\times Y_{\ell m}(\theta,\phi)h_\ell(Kr) \tag{3.35}$$

with only the $q_{\ell m}$'s remaining to be determined. These values are determined by requiring that total wave equation hold at $r=a$, i.e.,

$$P(\bar{r})\Big|_{r=a} = \left[P_i(\bar{r}) + P_s(\bar{r})\right]_{r=a} .$$

From the relation $j'_\ell(Ka)h_\ell(Ka) = j_\ell(Ka)h'_\ell(Ka) - i/K^2a^2$ (Morse and Ingard, 1968) and the total wave expression $\sum_{\ell m} Y_{\ell m}\, q_{\ell m}$, one has an expression for the $q_{\ell m}$'s, i.e.,

$$P_i(\bar{r})\Big|_{r=a} = -ia^2K^2 \sum_{\ell m} q_{\ell m}(Ka)Y_{\ell m}(\theta,\phi)j_\ell(Ka) \times [h'_\ell(Ka) + i\beta_\ell h_\ell(Ka)] . \quad (3.36)$$

Expanding the incident wave in a spherical harmonic series allows one to individually determine the $q_{\ell m}$'s in equation (3.36). For an incident plane wave of amplitude P_o and traveling along the z axis, the spherical wave expansion is

$$P_i = P_o e^{iKr\cos\theta} = P_o \sum_{\ell=0}^{\infty} (2\ell+1) i^\ell P_\ell(\cos\theta) j_\ell(Kr)$$

$$= P_o \sum_{\ell=0}^{\infty} \sum_{m=-\ell}^{\ell} (2\ell+1)\delta_{m0}\, Y_{\ell m}(\theta,\phi) j_\ell(Kr) \quad (3.37)$$

since $Y_{\ell 0}(\theta,\phi) = P_\ell(\cos\theta)$, where P is a Legendre function.

If the coefficients of expansion in equation (3.37) are equated on the surface $r=a$, the q_{mn} have values

$$q_{mn}(Ka) = P_o \frac{(2\ell+1)i^{\ell+1}}{h_\ell'(Ka) + i\beta_\ell h_\ell(Ka)} \frac{\delta_{m0}}{K^2a^2} . \tag{3.38}$$

Now substitute equation (3.38) into equation (3.26). The scattered wave is now in its well-determined form,

$$P_s(\bar{r}) = - P_o \sum_{\ell=0}^{\infty} (2\ell+1)i^\ell R_\ell \, P_\ell(\cos\theta) h_\ell(Kr) \tag{3.39}$$

$$\text{where } R_\ell = \frac{j_\ell'(Ka) + i\beta_\ell j_\ell(Ka)}{h_\ell'(Ka) + i\beta_\ell h_\ell(Ka)} .$$

simplified by the coefficient R_ℓ. As expected for spherical symmetry, the scattered wave is independent of the spherical coordinate ϕ.

In most scattering problems, interest is in the asymptotic form of the scattered wave. For this case $Kr >> 1$ and

$$\lim_{Kr \to \infty} h_\ell(Kr) = \frac{i^{-\ell-1}}{Kr} e^{iKr} .$$

The scattered wave is then

$$P_s(\bar{r}) = P_o \frac{e^{iKr}}{-iKr} \Phi(\theta) \tag{3.40}$$

where

$$\Phi(\theta) = \sum_{\ell} (2\ell+1) R_{\ell} P_{\ell}(\cos\theta) \ . \tag{3.41}$$

The function $\Phi(\theta)$, recognized as the scattering amplitude of equation (3.1), may be expressed as sum of individual amplitudes Φ_{ℓ} where $\Phi = \sum_{\ell} \Phi_{\ell}$. Each Φ_{ℓ} is the amplitude of a partial wave of the scattered wave. Equation (3.40) is often termed a partial wave expansion.

The scattering amplitude deserves more investigation. For any given angle of scatter θ, the value of Φ_{ℓ} is essentially the value of R_{ℓ}. Rewriting R_{ℓ}, using equation (3.34) one has

$$R_{\ell} = \frac{j'_{\ell}(x) - \gamma_{\ell}(x_e) j_{\ell}(x)}{h'_{\ell}(x) - \gamma_{\ell}(x_e) h_{\ell}(x)} \tag{3.42}$$

where $\gamma_{\ell} = -i\beta_{\ell}$ and the size parameters are defined $x = Ka$, $x_e = K_e a$. If the surrounding medium is nonabsorbing, then K is real. From the definition of $h_{\ell} = j_{\ell} + in_{\ell}$, R_{ℓ} becomes

$$R_{\ell} = \frac{1}{2} [1 + \mathscr{R}_{\ell}] \tag{3.43}$$

where

$$\mathscr{R}_{\ell} = \frac{h'^{*}_{\ell}(x) - \gamma_{\ell} h^{*}_{\ell}(x)}{h'_{\ell}(x) - \gamma_{\ell} h_{\ell}(x)}$$

The function $\mathscr{R}_{\ell}$ is defined as the reflection coefficient and provides much insight into the scattering. Whether the

medium of the sphere is absorbing or not depends on K_e. If K_e is real, or complex, the sphere is respectively nonabsorbing or partially absorbing. Whatever the nature of K_e, so the nature of γ. For a nonabsorbing medium, γ is real and, as is easily shown, $\mathcal{R}_\ell = 1$. Thus, each partial wave is reflected from the sphere with no change in amplitude, only a change in phase. No energy is lost at the sphere's surface. For a partially absorbing medium $\mathcal{R}_\ell < 1$ and some of each partial wave is absorbed. As a limiting case, if $\rho = \rho_e$ and $c = c_e$, $\mathcal{R}_\ell = -1$ and no wave is scattered.

Consider further the case of the nonabsorbing sphere. Since $\mathcal{R}_\ell = 1$, one may choose $\mathcal{R}_\ell$ as a pure phase function. Let $\mathcal{R}_\ell = -e^{-i2\delta_\ell}$ where δ_ℓ is called the phase angle. Then

$$R_\ell = \frac{1 - e^{-2i\delta_\ell}}{2} . \tag{3.44}$$

The phase angle concept is sometimes useful in calculation of resonances in scattering.

With the scattered wave known, the scattering cross-section σ_s may be calculated. From equation (3.2), $\sigma_s = \frac{1}{K^2} \oint |\Phi(\theta)|^2 \, d\Omega$. Using equation (3.41) and the orthogonality property

$$\int_{-1}^{1} P_n(\eta) P_m(\eta) \, d\eta = \frac{2\delta_{mn}}{2n+1} ,$$

one has

$$\sigma_s = \frac{4\pi}{K^2} \sum_{\ell} (2\ell+1) |R_\ell|^2 \quad . \tag{3.45}$$

For a nonabsorbing sphere, the cross-section becomes, with the aid of equations (3.43) and (3.44),

$$\sigma_s = \frac{4\pi}{K^2} \sum_{\ell} (2\ell+1) \frac{|1+\mathscr{R}_\ell|^2}{4}$$

$$= \frac{4\pi}{K^2} \sum_{\ell} (2\ell+1) \sin^2\delta_\ell \quad . \tag{3.46}$$

Whatever the type of scatterer, σ_s is a direct function of R_ℓ.

Utilizing σ_s for the nonabsorbing sphere, a more powerful and general result can be derived. First, rewrite the $|1+\mathscr{R}_\ell|^2$ term in equation (3.46). Then,

$$\frac{|1+\mathscr{R}_\ell|^2}{4} = \frac{1 + Re\{\mathscr{R}_\ell\}}{2} = Re\{\mathscr{R}_\ell\} \ ,$$

from equation (3.43) and the property $|\mathscr{R}_\ell| = 1$. However,

$$Re\{\Phi(\theta=0)\} = \sum_{\ell} (2\ell+1) Re\{R_\ell\} \ . \tag{3.47}$$

From equation (3.4), the extinction cross-section is $\sigma_t = \sigma_s+\sigma_a$. For a nonabsorbing sphere, $\sigma_a = 0$ and, using the relations in this paragraph and equation (3.45), the extinction cross-section is

$$\sigma_t = \frac{4\pi}{K^2} Re\{\Phi(0)\} . \qquad (3.48)$$

In other words, the total radiation removed from the incident wave is proportional to the real part of the scattering amplitude in the forward direction. This relation is called the optical theorem and is very useful in calculating extinction cross-sections. [In some references, $Re\{\Phi(0)\}$ is replaced by $Im\{\Phi(0)\}$. The determining factor is the i in the definition of Φ]. Since $Re\{\Phi(0)\}$ forms the shadow of the scattering sphere, it is not surprising that it measures the total power extracted from the incident wave.

The optical theorem is quite general. If the sphere is absorbing, the absorption cross-section can be easily derived. Recall $\sigma_a = \sigma_t - \sigma_s$. From equations (3.45), (3.47), and (3.48),

$$\sigma_a = \frac{4\pi}{K^2} \sum_{\ell} (2\ell+1) \left[|R_\ell|^2 - Re\{R_\ell\} \right] . \qquad (3.49)$$

The cross-sections are all functions of the wavelength. A more convenient expression for calculations is the efficiency Q defined in equations (3.5) through (3.7). Listed are the various efficiencies calculated in this section.

$$
\begin{aligned}
Q_t &= \frac{4}{x^2} Re[\Phi(0)] \\
Q_s &= \frac{4}{x^2} \sum_{\ell} (2\ell+1)|R_\ell|^2 \qquad (3.50) \\
Q_a &= \frac{4}{x^2} \sum_{\ell} (2\ell+1)\left[|R_\ell|^2 - Re\{R_\ell\}\right].
\end{aligned}
$$

Note that $\Phi(0)$ and R_ℓ are functions of x, the size parameter, and the acoustic constants which characterize the medium (ρ,c) and the scatterer (ρ_e,c_e). [The size parameter x_e may be written as $x_e = \frac{c}{c_e} x$]. Thus, the efficiencies of equations (3.49) are functions only of x and the acoustic parameters of the scattering process. For a general x, the efficiencies in equation (3.50) must be evaluated numerically. Shown in Figs. 3.3 through 3.7 are computed scattering efficiencies Q_t as a function of the size parameter x for various ratios of density and speed of the scattering to the surrounding medium. These curves are in excellent agreement with the literature. Figures 3.5 through 3.7 should be compared to the curves in Fig. 5 in Anderson (1950), and Fig. 3.3 should be compared to the curve in Fig. 1 in Hart and Montroll (1951). Note that for a nonabsorbing sphere, $Q_t = Q_s$. Each curve is unique to these ratios and thereby characterizes the scatterer and

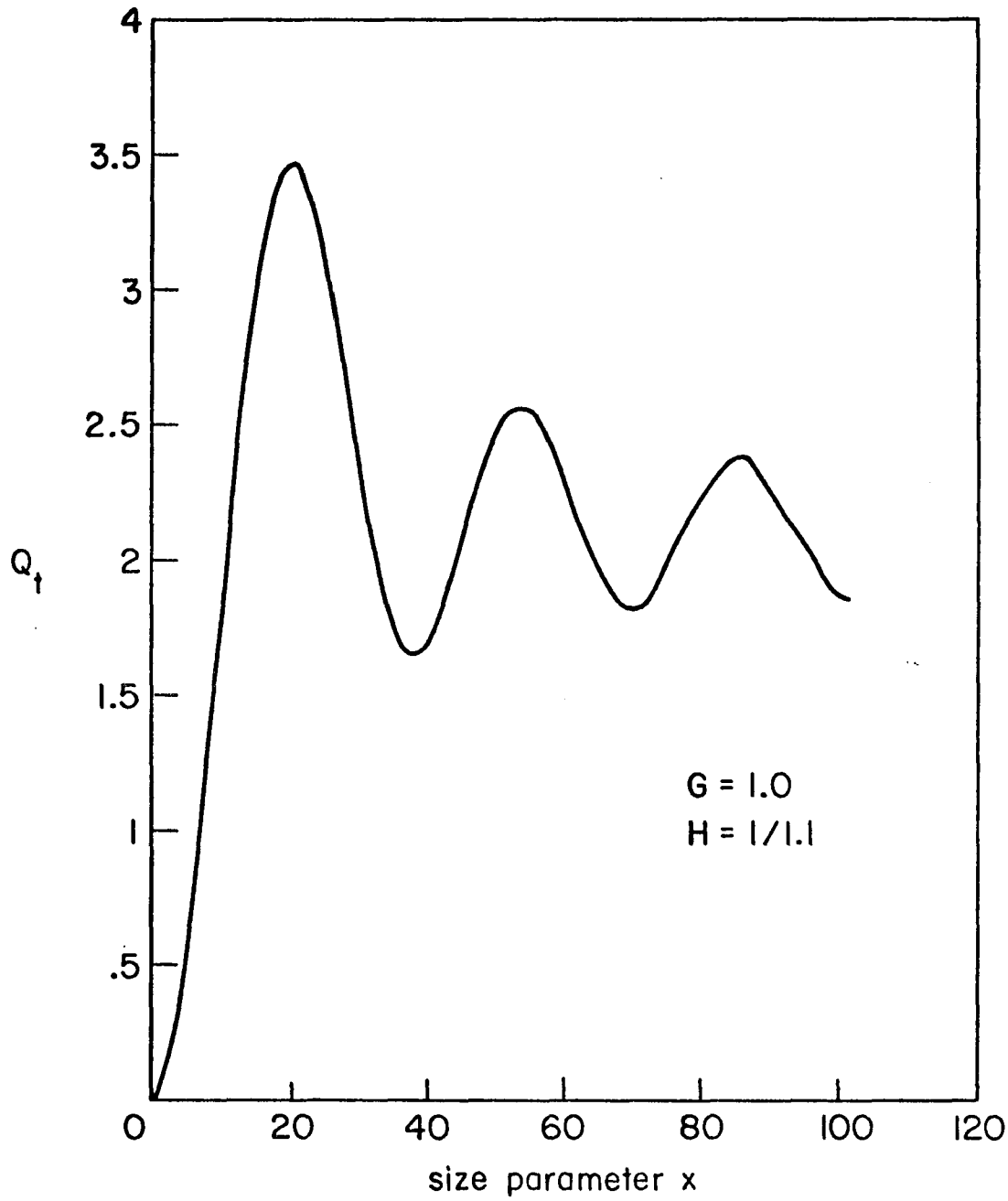

Fig. 3.3. Total scattering efficiency for a fluid sphere as a function of the size parameter x. $G \equiv$ (density of sphere)/(density of medium), $H \equiv$ (sound speed in sphere)/(sound speed in medium).

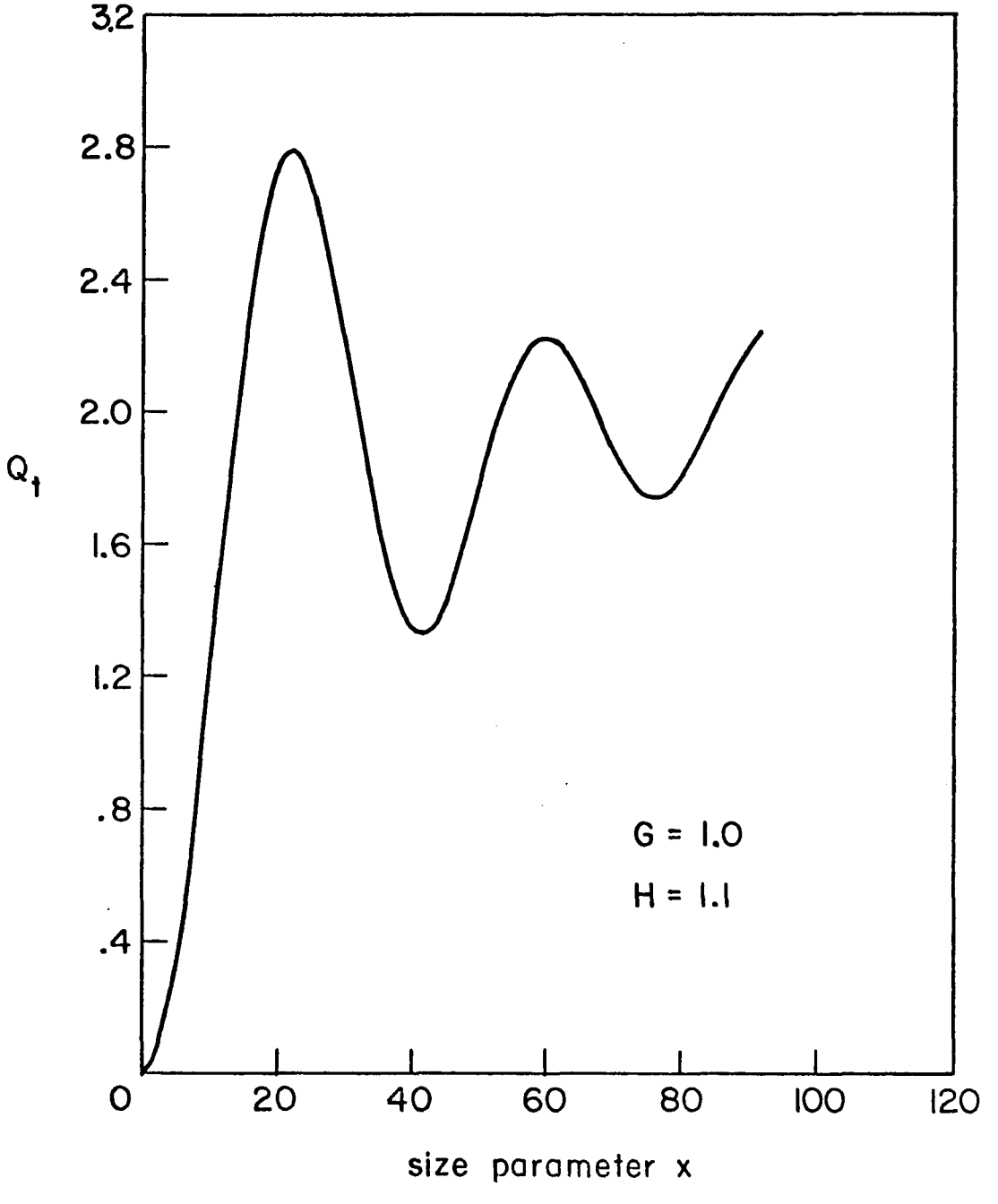

Fig. 3.4. Total scattering efficiency for a fluid sphere as a function of the size parameter x. G and H defined in Fig. 3.3. caption.

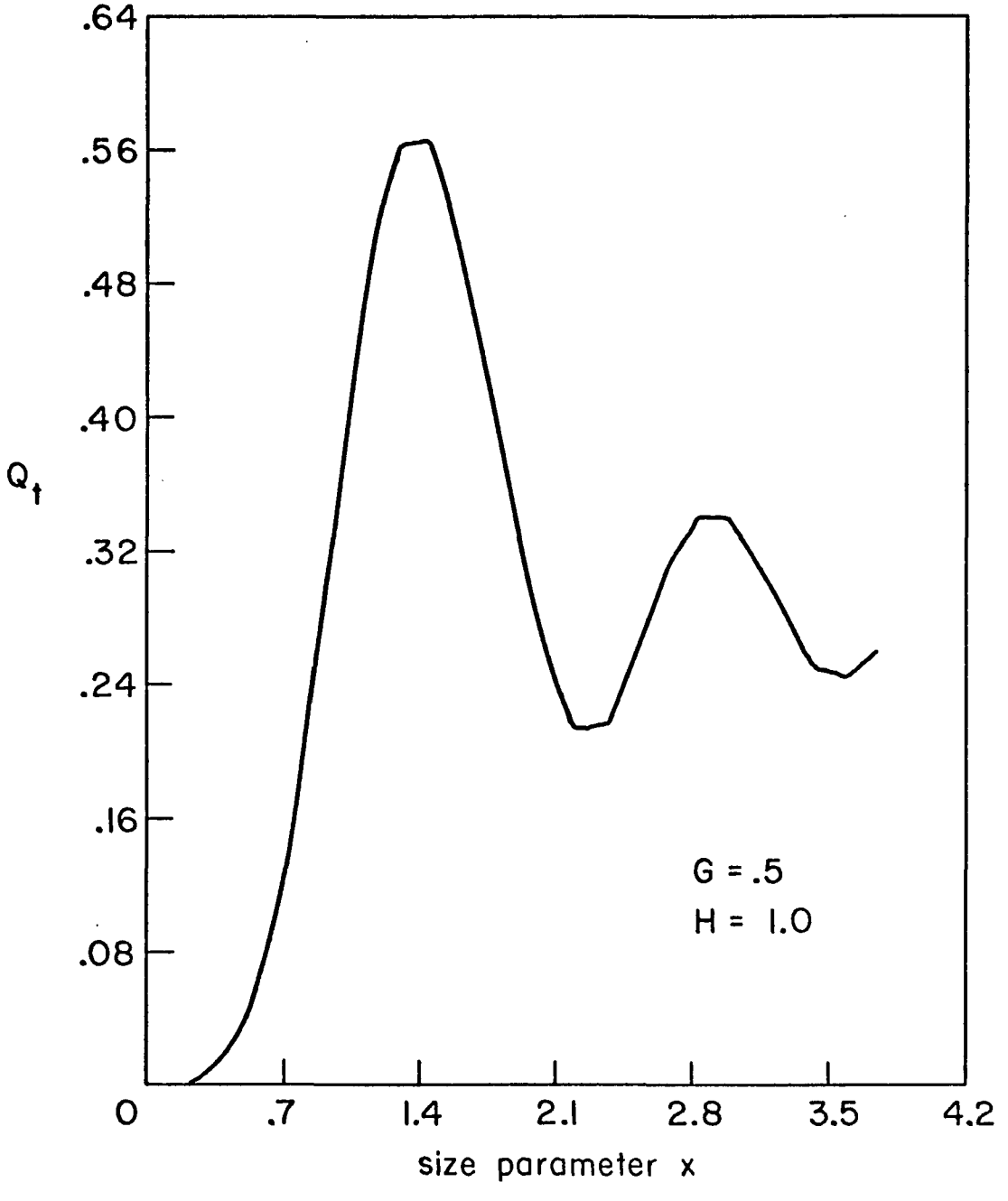

Fig. 3.5. Total scattering efficiency for a fluid sphere as a function of the size parameter x. G and H defined in Fig. 3.3. caption.

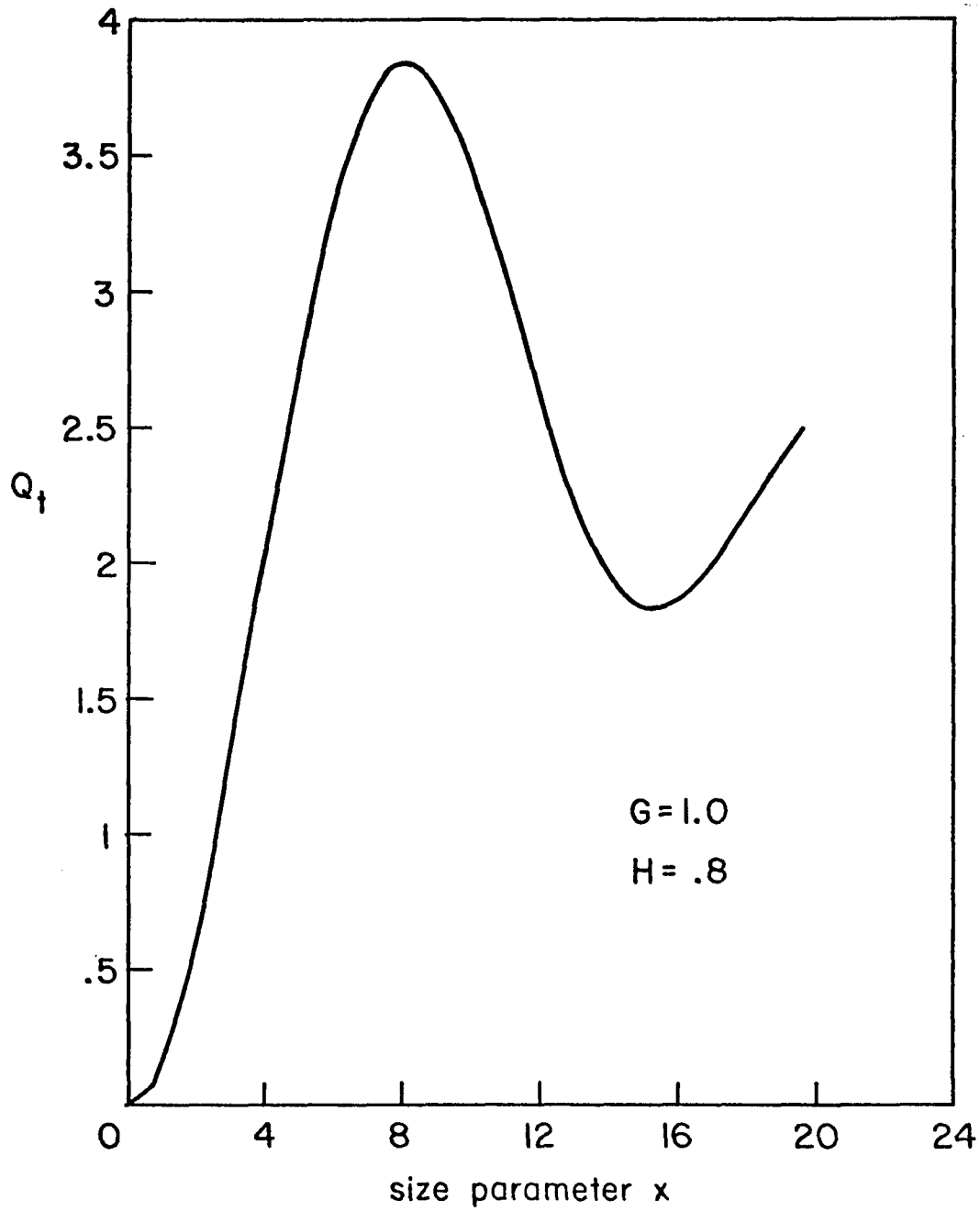

Fig. 3.6. Total scattering efficiency for a fluid sphere as a function of the size parameter x. G and H defined in Fig. 3.3. caption.

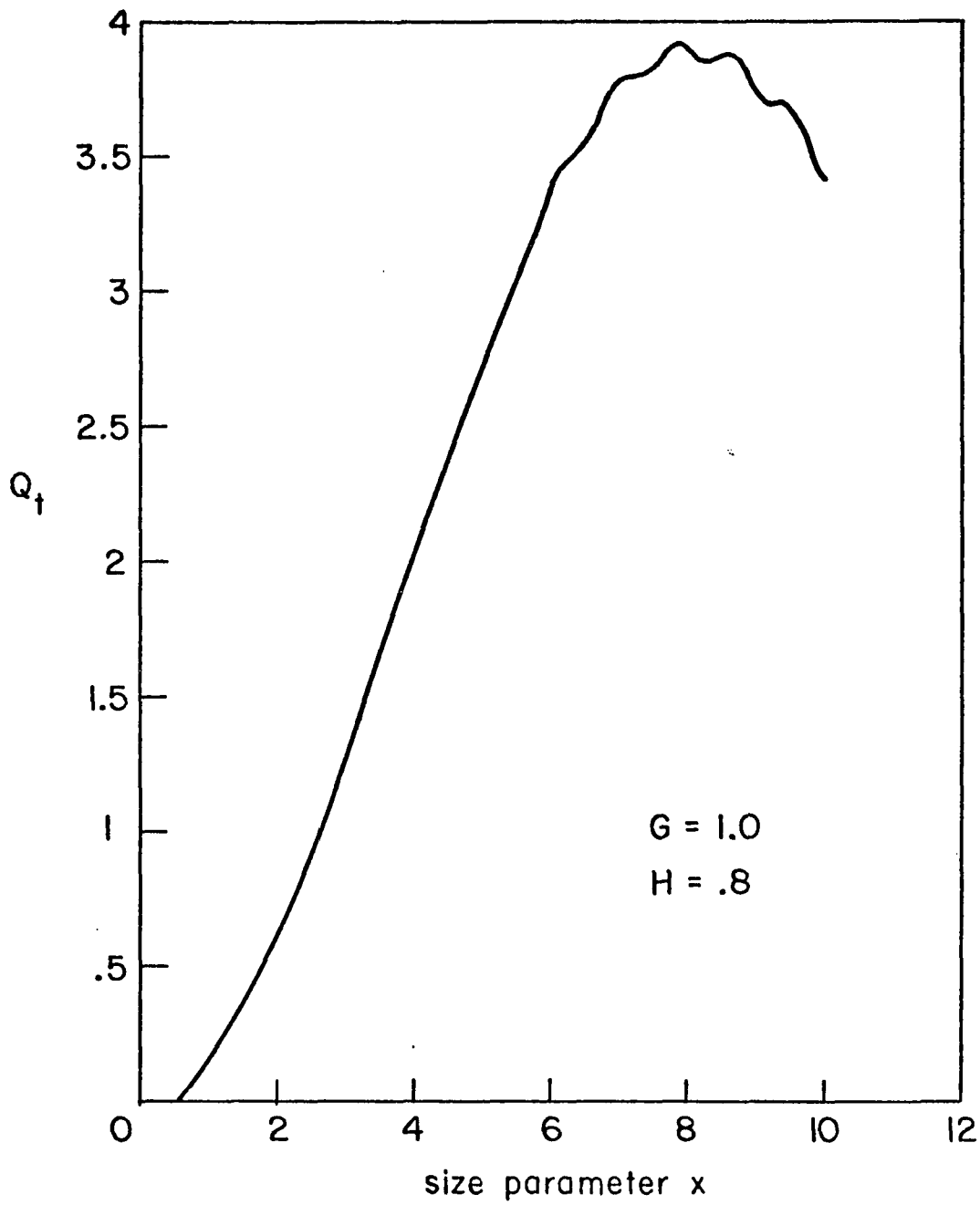

Fig. 3.7. Total scattering efficiency for a fluid sphere as a function of the size parameter x. G and H defined in Fig. 3.3. caption.

its environs. In the next section, some aspects of the structure of these curves will be discussed.

The scattering parameters derived were all for a single scattering sphere. Though many scattering particles can be modeled individually as spheres, how valid are these results for many-particle scattering? Very valid <u>if</u> the collections of particles of arbitrary size are separated by distances large compared to the wavelength. A rigorous expression (Ishimaru, 1978) of this statement is possible through use of the definition of the optical distance G. With scattering volume V and number particle density ρ_d, the single-scattering approximation requires that

$$G = \int_o^L \rho_d \sigma_t ds \approx \rho_d \sigma_t L << 1 , \qquad (3.51)$$

where the integration is taken over a path though the volume V and L is some linear dimension of V. For multiple scattering, refer to the references Ishimaru, (1978) and Morse and Ingard (1968).

This completes the section on Mie scattering. The next section will deal with limits and approximations of the rigorously derived relations of this section. Mie scattering theory does not always deal with scattering from spheres. Cylinders, spheroids, wedges, bubbles, etc. have all fallen victim to the theory derived in this section. Many of these are discussed in the references.

The theoretical approach used in this section is often not the most convenient for deriving the scattered wave. The most common technique is to know the forms of the field everywhere and match boundary conditions, completely disregarding the surface integral process. The approach taken here was illustrative and intended to provide insight into the completeness of scattering theory provided by Green's theorem.

Approximations and Resonances in the Mie Theory; Forward Scattering

A most useful and well-known scattering situation is for the case of the size parameter $x << 1$. [Or the wavelength $\lambda >> a$]. This is called the Rayleigh regime, and the expressions for the scattering amplitude and efficiency are much simplified. Using the small-x approximations for the spherical Bessel, Neumann, and Hankel functions,

$$j_\ell(x) \sim \frac{x^\ell}{(2\ell+1)!!}$$

$$n_\ell(x) \sim \frac{(2\ell-1)!!}{x^{\ell+1}}$$

$$n_\ell(x) \sim \frac{(2\ell)!}{i\ell!} \frac{1}{2^\ell x^{\ell+1}}$$

and substituting into equation (3.42) for the reflection coefficient R_ℓ, one has, after some manipulation (Morse

and Ingard 1968),

$$\Phi(\theta) = \frac{1}{2} K^2 a^2 \left\{ \frac{\kappa_e - \kappa}{\kappa} + \frac{3\rho_e - 3\rho}{2\rho_e + \rho} \cos\theta \right\}$$

$$Q_s = \frac{4}{9} (Ka)^4 \left\{ \left| \frac{\kappa_e - \kappa}{\kappa} \right|^2 + \frac{1}{3} \left| \frac{3\rho_e - 3\rho}{2\rho_e + \rho} \right|^2 \right\}$$

where κ, κ_e are the compressibilities of the surrounding medium and scattering sphere. As expected, Q_s varies as ω^4. The scattering amplitude Φ has one constant and one cosine dependent term, indicative of the monopole and dipole natures of the compressibility and density in scattering from an acoustic sphere.

Another feature of scattering, especially of interest to this work, is resonant structure in the scattered radiation. Such information can be gained from the scattering efficiency Q_s. From equations (3.50), Q_s essentially varies as $|R_\ell|^2$. Thus, the maxima and minima of $|R_\ell|^2$ would be indicative of the maxima and minima of Q_s and scattering in general. For a nonabsorbing sphere, from equation (3.41), one has

$$|R_\ell|^2 = \frac{U_\ell^2}{U_\ell^2 + V_\ell^2} \tag{3.52}$$

where

$$\begin{aligned} U_\ell &= j'_\ell(x) j_\ell(x_e) - (z/z_e) j'_\ell(x_e) j_\ell(x) \\ V_\ell &= n'_\ell(x) j_\ell(x_e) - (z/z_e) j'_\ell(x_e) n_\ell(x) \end{aligned} \tag{3.53}$$

and

$$z = \rho c, \quad z_e = \rho_e c_e \quad .$$

It is obvious that $|R_\ell|^2$ is a maximum and a minimum for, respectively, V_ℓ and U_ℓ very small. The limiting cases V_ℓ and $U_\ell = 0$, yielding $|R_\ell|^2$ unity and zero, are nonphysical. For $|R_\ell|^2 = 1$, the series for Q_s in equation (3.50) cannot converge and, for $|R_\ell|^2 = 0$, there is no scattered radiation. Any condition on $|R_\ell|^2$ and V_ℓ, U_ℓ should be independent of ℓ and, therefore, not dependent on the summing process. In general, such extrema would be difficult to ascertain.

For large x, i.e., the wavelength much less than that of the particle size, the analysis is possible. From the asymptotic formulas for j_ℓ and n_ℓ,

$$j_\ell \sim \frac{1}{x} \sin\left(x - \frac{\ell\pi}{2}\right) \quad ; \quad n_\ell \sim -\frac{1}{x} \cos\left(x - \frac{\ell\pi}{2}\right) ,$$

one may write V_ℓ as approximately

$$V_\ell \sim \sin\left(x - \frac{\ell\pi}{2}\right) \sin\left(x_e - \frac{\ell\pi}{2}\right) + \frac{z}{z_e} \cos\left(x - \frac{\ell\pi}{2}\right) \cos\left(x_e - \frac{\ell\pi}{2}\right)$$

ignoring the $\frac{1}{xx_e}$ term since it is cancelled in $|R_\ell|^2$. Rewriting, one has

$$V_\ell \sim \left(\frac{z}{z_e} + 1\right) \cos(x - x_e) + \left(\frac{z}{z_e} - 1\right) \cos(x + x_e - \ell\pi) \quad .$$

The first term, ℓ independent, yields a minimum for V_ℓ and a maximum for $|R_\ell|$ if

$$x-x_e = (m + \frac{1}{2})\pi, \tag{3.54}$$

m an arbitrary integer. A similar analysis on U_ℓ leads to minimum for $|R_\ell|$ if $x-x_e = m\pi$. Rewriting equation (3.54),

$$2Ka - 2K_e a = (2m+1)\pi , \tag{3.55}$$

or the path difference between a ray traveling through the particle and missing the particle produces a maximum in Q_s if the phase difference is odd multiples of π. This is different from the result predicted by ray optics by a factor of π. However, for large x, the difference Δx between maxima, not the absolute position of the maxima, is the measurable value. From $x_e = \frac{c}{c_e} x$,

$$\Delta x = \frac{\pi}{1 - \frac{c}{c_e}} , \tag{3.56}$$

or the difference in maxima or minima is only a function of the acoustic speeds. Any scattering sphere which has the same acoustic speed as the surrounding medium, but has a different density, will have none of the resonant structure described here. This large resonant structure for Q_s is seen in Fig. 3.3. For this curve, $\frac{c}{c_e} = 1.1$ and $\Delta x = 31.4$, which is very close to the Δx observed in Fig. 3.3.

Scattering in the forward direction is quite useful in many measurements. However, in the forward direction, the detector sees not only the forward-scattered wave but also the unscattered portion of the incident wave. Consider the problem of the total forward-scattered wave from N particles. If the optical distance G between particles, defined in equation (3.51), is much less than one, then one may assume that there is no multiple scattering and the scattered wave from each particle is not rescattered by another particle. The forward-scattered wave P_f may be written as

$$P_f = P_i + \sum_n^N P_{sn} (=0),$$

the sum of the incident wave and the forward-scattered waves from each particle.

If the incident wave is assumed planar and each scattered wave is a spherical wave of the form given by equation (3.40) [valid for the single scattering assumption and the condition $Kr >> 1$], then the forward-scattered time-averaged intensity I_f from equations (A17) and (A18) is proportional to $|P_f|^2$ or

$$\begin{aligned} |P_f|^2 &= |P_i + \sum_n^N P_{sn}|^2 \\ &= |P_i|^2 + 2 \sum_n^N Re\{P_i^* P_{sn}\} + \sum_m^N \sum_n^N P_{sm}^* P_{sn} \quad . \end{aligned} \tag{3.57}$$

Note that exactly in the forward direction, the scattered fields from an incident plane wave arrive in phase. If the scatterers are assumed identical, then $P_{sn} = P_{sm}$ and equation (3.57) becomes

$$\begin{aligned} |P_f|^2 &= |P_i|^2 + 2N\ Re\{P_i^* P_s\} + N^2\ |P_s|^2 \\ &= |P_i + N\ P_s|^2 \end{aligned} \tag{3.58}$$

With the expressions for an incident plane wave and the spherical scattered wave from equation (3.40), the intensity I_f with the aid of equations (A17) and (A18) becomes

$$I_f = \frac{P_o^2}{2\rho c}\left|1 - \frac{N\Phi(0)}{iKz}\right|^2 \tag{3.59}$$

$$\simeq I_o\left(1 - \frac{2N}{Kz}\ Im\{\Phi(0)\}\right) \text{ for } Kz >> I$$

$$= I_o\left[1 - \frac{2N}{Kz}[\Phi^2(0) - (4x^2Q_t)^2]^{\frac{1}{2}}\right], \tag{3.60}$$

using equation (3.50) and $I_o = \frac{P_o^2}{2\rho c}$. If little radiation is scattered; then $\Phi^2(0) >> (4x^2Q_t)^2$ and

$$I_f \simeq I_o\left[1 - \frac{2N}{Kz}\ \Phi^2(0) + \frac{N(4x^2)^2}{Kz}\ \frac{Q_t^2}{\Phi^2(0)}\right], \tag{3.61}$$

and the intensity in the forward direction is a measure of the extinction efficiency.

Scattering of a Pulsed Wave

All scattering expressions derived have been for time-harmonic waves of the form $e^{-i\omega t}$. Thus the scattered response to such an input as a function of ω is essentially the temporal transfer function of the scattering system. If one rewrites equation (3.40) with the frequency variable,

$$P_s(\omega;\bar{r}) = P_o \frac{e^{i\frac{\omega r}{c}}}{-i\frac{\omega r}{c}} \Phi(\omega,\theta) \quad . \tag{3.62}$$

If the incident wave is not time-harmonic, then the resultant scattered wave P_{so} in frequency space is

$$P_{so}(\omega) = P_s(\omega) \cdot A(\omega) \tag{3.63}$$

where $A(\omega) = \int_{-\infty}^{\infty} a(t)e^{-i\omega t}dt$; $a(t)$ is the temporal amplitude of the incident wave. [The r's in the argument have been conveniently dropped]. For a square pulsed wave of carrier frequency ω_o,

$$a(t) = rect(t/T)e^{-i\omega_o t}$$

where $rect(x)$ is the rectangle function defined in Goodman (1968) and T is the duration of the pulse. For this particular $a(t)$, it is easy to show (Goodman, 1968) that $A(\omega) = T\text{sinc}(T(\omega-\omega_o))$, where $\text{sinc}(x) \equiv \sin(\pi x)/\pi x$. By the definition of equation (3.60), the temporal form of the scattered

wave is

$$P_{so}(t) = \frac{1}{2\pi}\int_{-\infty}^{\infty} P_s(\omega)A(\omega)e^{i\omega t}d\omega \ . \qquad (3.64)$$

The effects of the limits of $a(t)$ on $P_{so}(t)$ are quite illuminating. First, let the pulse width T become quite large. Then, $\lim_{T\to\infty} T\text{sinc}T(\omega-\omega_o) = \delta(\omega-\omega_o)$ and $P_{so}(t) = P_s(\omega_o)e^{-i\omega_o t}$, illustrating that, indeed, $P_s(\omega)$ was the transfer function of the scattering system. Now, let the pulse width become extremely narrow. The sinc function becomes very flat and is approximately unity for all ω. The scattered wave $P_{so}(t)$ is now $P_{so}(t) = \frac{1}{2\pi}\int_{-\infty}^{\infty} P_s(\omega)e^{i\omega t}d\omega$, the temporal impulse response of the scattering system.

For conditions between the previous extremes, the form of $\Phi(\omega)$ in $P_s(\omega)$ must be explicit. From equations (3.42) and (3.43) the functional dependence of ω is with R_ℓ. Each x or x_e must be replaced by $\frac{\omega a}{c}$ or $\frac{\omega a}{c_e}$, which leads to a very complex dependence on ω, even for scattering in the forward direction. For any size parameter x, the wave $P_{so}(t)$ must be evaluated numerically. However, in certain cases of x and Δx, the form of $\Phi(\omega)$ reduces to a much simpler expression and the equation (3.62) is solvable analytically. Such an example could be for $x << 1$, the regime of Rayleigh scattering.

CHAPTER 4

THE EXPERIMENT

The experimental apparatus to be described in this chapter measures the scattering of a pulsed ultrasonic wave in the forward direction. Before the experiment is described, there is a discussion of what is actually measured, using freely the concepts developed in Chapter 3 and the appendices. A detailed description of the experiments and procedure follows. Emphasis is placed on the experimental parameters that affect the scattering measurements.

The Measurement

To understand what is measured, a brief presentation of the experimental apparatus is necessary. A single-frequency continuous electrical wave, after being pulse-modulated, is amplified and then transduced to an ultrasonic wave of the same frequency. This ultrasonic signal is then scattered by a sample, and the forward-scattered wave is transduced back to an electrical signal, which is reamplified, square-law detected, and time-sampled. The temporal sampling is performed by a sample-and-hold device [S/H], the output of the S/H is fed into a chart recorder, and the sampled signal is recorded as a function of signal frequency.

The S/H is very important because its temporal placement on the received pulse allows various portions of that pulse to be recorded.

The output pulse maintains its square nature. It will be assumed that this pulse is broad enough that a small bandwidth of frequencies passes thru the system. In practice, the frequency range scanned was 100 to 400 MHz and the pulse width in the frequency domain was approximately 2 MHz. Such a pulse width will average out the more narrow scattering resonances, but easily see those of greater width than 2 MHz. Thus, the scattered wave will be assumed to have one frequency ω_o so that the scattered amplitude is $\Phi(\omega_o)$. With reference to the last section of Chapter 3, this implies that the width of $A(\omega)$ in equation (3.64) is narrow enough such that $P_s(\omega)$ becomes $P_s(\omega_o)$ and is removed from the integral. Then $P_{so}(t) = a(t)P_s(\omega_o)$, as the pulse is only a multiplicative factor on the scattered wave.

The scattered intensity in the forward direction is given by equation (3.61). From this equation, one has $I_f \propto a + bQ_t^2$. Since Q_t is always positive, the extrema of Q_t^2 are also extrema of I_f. In Chapter 3 these extrema for large x were discussed. The conclusion was that the difference between the maxima or minima could be interpreted as the phase difference between a ray traveling through a particle and one missing the particle. From the analysis

of the preceding paragraph, one could construct for scattering in the forward direction a geometrical scattering model as illustrated in Fig. 4.1. The pulsed incident beam can be thought of as decomposing into two incident beams, one that misses and one that passes through the scatterer. After scattering, the beams recombine and interference between the two beams occurs at the region of overlap shown in Fig. 4.1. This interference was actually observed, and photographs and further discussion of this effect are in Chapter 5. The S/H, temporally placed at this overlap region, would see this interference effect.

Instrumentation

Now that one has a feeling for what is actually measured, the instrumentation will be described in detail. The system described is shown in Fig. 4.2. A VHF oscillator emits a high-frequency continuous-wave [CW] signal that is gated by a diode gate driven by pulser 1. This pulser is also the main clock of the electronic timing, and synchronizes pulse 2 and the oscilloscope. The diode gate sees from pulser 1 a train of pulses .6 μsec in width at a repetition rate of 5 KHz. From the nonlinear properties of the diode, the product of the CW signal and the pulse emerges from the diode gate. At this stage the power of the pulsed CW signal is from 50 to 400 mwatts. The next

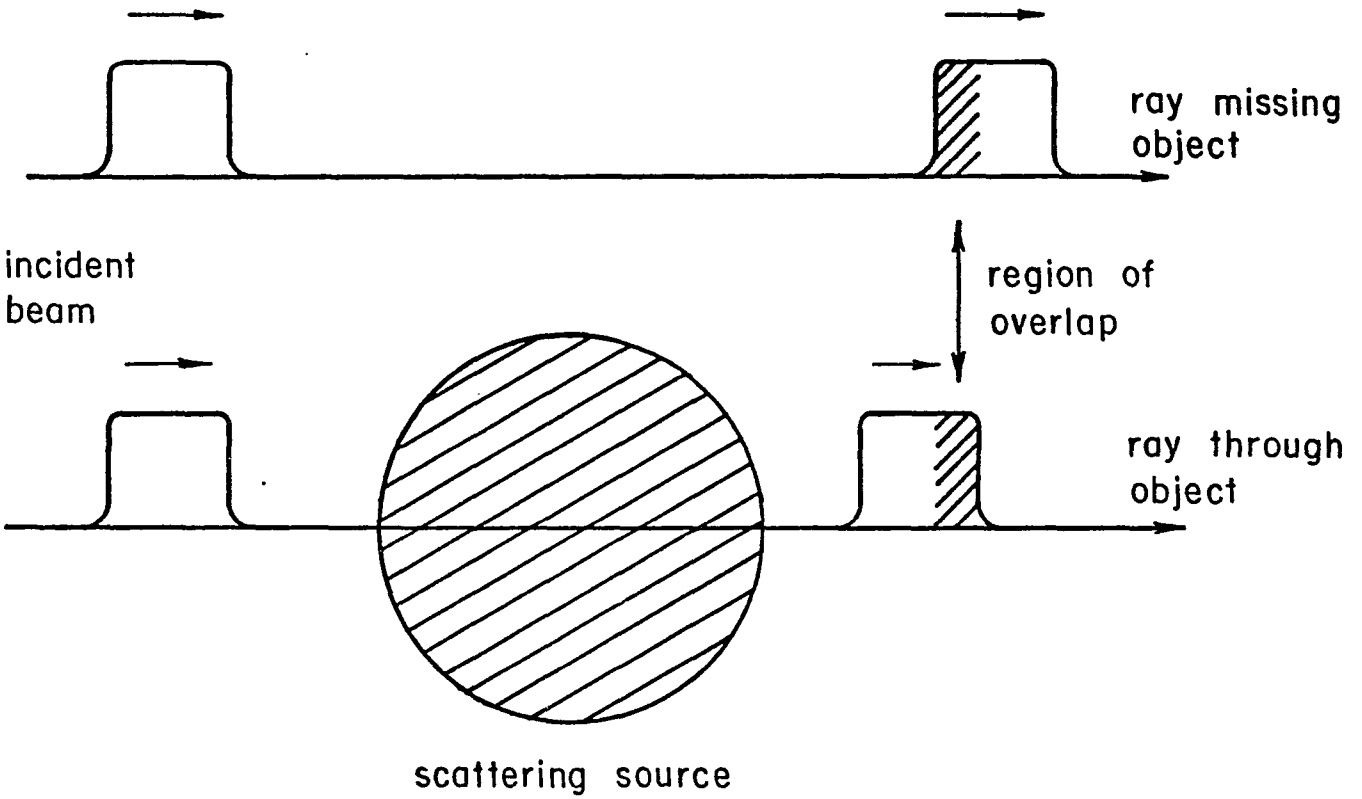

Fig. 4.1. Geometrical scattering model.

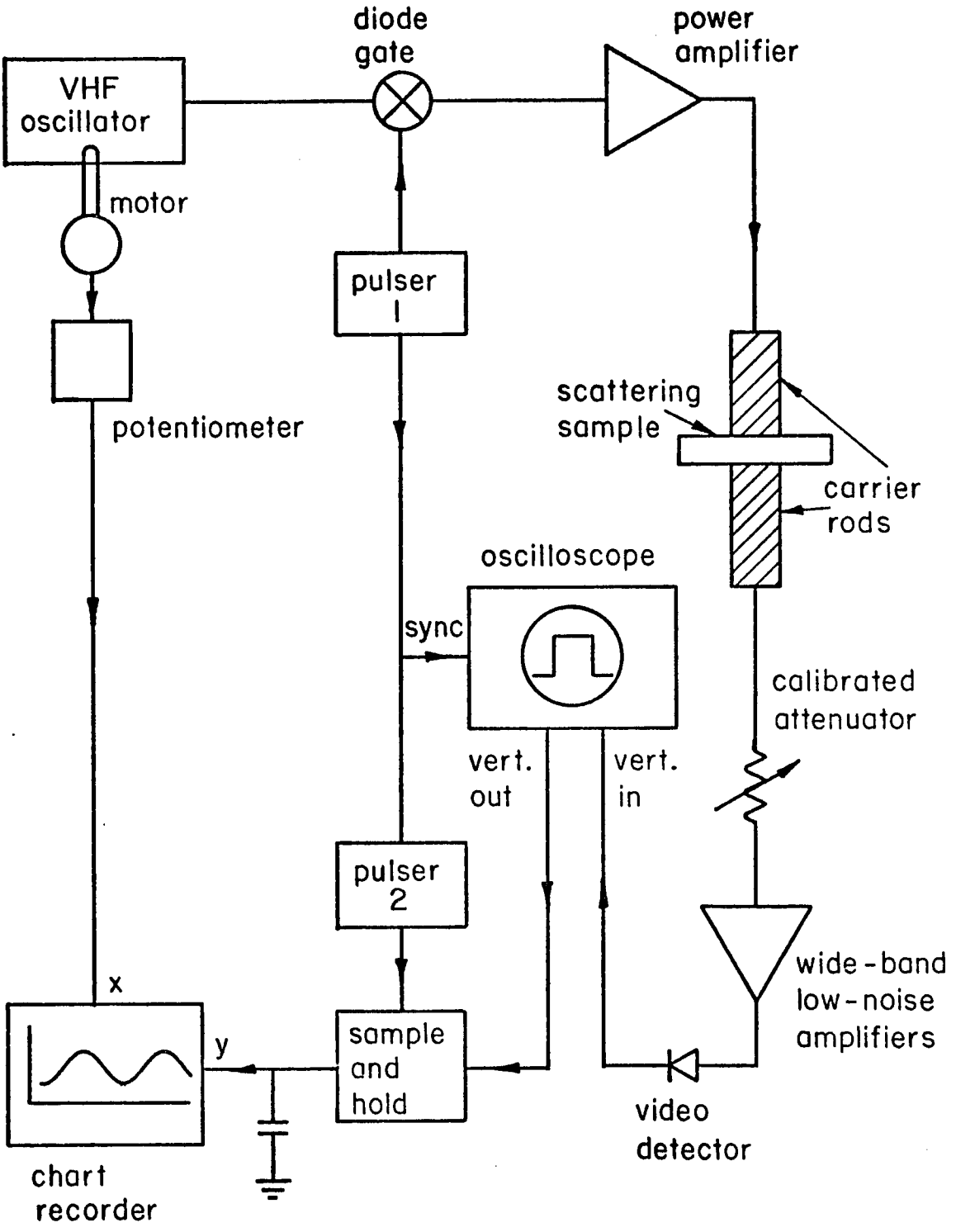

Fig. 4.2. Instrumentation schematic.

stage is a 5 watt power amplifier. The amplified pulse is then attenuated by 12 dB (now shown in Fig. 4.2) to protect the transducers.

The piezolectric transducers, illustrated in Fig. 4.3, were specially made by Itek Corporation, and their method of construction is proprietary. This much is known by the author: they are thin wafers of $LiNbO_3$ approximately 1.5 mm square, that have been gold-bonded onto the small ends of $LiNbO_3$ carrier rods of dimensions 10.2 mm x 10.2 mm x 20.3 mm. The cut of the transducer crystal is such as to be the most responsive to the generation of longitudinal waves and yet generate no transverse waves. The transducers are wideband with a center frequency response of 350 MHz are are acoustically impedance-matched to the carrier rods of $LiNbO_3$, whose purpose is to provide the interfacing between the ultrasonic waves and the scattering region. The sample holder is shown schematically in Fig. 4.3, and the entire transducer mounting is seen in the photograph in Fig. 4.4.

The transducer mounting shown in the photograph of Fig. 4.4 merits more discussion. The carrier rods are mounted vertically with the sample chamber or bath in between. The top rod has one vertical and two angular adjustments, and the bottom rod has two horizontal adjustments; thus, there are five degrees of freedom. For most cases, the

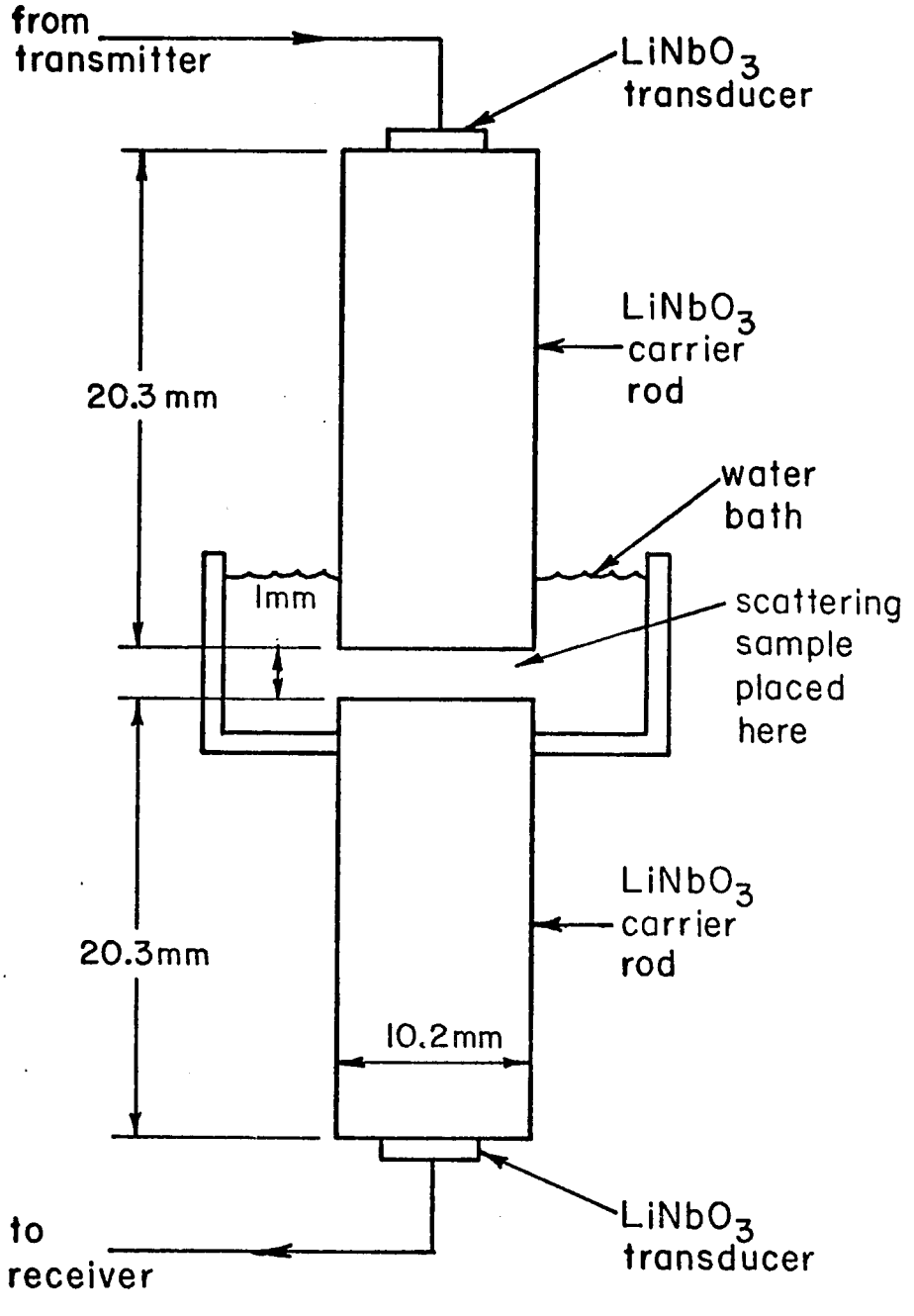

Fig. 4.3. Transducer configuration and sample chamber.

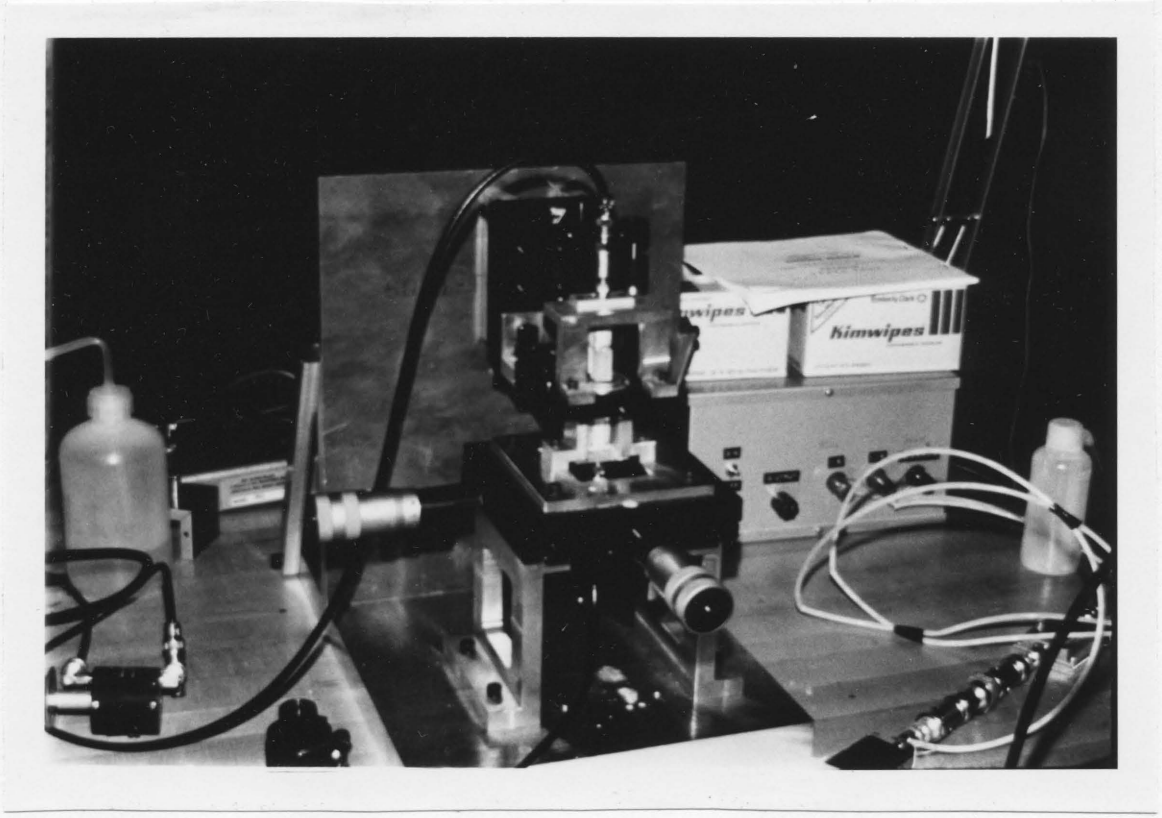

Fig. 4.4. Transducer mounting.

carrier rod separation was 1 mm. This value and the alignment of the rods will be discussed in the next section.

The forward-scattered ultrasonic wave, piezoelectrically transduced to an electrical pulse, proceeds to a calibrated attenuator. This attenuator, of range 110 dB in steps of 1 dB, keeps the to-be-amplified signal in the operating range of the low-noise amplifier. It also provides system calibration for data reduction. After the low-noise amplifier, the video detector takes the absolute-value-squared of the signal, which is then displayed on the oscilloscope. The pulse, now approximately 1 millivolt in magnitude, is amplified 100x by the oscilloscope and fed to the S/H. The sample pulse of the S/H is simultaneously displayed on the oscilloscope, thereby allowing one to visually choose the portion of the pulse to be sampled. The S/H, taking 15 nanoseconds to respond to the signal, averages the sampled voltage over about 100 nanoseconds. The sampled portion, held at a constant voltage, is recorded by the y-axis of the chart recorder. While the pulse is quickly traversing the prescribed path, an electric motor is slowly turning the mechanical frequency control on the VHF oscillator. Also connected to this motor is a simple potentiometer that provides a DC voltage to the x-axis of the chart recorder. Essentially, the chart recorder is now plotting received signal versus frequency

of that signal. Such a plot takes approximately thirty seconds. In practice, the VHF oscillator does not cover the full frequency range of 100 to 400 MHz on one scale, and at least three separate runs must be made.

Validity of Theoretical Model to Experiment

With the transducer and carrier rod dimensions in mind, one may consider the validity of the application of the theoretical model developed in Chapter 3. The expression for the forward scattered wave was derived from the assumption of plane wave illumination. Seki, Granato and Truell (1956) found that with an acoustic piston source of diameter 75 wavelengths, the radiated field normal to the axis of the transducer was a good approximation to a plane wave for ratios of the axial distance to piston diameter as small as 13. This is the approximate ratio of the carrier rod length to the $LiNbO_3$ transducer width. Seki et al. (1956) also found this plane wave approximation to be good over an angular subtense of 0.04 radians. Experiments in obscuring the transmitted beam with a 0.5 mm wire indicated that the primary region of pressure wave illumination in the water gap was an area approximately 1 mm^2. The ratio of 1 mm to 20.3 mm for the carrier rod length yields an angular subtense of approximately 0.05 radians. For a

frequency range of 100 to 400 MHz, the $LiNbO_3$[1] transducer was 23 to 91 wavelengths in diameter. Thus, to a good approximation the illuminating wave could be considered planar.

The asymptotic expression for the scattered field assumed $Kr >> 1$. For the frequency range of 100 to 400 MHz, the wavelength range in the $LiNbO_3$ carrier rods is 66 to 17 μ. If r is assumed to be 20.3 mm, the length of the receiver carrier rod, the asymptotic condition $Kr >> 1$ is easily satisfied.

In the expression, equation (3.59), for the forward-scattered wave, one assumes that there is no multiple particle scattering, that the scattering from N particles is a coherent sum of the scattering from each particle, and that the scattering amplitude Φ is completely determined from a measurement of $\Phi(\theta=0)$. The validity of the first assumption is discussed in Chapter 5. To test the validity of the last assumption, one determines the range of θ seen by the detector. An ultrasonic beam scattered from the scattering area, which is approximately 1 mm^2, will miss the receiver detector if $\theta > D/z$, where D is the detector diameter and z is the distance from the scattering region to the detector. From Fig. 4.3 and the previous section,

---

1. The compressional wave speed was that of the T_{11} stress wave, 6.6 x 10^6 mm/sec.

one has z = 20.3 mm and D = 1.5 mm. The upper limit of θ is therefore 0.074 radians, very close to θ=0.

Another measure of the validity of this assumption is to consider the detector illuminated by an angular spectrum of plane waves. If the angular spread θ of a plane wave is such that $\theta > \lambda/D$, then this wave will be phase cancelled over the detector face. The wavelength range in $LiNbO_3$ of 66 to 17μ yields a θ variation of 0.011 to 0.044 radians. If Φ is assumed to vary little over this range of θ, then the assumption of $\Phi(\theta=0)$ is indeed a valid one.

To check the coherent sum assumption, one may calculate the difference in the phase variation across the detector face for a scattering particle located at the center of scattering region versus a scattering particle located at the edge of the scattering region. For a one dimensional calculation with a scattering region of 1.5 mm, and with the assumption of Φ slowly varing across the detector surface, this phase variation difference is easily calculated to be approximately 0.9 radians. Thus, the waves do not cancel when superimposed on the detector face. If there is a significant variation in the scattering amplitude Φ across the detector, then one observes the average value of Φ.

For attenuation measurements, the assumptions of single particle scattering need not be considered. Seki et al. (1956) found that if two identical transducers are used in a coaxial source-detector mode, a diffraction attenuation of 1 dB results when the transducer separation is increased by a^2/λ, where a is the transducer radius. For the cell suspension measurements to be discussed in Chapter 5, the transducers were not actually moved, but the wavelength in $LiNbO_3$ was changed from approximately 4.4×10^{-3} to 1.9×10^{-3} centimeters (150 to 350 MHz). This corresponds to a a^2/λ range of 1.28 cm to 3.0 cm. Thus, a diffraction attenuation of 2 dB can result in this frequency range, and the attenuation values are slightly larger than they would be without this effect.

Experimental Parameters

In an actual experiment, various parameters must be considered and established. Some estimation or measure must be made of the accuracy of the measurement. This section deals with such topics.

Of great importance is the medium in which the scatterers are immersed. For convenience, its relatively low absorption, and biological application, the medium was basically water. Some of the biological samples were in suspensions of a nutrient saline, which to the ultrasound

could not be distinguished from water. The absorption of water has been well studied (Kinsler and Frey 1962; Hueter and Bolt 1966; Beyer and Letcher 1969). In the frequency range of interest, water is a classical fluid, which means that the value of the incident wave P_o at any distance z into the fluid is $P_o e^{-\alpha z}$, where the attenuation coefficient α varies as ν^2, with ν being the frequency of the wave. A more useful measure of α is in terms of measurable intensity I, and, from the above, $I = I_o e^{-2\alpha z}$. If the intensity level is expressed in decibles, then $10 \log_{10} \frac{I}{I_o} = -8.7\alpha z = -az$. The constant a is a measure of the spatial rate of decrease in intensity level. The references above give for the low-MHz (< 10 MHz) frequencies a range of $\frac{a}{\nu^2}$ of 2 to 3 x 10^{-4} dB/(mm MHz^2), for 1 atm and temperatures of 15° to 20°C. The experimental results from Chapter 5 give a value of $\frac{a}{\nu^2}$ of 2.44 x 10^{-4} dB/(mm MHz^2) for frequencies from 150 to 400 MHz. For this frequency range one has an attenuation of 6 to 39 dB/mm. This attenuation at higher frequencies mixed with the fall-off of the transducer sensitivity, centered at 350 MHz, greatly affects the detected signals at frequencies beyond 400 MHz. The entire analysis leads us to one conclusion, the smaller the water gap, the better.

At this point another parameter enters the picture. The incident pulse leaks strongly from the transducers and appears temporally in the detected signal. In particular,

a pulse seems to jump the first carrier rod, probably due to stray capacitance, and appears at the top surface of the second. Another pulse apparently jumps the water gap all together. To add to the misery, these pulses also multiply reflect inside the carrier rods. The pulse of interest, taking its proper path through carrier, water, and carrier, must be temporally fit between the above pulses, otherwise interference will occur. The water-gap transit time, small compared to the carrier-rod transit time, must be increased so that the pulses are separate.

Finally, the pulse width itself must be wide enough so as not to be distorted by the limiting time constants of the system, and to allow interference between the rays of the geometrical scattering model as seen in Fig. 4.1. The pulses previously described are shown schematically in Fig. 4.5. With all the above in mind, a pulse width of .6 μsec and a sample gap width of 1 mm was experimentally decided upon. Since the transit time through 1 mm of water is 1.5 μsec, there is adequate temporal separation of the spurious pulses.

Another temporal parameter to be defined was the placement of the S/H sample signal. Since most scattering media have a larger sound velocity than water, the pulse passing through the scatterer is received earlier than the unscattered pulse. This will be seen in photographs of

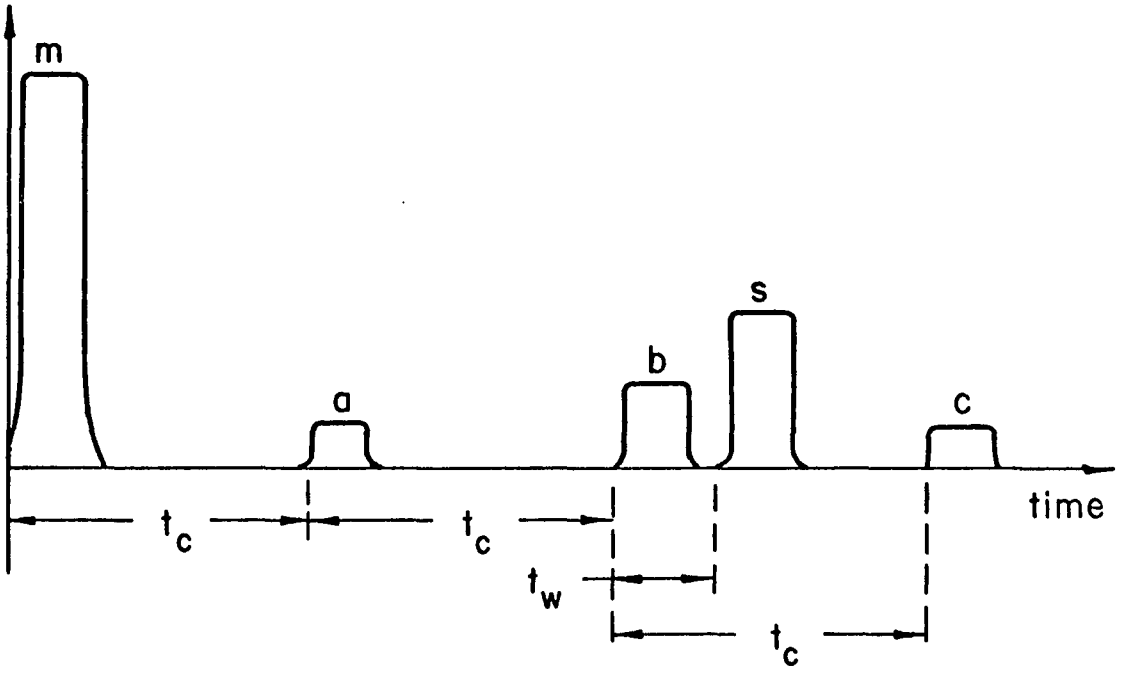

Fig. 4.5. Pulse position with time the horizontal axis. Pulse m is the main pulse. Pulses a, b, and c are leakage pulses. Pulse s is the signal pulse to be measured. The time intervals t_c and t_w are transit times for a carrier rod and the water gap.

pulses appearing in Chapter 5 and is shown schematically in Fig. 4.1. If the scattered wave is of small amplitude, it is best to position the S/H sample signal at the front of the unscattered pulse, since this is the most likely place for the scattered and unscattered waves to temporally overlap, thereby detecting all interference phenomena that occur.

There are many nonlinearities in the system, from amplification to transducer response. To eliminate them, signals of equal magnitude were compared with each other. For example, a scattered signal would be recorded by the detector with a certain calibrated attenuator reading. The same signal magnitude at the detector would be produced with only water in sample chamber and the attenuator reading would be recorded. The attenuation would be the difference between the above readings. Therefore, all attenuation values for nonresonant scattering media are relative to the attenuation of water at that frequency. For large resonant scattering, only the resonant structure is of interest.

Experimentally, it was observed that all water attenuation measurements could be reproduced to well within ± 1 dB. Therefore, all measurements are assumed accurate to within this range. The accuracy of measurement can be estimated from the water attenuation measurements described

in Chapter 5. The measured value for $\frac{a}{\nu^2}$ was 2.44×10^{-4} dB/(mm MHz^2). The author was unable to find attenuation values in the frequency range of 100 to 400 MHz. However, this value extrapolated to the lower MHz frequencies gives good agreement with the literature. See the values quoted earlier in this section.

Sample Preparation and Handling

For physical objects such as Crofon fibers, several scattering objects would be placed in the sample chamber; for a single object the scattered signal was too small for measurement. The surrounding media for all physical samples was water, always at room temperature.

For biological cell suspensions, it was found that large concentration of cells, on the order of 200 million cells per milliliter, were necessary to observe any attenuation in the received pulse. Such concentrations could violate the single-scatterer approximation previously discussed. Further consideration will be given to this in Chapter 6. All cells suspensions were at room temperature. No attempt was made to monitor the temperature of the cell suspensions.

CHAPTER 5

MEASUREMENTS AND ANALYSIS

This chapter presents the results of the experiment described in the previous chapter. The first section describes the measurement of the absorption of ultrasound in water in the frequency range of 150 to 400 MHz, and establishes the accuracy of the scattering results. The next section is concerned with the scattering from physical objects, such as Crofon fibers, and gives experimental evidence for the geometrical scattering model discussed in Chapter 4. The third section describes the scattering from cell suspensions. The data here indicates no resonant structure.

Ultrasound Attenuation in Water

In this experiment, ultrasound attenuation in water was measured at four frequencies using the calibrated attenuator and the procedure described in Chapter 4. The output signal level was always brought back to its same magnitude using the calibrated attenuator. By varying the water-gap separation, a plot of attenuation in dB versus distance in mm can be constructed for frequency. The slope of the best fit straight line through this data, shown in Fig. 5.1, is

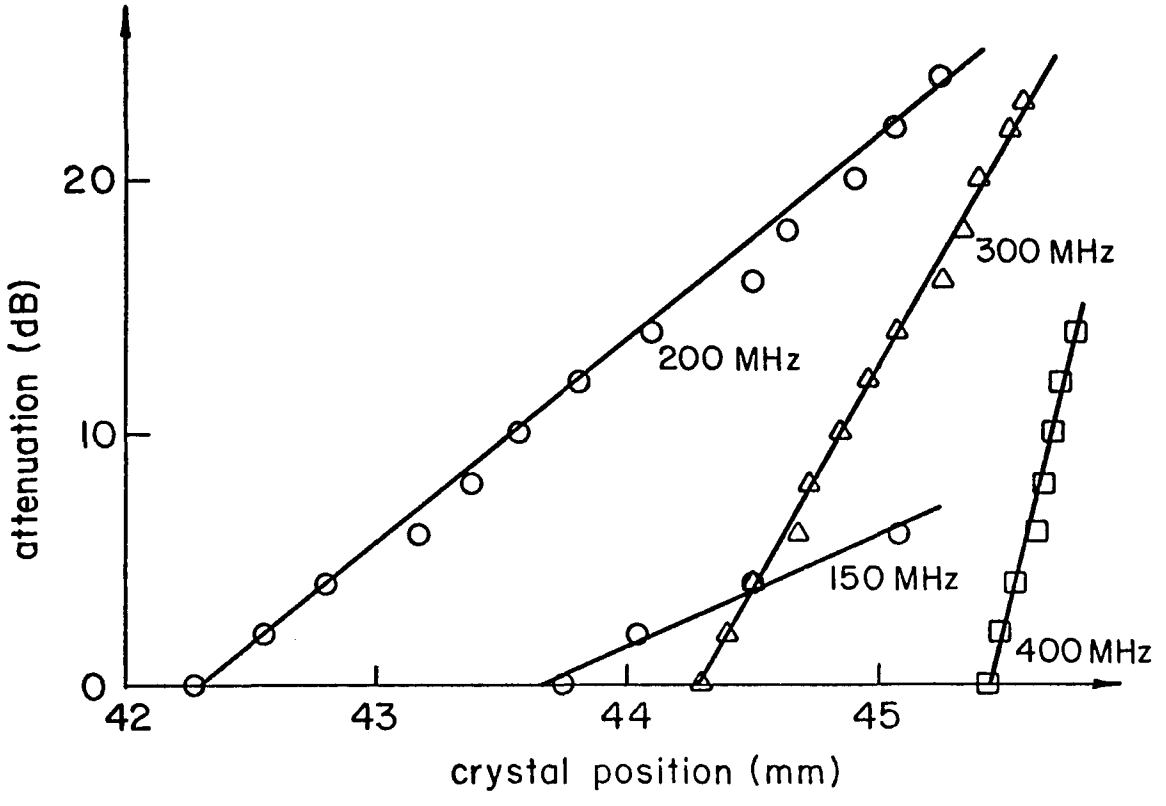

Fig. 5.1 Attenuation of ultrasound in water for different crystal (carrier rod) positions for different frequencies.

the attenuation coefficient a, discussed in Chapter 4. For a/ν^2, one determines the slope of the a values plotted against their respective frequencies squared. This data is shown in Fig. 5.2. The slope of the straight line is 2.44×10^{-4} dB/(mm MHz^2). This value, extrapolated to the lower megahertz frequency range, agrees quite favorably with values found in the literature. Kinsler and Frey (1962) for 15°C, report $a/\nu^2 = 2.4 \times 10^{-4}$ dB/(mm MHz^2), and

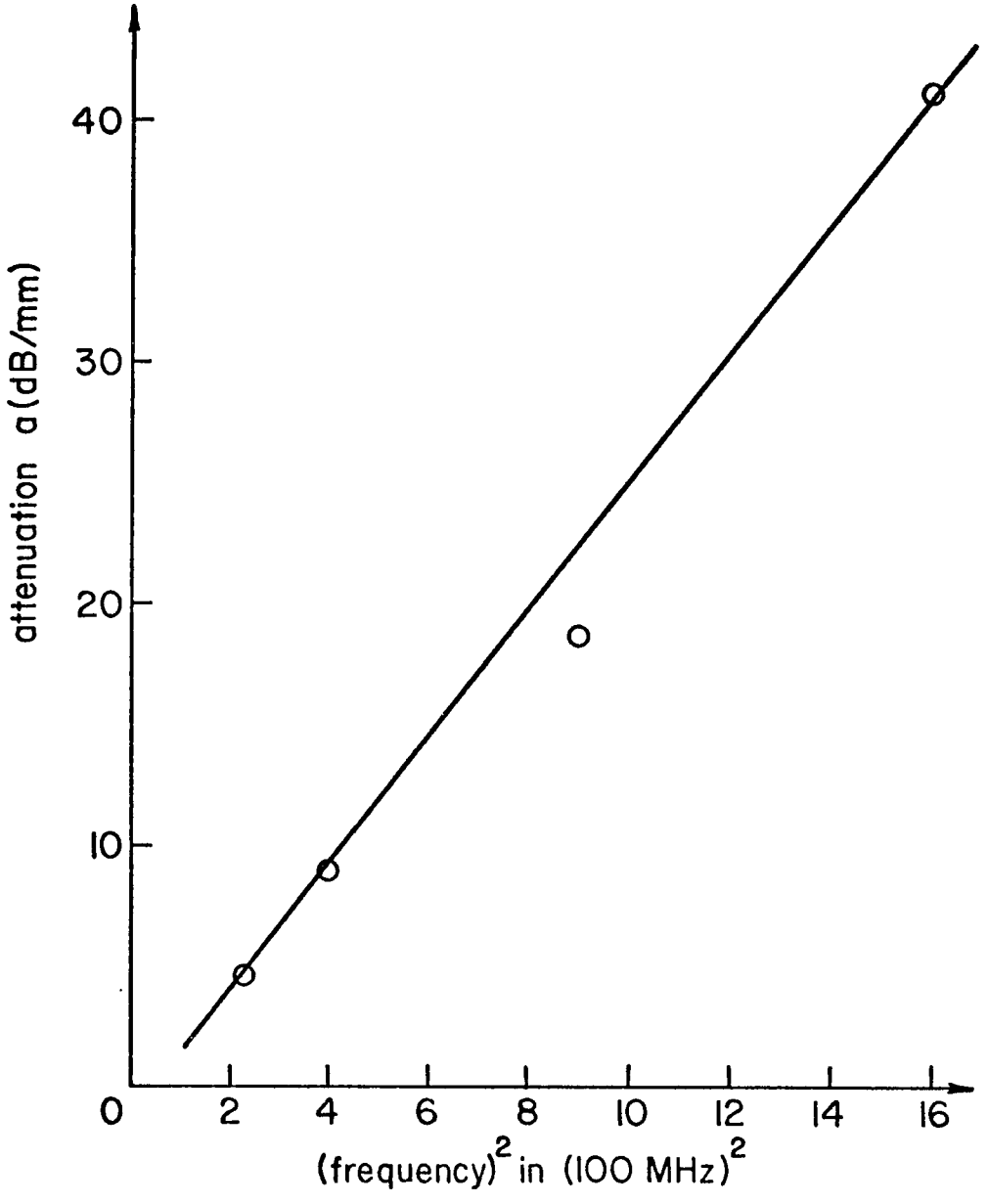

Fig. 5.2. Water attenuation in dB/mm for the ultrasound frequencies of Fig. 5.1.

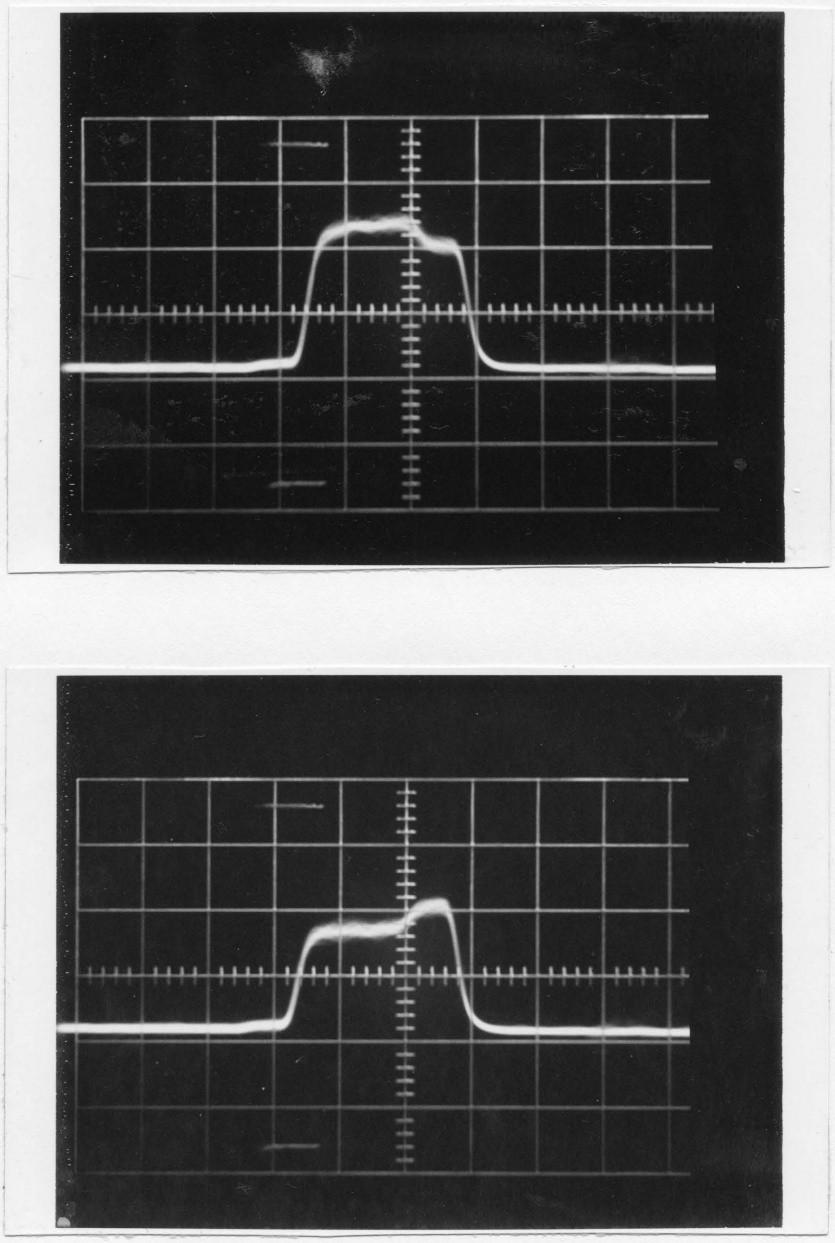

Fig. 5.3. Oscilloscope traces of the received pulse for slightly different frequencies for a 470μ Crofon fiber.

Hueter (1966) for 20°C gives the value of $\alpha/\nu^2 = 2.2\text{x}10^{-4}$ dB/(mm MHz^2). To the author's knowledge, these are the first attenuation measurements of water in this frequency regime. Diffraction attenuation for these measurements are negligible since the least a^2/λ distance is 1.28 cm (see Chapter 4) and the greatest distance traversed is 3 mm, which means the diffraction attenuation is less than 1 dB. However, for such a small a^2/λ distance, there is some fluctuation in the diffraction attenuation though of magnitude much less than 1 dB (Seki, et at., 1956). This could account for some of the fluctuation seen in the data in Fig. 5.1.

Ultrasound Scattering from Physical Objects

This section concerns itself with many experiments. The first is the scattering from Crofon fibers. Several of these fibers were aligned collinearly in the sample chamber. The fibers were then irradiated by ultrasound. Shown at the top of Fig. 5.3 is a photograph of the detected pulse as seen by the oscilloscope. At the bottom is the same pulse with the frequency slightly changed. Note the interference effect at the front of the pulse and the steady value of the pulse at the tailing edge. Closer inspection reveals a small constant pulse preceding the obvious pulse. This can be interpreted using the geometrical model shown

in Fig. 4.1 as part of the pulse that passes through the Crofon while the larger pulse is the one that misses the Crofon. The photographs of Fig. 5.3 show the interference effect of these two pulses. The pulse width is 0.5 μsec and each horizontal block is 0.2 μsec. From the photographs the unscattered pulse lags the scattered pulse by approximately 1.5 μsec. It is interesting to compare this value with the one predicted by the geometrical mode. Let the fiber diameter be d, the velocity of sound in Crofon be c_c and in water be c_w. The time lag between a pulse passing through equal distances d in Crofon and water is $\Delta t = d/c_w - d/c_c$. For d = 470μ, $c_c = 2.65 \times 10^6$ mm/sec,[1] $c_w = 1.48 \times 10^6$ mm/sec (Kinsler and Frey, 1962), one has Δt = 1.58 μsec. If one uses the value of c_c derived from the resonant curves to be discussed below, Δt = 1.55 μsec. Both values are in excellent agreement with the photographs.

If the S/H is positioned to sample at the interfering portion of the detected signal, then a plot of this signal versus frequencies can be made on the chart recorder. Such curves are shown in Fig. 5.4 and 5.5 for Crofon diameters of 470μ and 265μ. From these figures it is easy to measure the difference $\Delta\nu$ between frequency resonances.

---

1. This value of c_c is the speed of a longitudinal wave in lucite (Kinsler and Frey, 1962). According to E. I. duPont de Nemours and Co., Crofon is made of lucite.

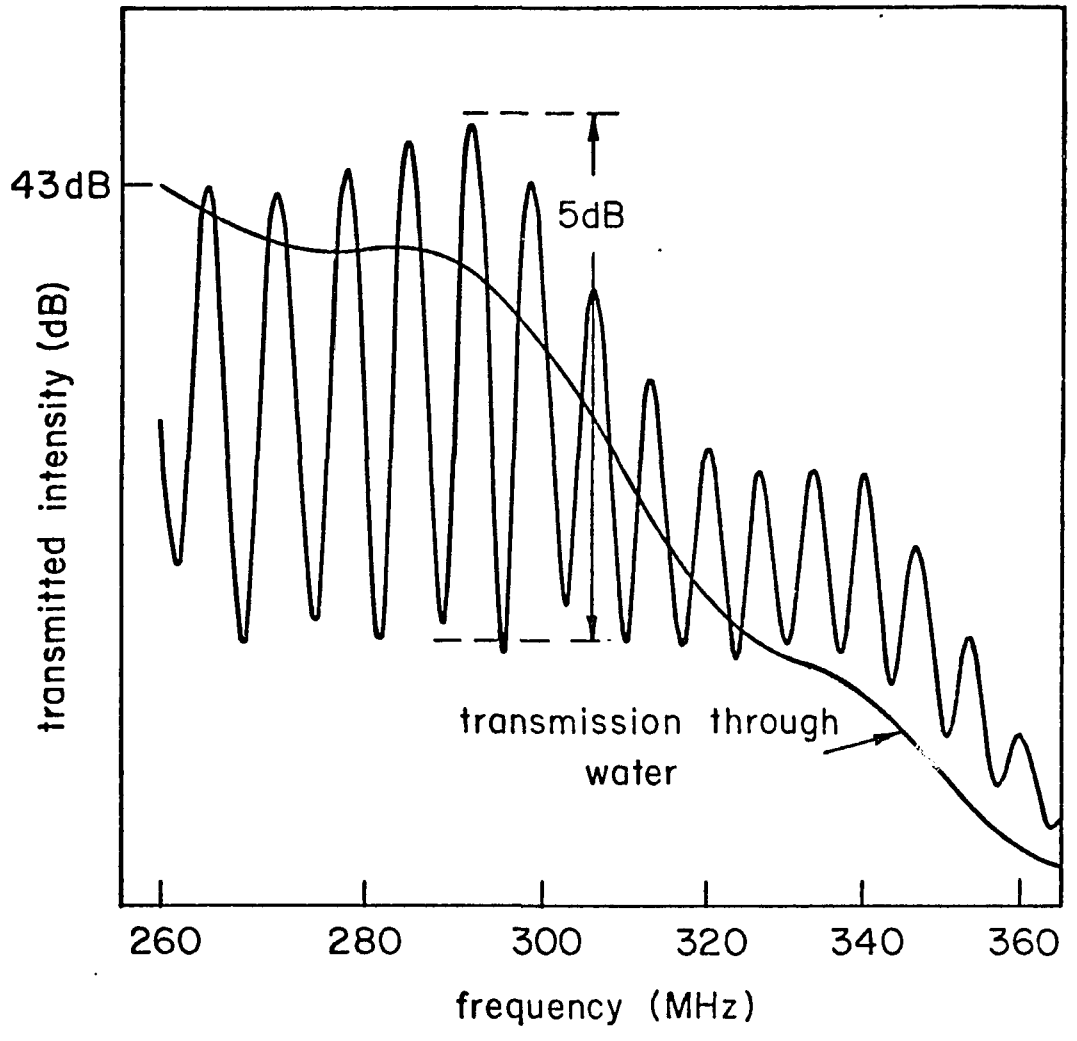

Fig. 5.4. Chart recorder plot of forward-scattered signal from 470 μ diameter Crofon fiber. The data is unnormalized. The signal fall-off and fluctuation is due to, respectively, water absorption and system nonlinearities.

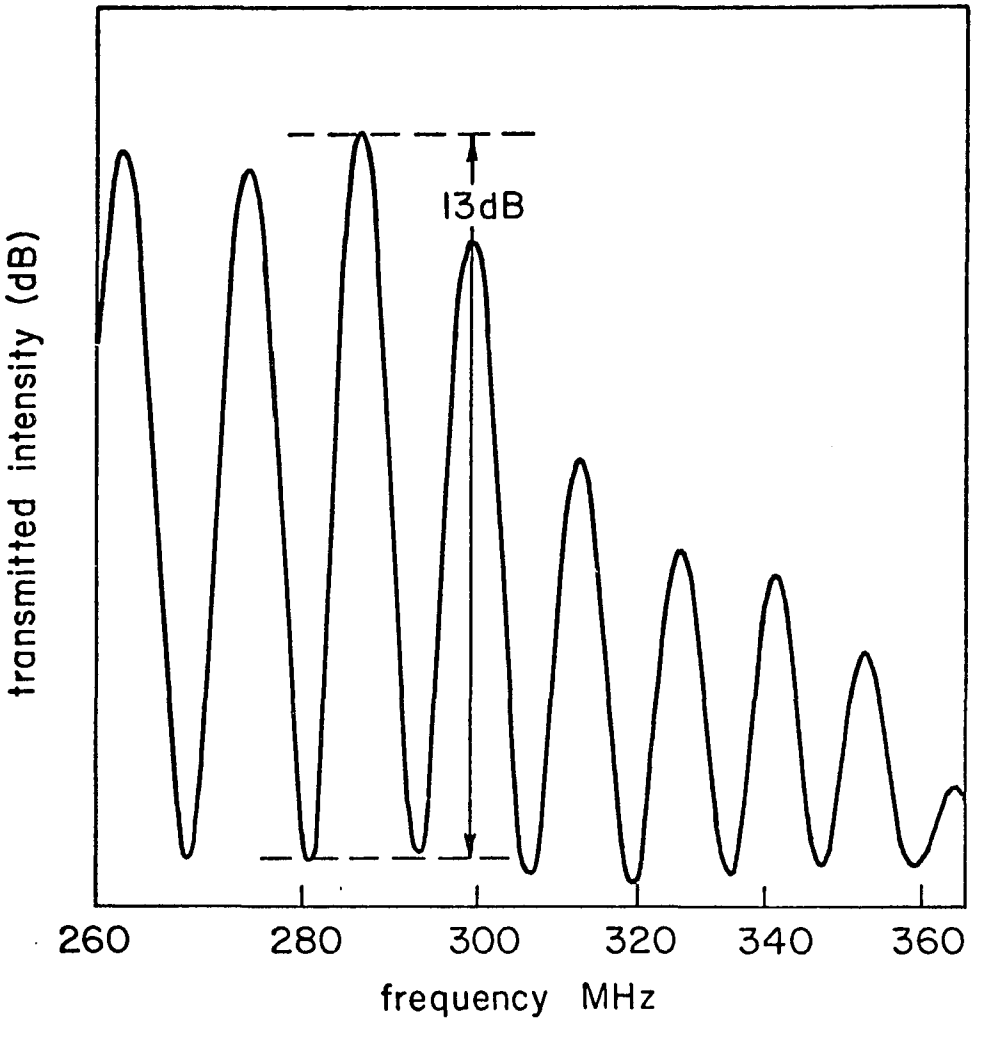

Fig. 5.5. Chart recorder plot of forward-scattered signal from 265 μ diameter Crofon fiber.

For the 470μ and 265μ diameter Crofon, the average measured $\Delta\nu$ is 7.03 MHz and 12.6 MHz, respectively. From the Mie theory developed in Chapter 3 and extended to cylinders in Appendix B, the spacing between resonances in the forward-scattered radiation is the same as the separation in Q_t or the total scattered power. For large size parameters, this resonant spacing assumes a simple form and, from Appendix B, is the same form for both spheres and cylinders. From the definition of x, $x = Kb = 2\pi b\nu/c$ where c is the surrounding medium and b is the radius of the scatterer. For frequencies of 100 to 400 MHz and the two radii of the Crofon fibers, x varies from 100 to 800. Thus, one does have large size parameters, and the resonant separation Δx is from equation (3.56)

$$\Delta x = \frac{\pi}{1 - c_w/c_c} . \tag{5.1}$$

From the definition of x,

$$\Delta x = b\Delta K = \frac{2\pi b}{c_w} \Delta\nu \tag{5.2}$$

since b, the radius of the cylinder, is constant and the speed of sound in x is always the speed of the medium surrounding the scatterer. Combined, equations (5.1) and (5.2) yield

$$\Delta\nu = \frac{1}{2b}\left(\frac{1}{c_w} - \frac{1}{c_c}\right)^{-1} . \qquad (5.3)$$

For the values of c_w and c_c in the previous paragraph, the calculated separation of resonances is

$$\Delta\nu = 7.13 \text{ MHz, } 470\mu \text{ fiber diameter,}$$
$$\Delta\nu = 12.4 \text{ MHz, } 270\mu \text{ fiber diameter.}$$

For each case, the worst error is approximately 2%. If equation (5.3) is used to calculate c_c for the measured $\Delta\nu$'s, c_c equals $2.68\text{x}10^6$ mm/sec for the 470μ diameter and $2.66\text{x}10^6$ mm/sec for the 270μ diameter. These values of c_c, calculated from the measured $\Delta\nu$'s and the well-known value of c_w, are in excellent agreement with the reported speed of sound for lucite. Thus, $\Delta\nu$ is quite sensitive to small variations in the Crofon sound velocity c_c. These results are further discussed in Chapter 6.

Another scattering object investigated was sapphire spheres. Shown in Fig. 5.6 is forward-scattered radiation versus frequency for sapphire spheres 600μ in diameter. Note that the resonances are not nearly as prominent as those of the Crofon fibers. The average $\Delta\nu$ was measured to be 4.19 MHz. Sapphire is acoustically anisotropic, but if the average of the longitudinal velocities is chosen, c_L = $10.5\text{x}10^6$ mm/sec, the calculated resonant separation from

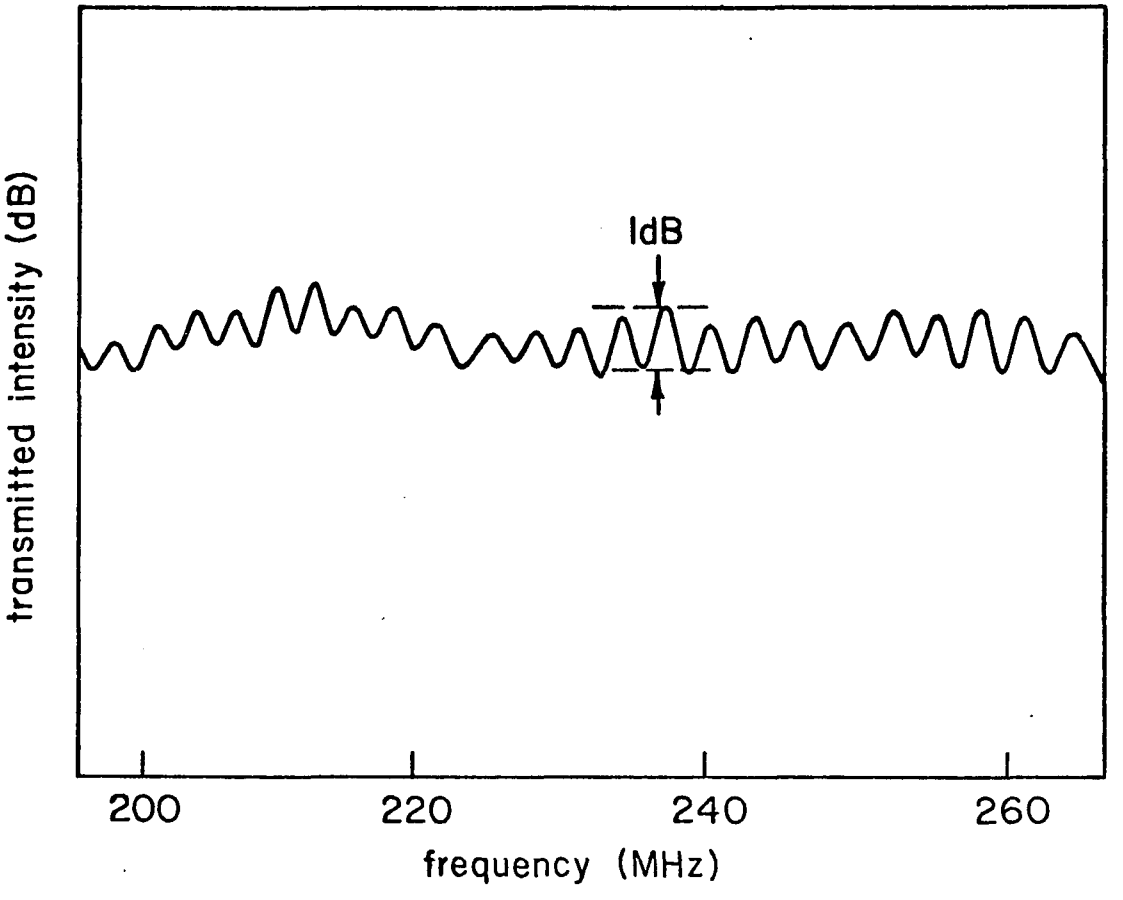

Fig. 5.6. Chart recorder plot of forward-scattered signal from 600 μ diameter sapphire spheres.

equation (5.3) is 2.87 MHz. The percent error between the measured and calculated $\Delta\nu$ is very large, -50%. In Fig. 5.7, one sees the resonant structure in the forward-scattered radiation from spheres 800μ in diameter. The average measured $\Delta\nu$ is 3.02 MHz; the calculated $\Delta\nu$ is 2.15 MHz. Again, a large percent error. Possible explanations for this discrepancy are discussed in Chapter 6.

In Fig. 5.8, one sees an entirely different type of resonance. A sheet of 140μ thick glass was placed in the water gap. Since the glass completely filled the water gap, there was no unscattered wave. In fact, the resonances here are completely due to a Fabry-Perot type phenomenon, the interference between the transmitted and internally reflected waves. The measured $\Delta\nu$ is 20.1 MHz. To calculate the resonant spacing one uses the optical cavity expression $\Delta\nu = 2d/c_g$ where d is the spacing and c_g the bulk speed of glass. For $c_g = 5.6\text{x}10^6$ mm/sec, $\Delta\nu = 20.0$ MHz. The agreement is excellent.

Though no figures are shown, it was very easy to obtain the same resonant effect with only the water gap as a cavity. Let d be the water gap separation. Then for $d = 1$ mm, $\Delta\nu = 2d/c_w = 1.33$ MHz. But these resonances were not observed in the data because they were carefully avoided by using short pulses. The temporal separation between two of these pulses for $d = 1$ mm is $\Delta t = 2d/c_w = 1.33$ μsec.

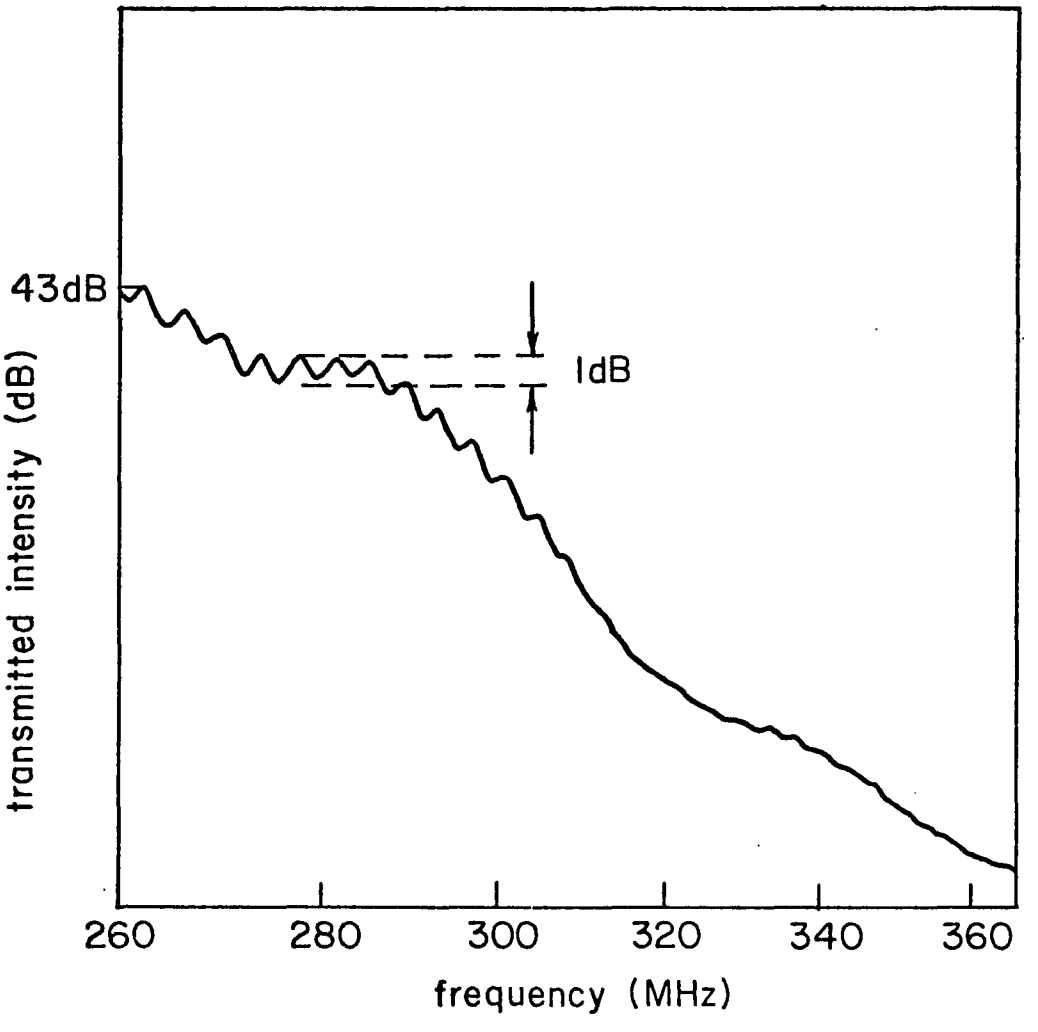

Fig. 5.7. Chart recorder plot for 800 μ diameter sapphire spheres.

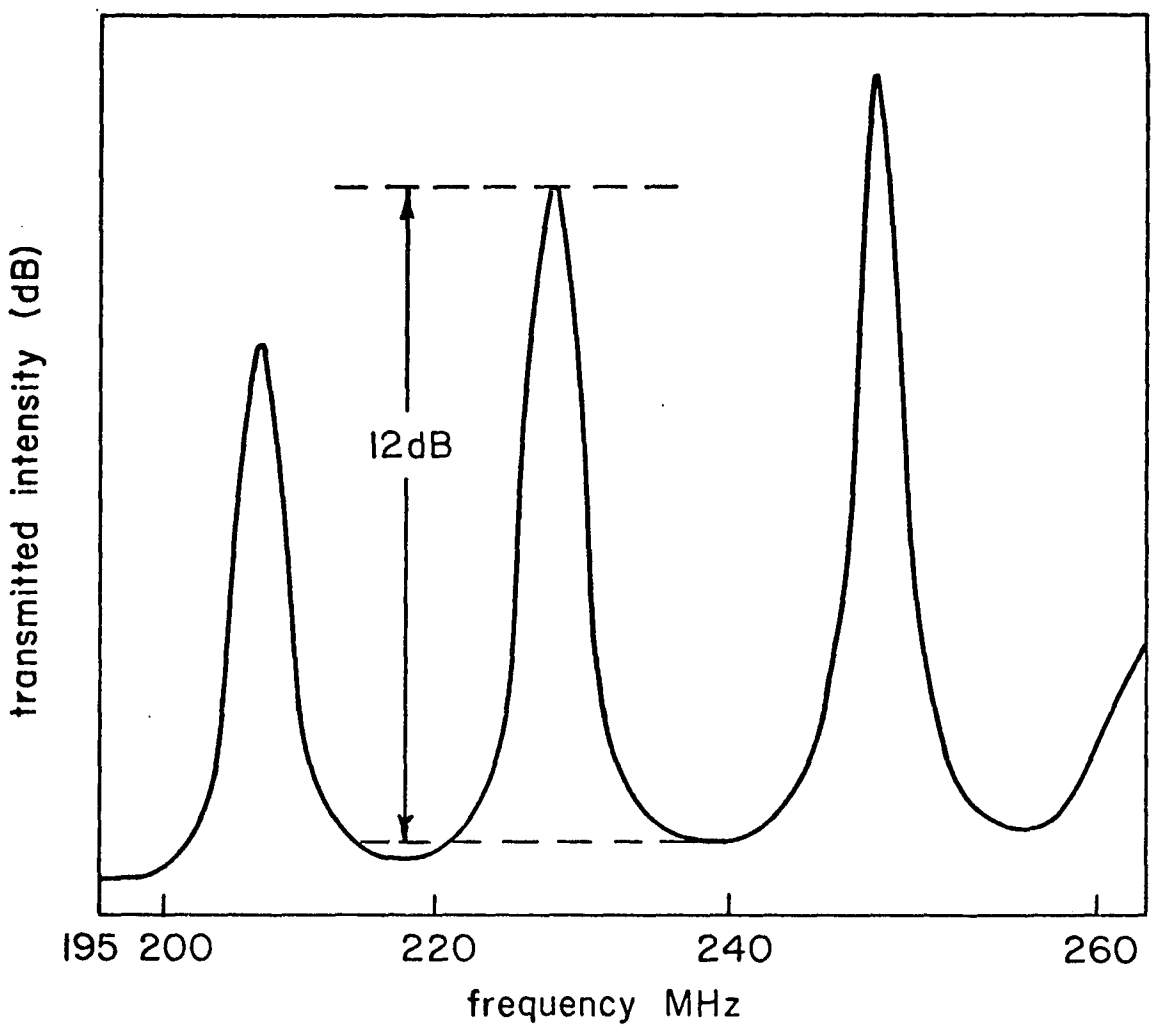

Fig. 5.8. Chart recorder plot of signal transmitted through 140 μ thick glass cover slide.

With a pulse width of .6 μsec, there could be no pulse overlap and, consequently, no interference due to the water gap.

To get some idea of cell modeling, suspensions of latex spheres were investigated. Immediately, problems arose. After a trial-and-error adjustment of concentration, the resonant curves proved to be irreproducible, and varied significantly not only between different trials, but also within a given trial. The 11.9μ latex spheres proved more manageable. Shown in Fig. 5.9 is graph of attenuation versus frequency for these spheres. A slight resonant structure is apparent. Data below 150 MHz have been ignored because of leakage of higher harmonics from the VHF oscillator to the detector. For this reason, all subsequent attenuation curves will be plotted for frequencies higher than 150 MHz. This apparent resonant structure is too broad for measurement. If one calculates the appropriate $\Delta\nu$ for an ultrasound speed of 2.32×10^6 mm/sec,[1] the resonance spacing is 172 MHz, which is near the experimental frequency range of the system. Therefore, the possible resonance seen in Fig. 5.9 is theoretically reasonable.

---

1. This value for the speed of ultrasound in latex was given by Dow Chemical Co.

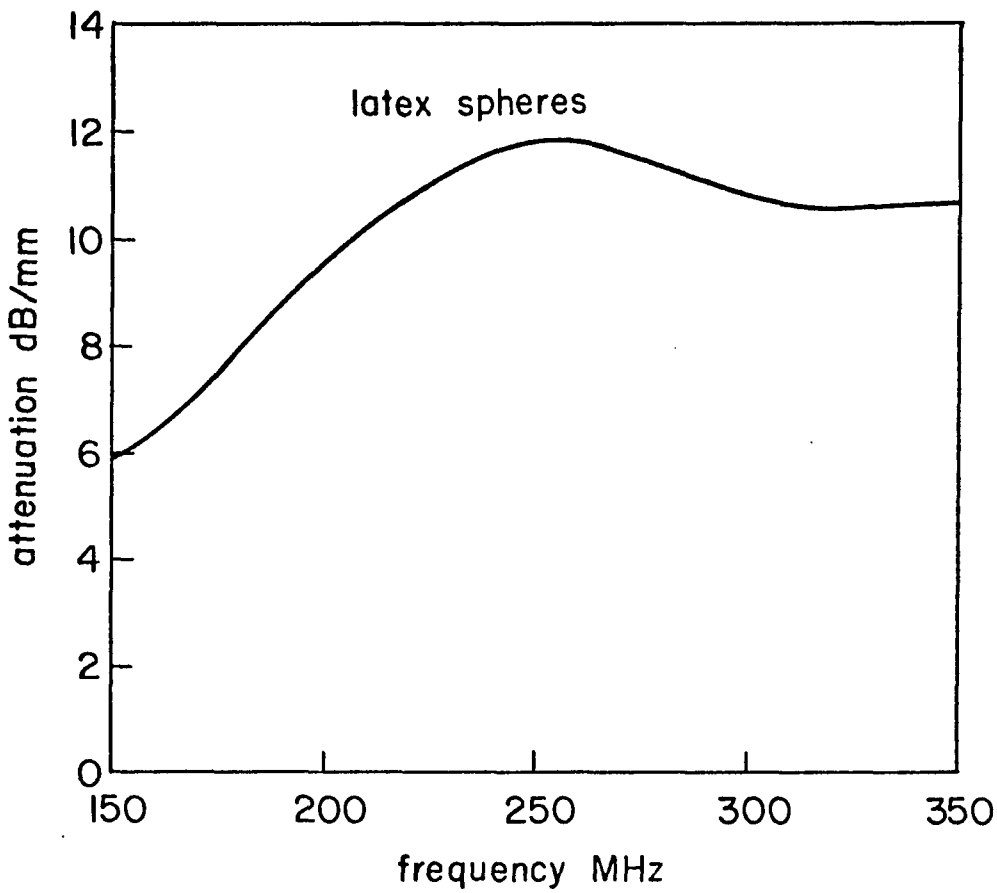

Fig. 5.9. Attenuation in dB/mm for 11.9 μ diameter latex spheres.

This completes the data analysis for scattering from physical objects. In some cases, resonances did occur. The next topic concerns forward scattering from biological suspensions.

Scattering from Biological Specimens

The data presented in this section are only from the scattering of cell suspensions. Attempts at measuring scattering from slabs of tissue proved unsuccessful. The tissue samples must be in contact with the carrier rod surfaces. Otherwise, variations in the surface shape can cause spurious scattering resonances. There can also be resonances due to the water, or more specifically saline, gap between one carrier rod and the tissue specimen surface. With the tissue specimen completely filling the gap between the carrier rods, the signal was often too small to detect. In the process of discovering these effects, tissues examined were fresh mouse liver, spleen, and red and white muscle. Also investigated were rat tumors and glycerated muscle. All specimens presented the above problems.

On the other hand, cell suspensions present none of the interfacing problems. After discovering that large concentrations were necessary in order that an attenuated signal could be observed, attenuation data were collected. Because of the large cell concentrations, the transmitted

signal at frequencies beyond 350 MHz was greatly reduced. As a consequence, all attenuation measurements for cell suspensions cease at 350 MHz. However, no obvious resonant structure was observed for any of the cell suspensions. Shown in Fig. 5.10 is the ultrasound attenuation of mouse leukemia cells at different cell growth phases. For two curves, as noted, the cells are in a plateau stage or in a growth stage. The cells were synchronized so as to be in a growth or non-growth phase. The plateau stage is the phase immediately following a growth stage. The remaining curve of Fig. 5.10 shows another specimen of the same cells in a growth phase 6 hours later. To within the accuracy of measurement and the variation in cell concentration, there is no apparent difference ultrasonically between these cell phases.

In search for resonances other cells suspensions were investigated. Shown in Figs. 5.11 and 5.12 are attenuation curves for the cell lines denoted as *RT1*, *CHO*, and *B77*. These are, respectively, rat tumor cells, chinese hamster ovary cells, and virus-transformed rat tumor cells. All of these curves plus those of Fig. 5.10 show a relatively linear dependence of attenuation in dB/mm on frequency, which is the same frequency dependence exhibited by tissues in the low megahertz range, (Wells 1977, Dunn and O'Brien, Jr. 1978). Thus, as ultrasound absorbers, cell suspensions

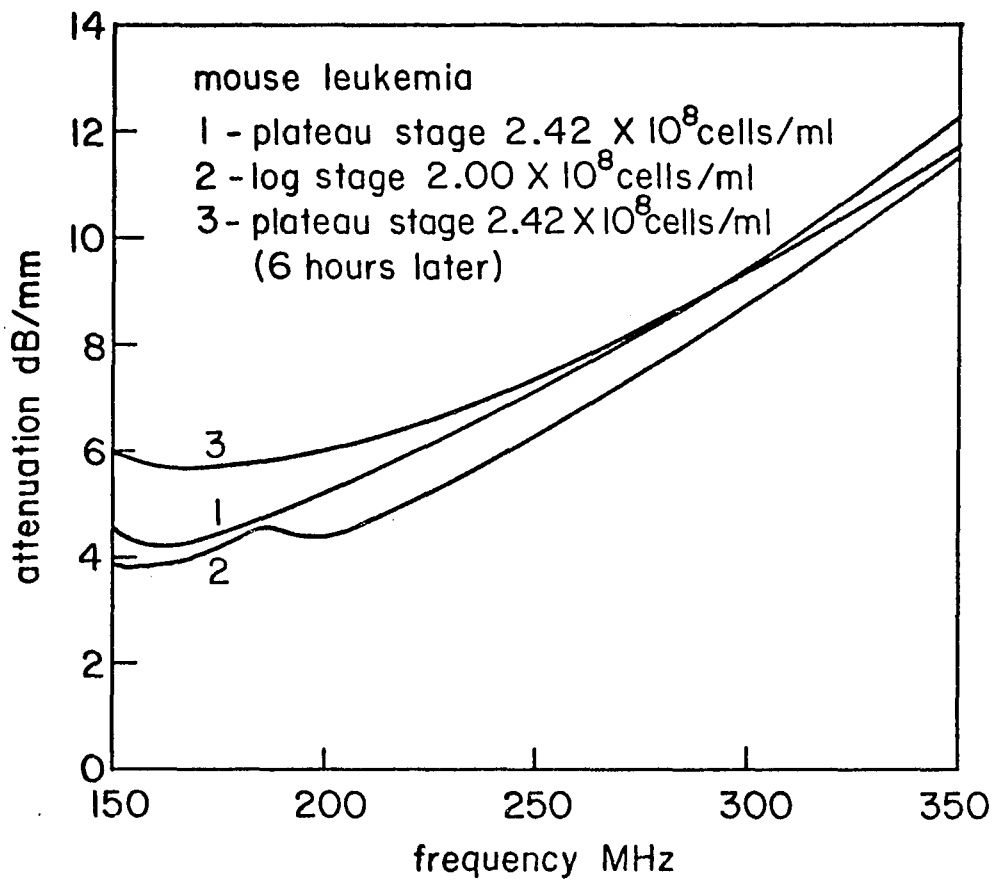

Fig. 5.10. Attenuation in dB/mm for mouse leukemia cell suspensions for different cell growth phases.

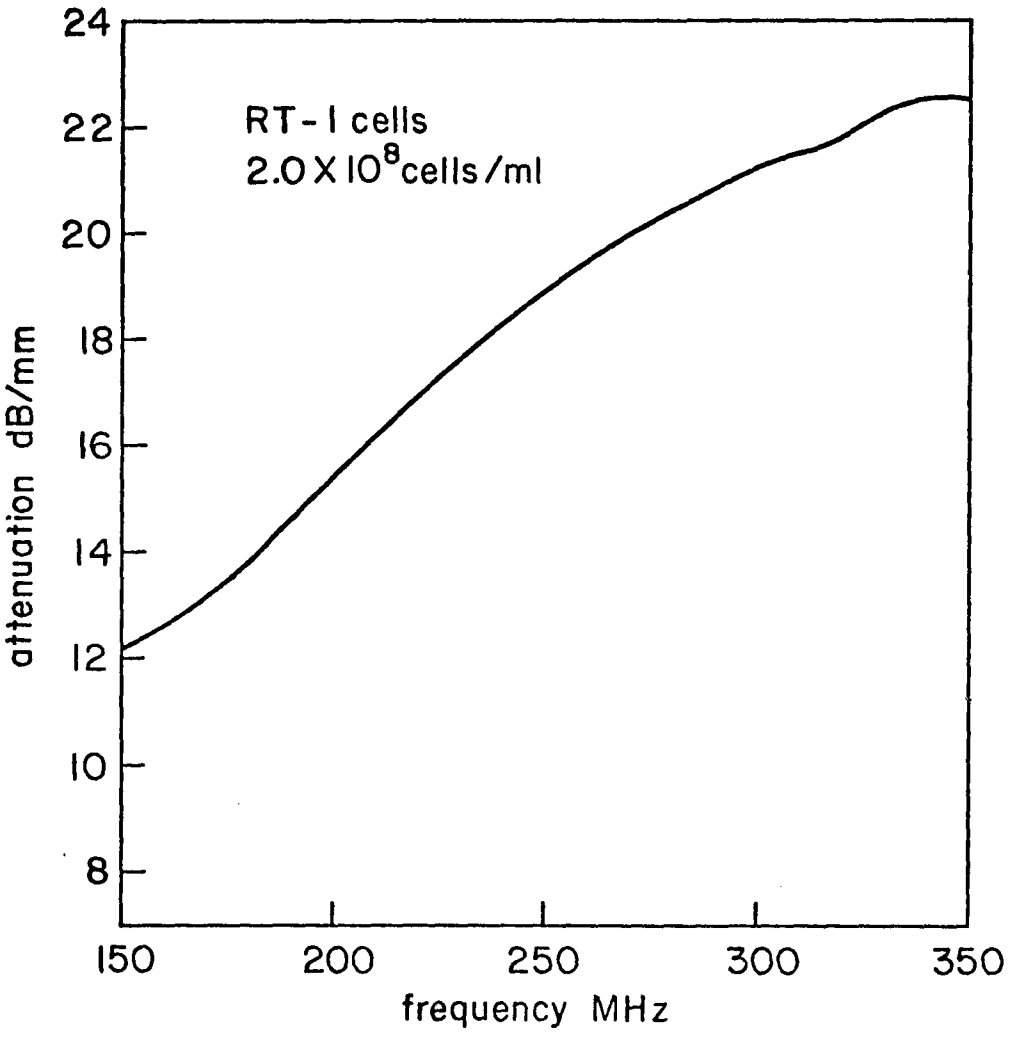

Fig. 5.11. Attenuation in dB/mm for a rat tumor cell suspension.

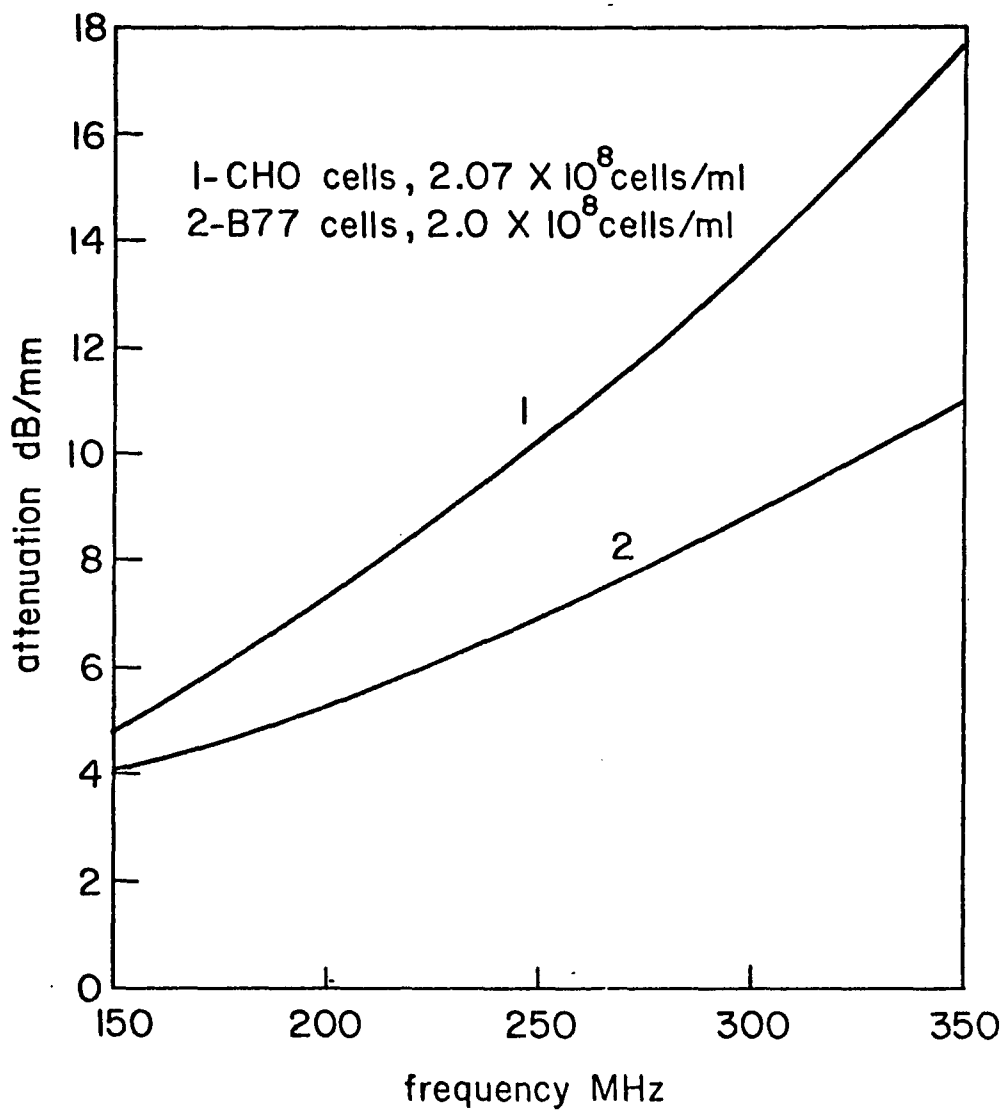

Fig. 5.12. Attenuation in dB/mm for chinese hamster ovary (*CHO*) and virus transformed rat tumor (*B77*) cell suspensions.

behave more like tissue than a classical fluid, such as water, which has a frequency-squared dependence. Also note that the virus-transformed cells have a significantly lower attenuation than the untransformed cells. Photographs comparing these two cells can be seen in Fig. 5.13.

The mean cell volume (MCV) for these cells was approximately $1000\mu^3$. For a concentration of 200 million cells per ml, these cells were packed extremely close together. For such concentrations, what is the value of the optical distance G defined in equation (3.51)? Recall $G \approx \rho_d \sigma_t L$. Let L be the width of the water gap, 1 mm. From the cell concentrations previously given, the particle density ρ_d is $2\text{x}10^5$ cells/mm^3. Assume that the scattering cross-section σ_t is approximately twice the projected area of cell. For a MCV of $1000\mu^3$, this would be $200\mu^2$ or $2\text{x}10^{-4}$ mm^2. For these numbers, G is 40, much greater than 1. Such a situation easily violates the condition for a single particle scattering model described in equation (3.51) and invalidates the expression derived for scattering in the forward direction.

Shown in Fig. 5.14 are the attenuation curves for melanoma. The different curves represent cells with and without melanin, the purple-brown colored pigment known to be correlated with skin cancer. Surprisingly, the cells without melanin have a measurably greater absorption.

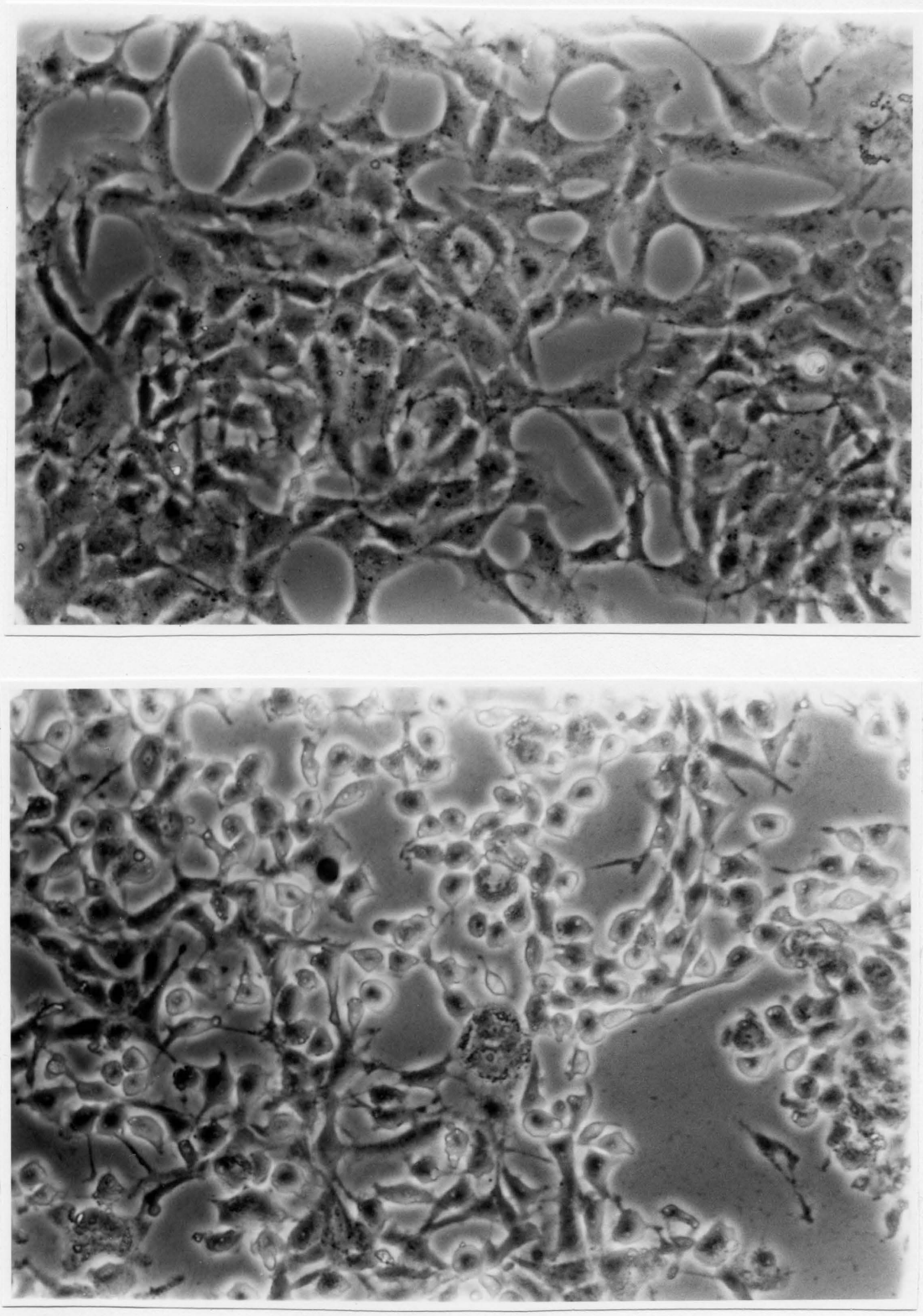

Fig. 5.13. Rat tumor cells (top), virus-transformed rat tumor cells (bottom).

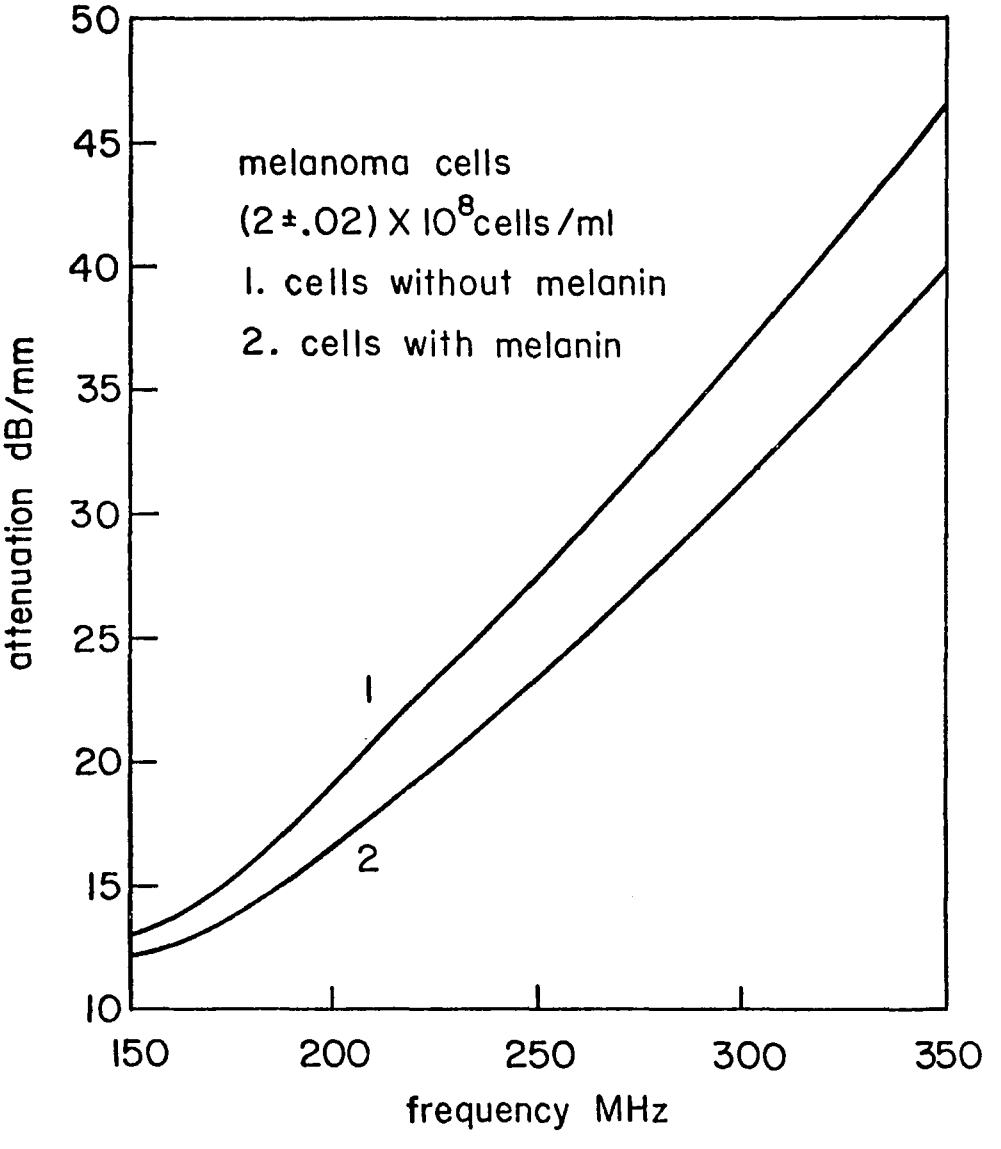

Fig. 5.14. Attenuation in dB/mm for melanoma cell suspensions with and without melanin.

This could be due to the variation in concentration of the cell suspensions. The absorption here, however, is much greater than that observed for previous cell suspensions of comparable concentrations. The dependence on frequency is still linear. These cells were also densely packed.

An attenuation that is definitely not linear with respect to frequency is shown for bovine blood in Fig. 5.15. Of all data displayed, this plot has greatest attenuation, with no signal detected after 300 MHz. The MCV was approximately $41\mu^3$. With a concentration of $4x10^9$ cells/ml, the cells were closely packed together. From the curve in Fig. 5.15, the attenuation at 200 MHz is 23 dB/mm. This agrees very well with the attenuation of ~ 17 dB/mm at 200 MHz measured by (Edmonds, 1962) for an aqueous solution of dissolved crystalline hemoglobin. The additional attenuation is probably due to the intact cell structure.

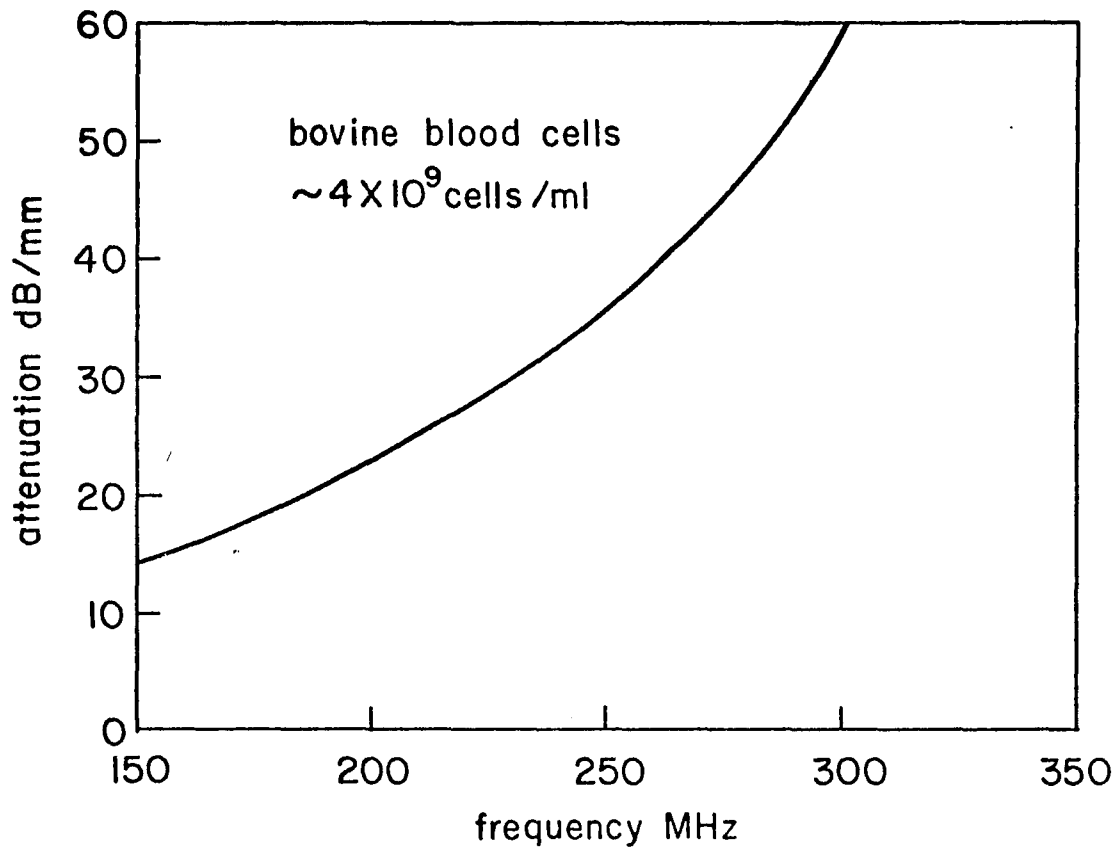

Fig. 5.15. Attenuation in dB/mm for bovine red blood cell suspension with a mean cell volume of 41 μ^3.

CHAPTER 6

CONCLUSIONS AND SUGGESTIONS FOR FURTHER WORK

Conclusions

Ultrasound spectroscopy, through the analysis of scattered radiation as a function of frequency, offers a method of characterization of individual scatterers or a collection of scatterers. The focus of this work has been on individual scatterers and their signatures, though scattering data has been obtained from both of the above sources. Furthermore, for certain ranges of size parameter x, either very large or very small, this characterization is more than just a unique signature and certain physical parameters of the scatterer can be gleaned from the scattered data without resorting to elaborate inversion techniques.

In order to investigate the scattering characteristics of individual particles, certain physical conditions must be imposed on the scattering medium and the detection system. Otherwise, the individual scattering signatures will be obscured. To observe individual-particle characteristics in a collection of particles, the usual criterion is that the particles are separated by a distance large compared to the wavelength of the radiation. For suspensions of cells, a large concentration was necessary to detect a scattered

signal, and, as a consequence, the above criterion was violated. For the Crofon fibers, sapphire and latex spheres, this condition was easily met.

Another condition is that the absorption of the scatterer or collection of scatters not be too great, or the scattered structure is completely damped out. It is hard to say what the absorption of a single cells is. However, the number of cells in the water gap between the carrier rods was approximately 20 million. Such a large number could cause significant absorption. For the Crofon fibers and sapphire spheres, their number was too small to cause obscuring absorption.

In theory, scattered radiation is present in all directions. In the forward direction, the form of the scattered radiation becomes particularly simple and is shown to be proportional to Q_t. The detected signal in the forward direction, however, has a significant contribution due to the unscattered incident wave. This portion of the signal can be extremely large and mask the forward-scattered wave. For large x, experiment indicates that the scattered wave is easier to discern. Also for large x, the resonant pattern of the scattered wave can give physical parameters about the scatterer, such as particle size or velocity of sound in the particle. This proved to be the case for the Crofon fibers and for the special case of the glass plate. For

the sapphire spheres, the problem was more complex. The simple fluid-sphere model proved inadequate. The correct model would be to assume an elastic sphere, which has an extremely complex scattering coefficient R_ℓ, (Hickling, 1962). A numerical analysis of the extrema of R_ℓ for large x would in all likelihood yield the observed separation.

Understood in any of the above scattering analyses is that the range of x covered by the experiment must be large enough to give detectable resonances, or $x_{max}-x_{min} > \Delta x$, where Δx is calculated from the large x analysis. This figure for Δx is sometimes a good approximation for intermediate x values also. For the resulting frequency range of this experiment, the $x_{max}-x_{min}$ difference for the sapphire spheres and Crofon cylinders was always larger than Δx. For particles of cellular sizes and of velocities comparable to the surrounding medium, this $x_{max}-x_{min}$ difference is comparable to Δx, which makes resonances not easily distinguishable. An example of the effect of scatterer size on the $x_{max}-x_{min}$ difference is the 11.9μ latex spheres. The experimental scattering curves shows possibly a resonance. Thus, for the frequency range experimentally available, one would be more likely to see resonant structure for large cells than for small ones.

Variation in size of the scattering particle has an inverse relation to resonant frequency spacing. Many cell

lines are a collection of cell sizes. If the variation in size is too large, resonances for different sizes overlap and essentially average out. In contrast, the sapphire spheres and Crofon fibers had excellent size regularity.

Most likely, the lack of resonant structure seen in the scattering of ultrasound from cell suspensions was due to a combination of the previously mentioned reasons. In order to ascertain the individual effects of the above parameters, further experimental work is necessary.

In summary, one can say that simple measurements of scattering resonants can certainly reveal physical characteristics of the scatterer. For large size parameters and for forward scattering, a simple geometrical scattering model for fluid spheres and cylinders has been experimentally verified and reveals for fluid particles information about the scattering particle's size and its characteristic speed of sound. For large x, the resonant spacing is the same for both spheres and cylinders. Such a fluid-particle model should be an excellent one for cells. However, no scattering resonances for cells were observed. It was observed that the attenuation of ultrasound in most cell suspensions was linear with respect to frequency, which corresponds to the observed attenuation in tissues for the low megahertz frequency range. Different cell suspensions of similar concentration have different attenuation curves and

different slopes. There appears to be no significant difference in the ultrasound attenuation of cells in the growth and non-growth phase.

The attenuation of ultrasound in water was measured from 150 to 400 MHz and agrees well with values reported in the literature. The attenuation of bovine blood was measured and agrees well with previously observed values of the attenuation of hemoglobin.

Suggestions for Further Work

Suggestions for further work fall into basically two categories; experimental and theoretical. The experimental considerations are addressed first. The crystal construction used in this experiment was designed for measurement of forward-scattered radiation. Backscattered signal measurements were theoretically possible, but, in practice, the unscattered reflected pulse from the interface between the carrier rods and the water gap proved to be extremely large and, for this author, impossible to remove. Scattering detection at 90° would solve the problem of the unscattered wave, but would present some interesting transducer carrier rod and interface problems. One solution might be larger, thinner carrier rods. The larger rods would allow more temporal spacing between unwanted stray pulses; the thinner rods would permit a smaller scattering sample thickness and less unwanted absorption from the

sample. Though the scattered wave at 90° is not proportional to Q_t, an analysis of the scattering amplitude $\Phi(90°)$ might yield a pliable enough equation from which scattering resonances might be determined.

With the same experimental apparatus, further experiments could be performed on the attenuation of cell suspensions. Placement of live cell suspensions in a controlled-temperature environment could reveal unexpected results. All experiments described in this dissertation were performed at room temperature. Small temperature variations around this temperature seemed to have little effect ultrasonically. However, certain cell activity can be limited to a narrow temperature range, often higher than room temperature. The use of an incubator could provide some interesting results. The effect of a variation in temperature on biological systems cannot be overestimated. The human body goes to great lengths to maintain homeostasis.

One might consider an experiment investigating the forward scattering of extremely large cells. Cells with diameters of hundreds of microns and with some degree of size regularity might circumvent the problem of resolution spacing. The author was unable to find such cells.

A theoretical study of Mie scattering for fluid spheres and cylinders with densities and velocities comparable to those of tissues might prove extremely enlightening.

Such a study could determine the expected variations in resonance structure for changes in cell size, density, and speed. The differential scattering cross-section could indicate the variation in angular scattering as a function of the cell's properties. Taken a step further, the cell could be modeled as a fluid sphere with a small fluid or solid boundary, the cell wall. Numerical Mie scattering solutions are often solved as a function of the size parameter x, which includes both frequency and particle size. Investigations of these scattered wave solutions can produce the range of x over which the most interesting scattering resonances occur. The experimenter can then juggle the experimental frequency range and particle size so that these interesting resonances are experimentally observable.

As a final theoretical suggestion unrelated to cell scattering, one might explore the equivalence of the volume and surface scattering formulations discussed in Chapter 3. The fluid sphere, cylinder, prolate spheriod, or whatever could be modeled individually as a source, using discontinuous functions. It should be possible to derive the same scattering formulation irrespective of the choice of the surface or volume integral formulation.

APPENDIX A

ACOUSTIC WAVE PROPAGATION

This appendix presents the basic equations describing the propagation of acoustic waves in an ideal (nonviscous and thus nonabsorbing) fluid. From these equations will be derived a wave equation, an energy flow relation, and boundary conditions for acoustic waves. The specific solutions of time-harmonic, plane and spherical waves to the wave equation will be considered. Finally, the concept of acoustic impedance is discussed. This appendix is intended to be only a summary of acoustic physics for those unfamiliar with the topic.

Acoustic waves are small-signal oscillations in a fluid. The basic equations of these acoustic waves are derived from a first-order perturbation of the classical state variables applied to the dynamical equations of a fluid and the thermodynamic equation of state. Presented here are the resulting linearized small-signal equations. An excellent derivation of these equations can be found in the references (Landau and Lifshitz 1959, Morse and Ingard 1968, and Hunt 1972).

Initially, the physical variables of interest must be defined. The variables which completely describe a

fluid are the fluid particle velocity[1] $\bar{u}(\bar{r},t)$ and any two of the three thermodynamic state variables of the fluid; density $\rho(\bar{r},t)$, pressure $P(\bar{r},t)$ and temperature $T(\bar{r},t)$. All problems considered in this appendix, unless otherwise stated, will be isothermal, reducing the number of unknown variables from six to five. For the acoustic equations, the variables will be the first-order perturbations of these quantities. Any subscripted variables will be the static or zero-order quantities.

The small-signal equations which classically describe acoustic phenomena are:

$$\text{Continuity of mass equation } \rho_o \nabla \cdot \bar{u} = -\frac{\partial \rho}{\partial t} \qquad \text{(A1)}$$

$$\text{Force equation (Newton's 2nd Law) } \rho_o \frac{\partial \bar{u}}{\partial t} = -\nabla P \qquad \text{(A2)}$$

$$\text{Thermodynamic equation of state } P = \left.\frac{\partial P}{\partial \rho}\right)_T \rho \ . \qquad \text{(A3)}$$

For nonisothermal conditions, an additional heat-exchange, conservation-of-energy equation is required. For the isothermal situation, the energy-conservation equation is derivable from the equations above. For a viscous fluid, an additional stress tensor with appropriate small-signal approximations is added to the right side of equation (A2).

---

1. A fluid particle is defined as a small enough volume of the fluid such that the thermodynamic state variables do not vary appreciably within that volume.

The thermodynamic equation of state is further clarified by the relation $\kappa_T = \rho_o \left.\frac{\partial P}{\partial \rho}\right)_T$ (Morse and Ingard, 1968) where κ_T is the isothermal compressibility. Also to first order, $\kappa_T = \kappa_S$ the adiabatic compressibility, and for convenience the subscript will be dropped. If one substitutes κ in equation (A1), the equations of motion become

$$\nabla \cdot \bar{u} = - \kappa \frac{\partial P}{\partial t} \qquad \text{(A4)}$$

$$\rho \frac{\partial \bar{u}}{\partial t} = - \nabla P \ , \qquad \text{(A5)}$$

where for convenience ρ_o will be represented by ρ, since the variable ρ will no longer appear in any equations.

To solve for a wave equation in pressure P, a time derivative of equation (A4) and a divergence of equation (A5) with the elimination of $\nabla \cdot \frac{\partial \bar{u}}{\partial t}$ yields

$$(\nabla^2 - \rho\kappa \frac{\partial^2}{\partial t^2}) P(\bar{r},t) = 0 \ . \qquad \text{(A6)}$$

From the wave equation (A6), the speed of the wave c must be $(\rho\kappa)^{-\frac{1}{2}}$, an expression that can also be derived from the kinetic theory of gases (Morse and Ingard, 1967). It is obvious that a reversal of the previous operations can lead to a similar wave equation for $\bar{u}$ with the same wave velocity c.

In the same manner that the Poynting vector is derived in the classical theory of electrodynamics

(Jackson, 1975), a similar energy flow equation can be derived from equations (A4) and (A5). Let equation (A4) be multiplied by P and equation (A5) by $-\bar{u}$. Adding the resulting equations and utilizing the vector identity $\nabla\cdot(P\bar{u}) = \nabla P\cdot\bar{u} + \bar{u}\nabla\cdot P$, one has

$$\frac{\partial}{\partial t}\left(\frac{\kappa P^2}{2} + \frac{\rho u^2}{2}\right) + \nabla\cdot(P\bar{u}) = 0 \ . \qquad \text{(A7)}$$

If one defines $\varepsilon = \frac{\kappa P^2}{2} + \frac{\rho u^2}{2}$ as the energy density of the wave and $\bar{I} = P\bar{u}$ as the wave intensity, equation (A7) becomes the conservation of energy equation

$$\frac{\partial \varepsilon}{\partial t} + \nabla\cdot\bar{I} = 0 \ , \qquad \text{(A8)}$$

which means that the time rate of energy created within a certain volume is equal to the rate of energy flow out through the boundary surfaces of that volume. The energy density terms $\frac{1}{2}\rho u^2$ and $\frac{1}{2}\kappa P^2$ are, respectively, the kinetic and potential energy densities. The kinetic energy term is readily identified from its velocity-squared dependence. The potential energy term can be easily seen from a simple work argument. The work per unit volume expended in compression by the pressure wave is $\int P\,\frac{dV}{V}$. Thermodynamically, the compressibility κ is defined as $\kappa = \frac{1}{V}\frac{\partial V}{\partial P}$ or $dV = V\kappa dP$. If

this expression is substituted into the previous integral, the work per unit volume, which is the potential energy density, is $\frac{1}{2}\kappa P^2$.

Establishing boundary conditions is of supreme importance in reflection and scattering problems. Consider the fluid boundary of Fig. A1 and the Gaussian pillbox drawn at that boundary. An acoustic wave $P_1\bar{u}_1$ is present on one side of the boundary and the wave $P_2\bar{u}_2$ on the other. The boundary conditions on $\bar{u}$ and P are derived from the equations of motion (A4) and (A5). First derive the boundary conditions on $\bar{u}$. Taking the volume integral of equation (A4) and using Gauss's divergence theorem, one has

$$\oint_S \bar{u}\cdot d\bar{S} = -\int_V \kappa \frac{\partial P}{\partial t}\, dV \ . \qquad \text{(A9)}$$

Let the volume enclosed be the pillbox of Fig. A1. For a small enough volume, one may write equation (A9) as

$$(\bar{u}_1\cdot\hat{n}_1 + \bar{u}_2\cdot\hat{n}_2)\Delta a + \bar{u}\cdot\Delta\bar{\ell}_{\text{circumference}} = -\kappa \frac{\partial P}{\partial t}\Delta a\Delta\ell$$

If $\Delta\ell$ approaches zero and $\lim_{\Delta\ell\to 0} \frac{\partial P}{\partial t}\Delta a\Delta\ell = 0$, i.e., no pressure current along the boundary, then

$$(\bar{u}_1-\bar{u}_2)\cdot\hat{n} = 0 \text{ since as } \Delta\ell \to 0,\ \hat{n}_1 \to -\hat{n}_2 \ . \qquad \text{(A10)}$$

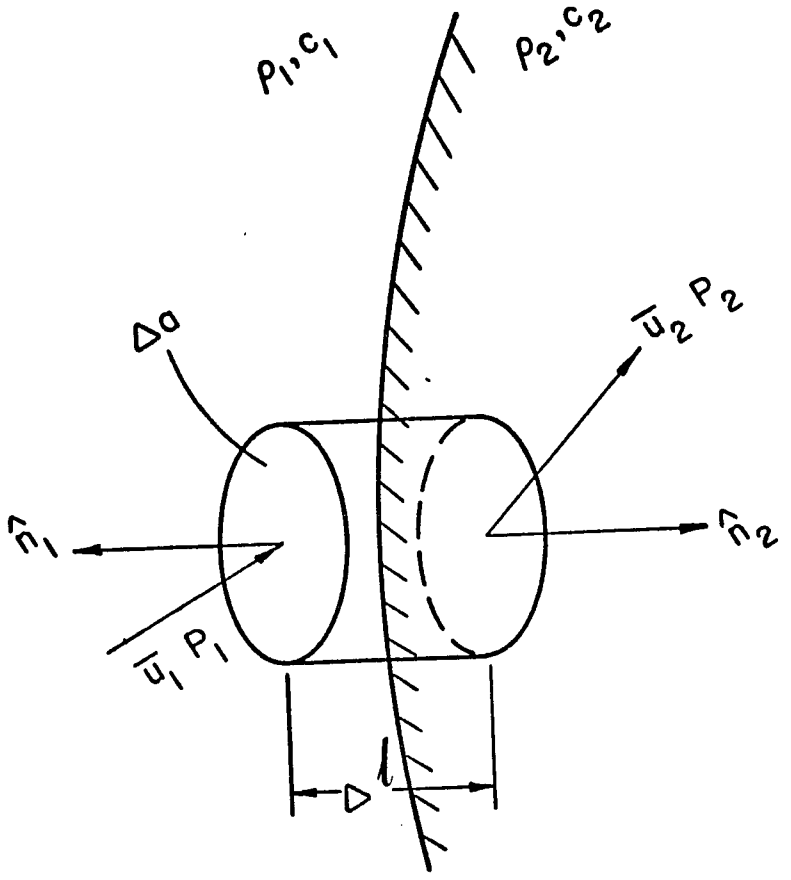

Fig. A1. Boundary interface between acoustic media.

Thus, the normal components of the fluid velocity are continuous at a boundary. Performing the same operation with equation (A5), utilizing the relation $\int_v \nabla P \, dV = \oint_s P \, d\bar{S}$ and assuming $\Delta \lim_{\ell \to 0} \rho \frac{\partial \bar{u}}{\partial t} \Delta a \Delta \ell = 0$, i.e., no velocity current at boundary, one obtains the boundary condition

$$P_1 - P_2 = 0, \qquad \text{(A11)}$$

i.e., the pressures are continuous across the boundary interface. Utilizing the above boundary condition, one may now derive various reflection and refraction relations for various interfaces. Certain special cases are of interest. In a scattering medium that is either acoustically soft or hard (also denoted as rigid), the particle velocity and it's associated pressure are both zero. However, the boundary conditions are quite different. At the surface of an acoustically soft medium, the boundary condition is that the pressure inside the soft medium is zero. At the surface of an acoustically hard medium, the boundary condition is that the normal component of the particle velocity inside the hard medium is zero.

It is now appropriate to consider certain classes of solutions to the wave equation (A6). First consider time harmonic waves such that

$$\begin{Bmatrix} P(\bar{r},t) \\ \bar{u}(\bar{r},t) \end{Bmatrix} = \begin{Bmatrix} P(\bar{r}) \\ \bar{u}(\bar{r}) \end{Bmatrix} e^{-i\omega t} .$$

In this case the time-average intensity is

$$\langle \bar{I} \rangle = \frac{1}{2} Re(P^* \bar{u}). \tag{A12}$$

With equation (A5), this value becomes

$$\frac{1}{2} Re\left(\frac{1}{i\omega\rho} P^* \nabla P\right) = \frac{1}{2} Im\left(\frac{P^* \nabla P}{\omega\rho}\right) \quad \text{or}$$

$$\langle \bar{I} \rangle = \frac{1}{\omega\rho} (P^* \nabla P - P \nabla P^*), \tag{A13}$$

a result often seen in the literature and described as the direction of energy flow for a scalar wave.

For a plane wave

$$\begin{Bmatrix} P(\bar{r},t) \\ \bar{u}(\bar{r},t) \end{Bmatrix} = \begin{Bmatrix} P_o \\ \bar{u}_o \end{Bmatrix} e^{i(\bar{K}\cdot\bar{r} - \omega t)}$$

where K is the wave number, the equation of motion (A5) yields

$$\bar{u} = \frac{P}{\rho\omega} \bar{K}, \tag{A14}$$

so that the particle velocity is in the same direction as the wave. The magnitude of equation (A14) gives a direct relation between u and P;

$$u = \frac{P}{\rho c} \tag{A15}$$

where ρc is defined as z_c, the characteristic acoustic impedance of the medium. The time averaged intensity of a

plane wave is

$$\langle I \rangle = |Pu| = \frac{P_o u_o}{2} \tag{A16}$$

Alternate forms are

$$\langle I \rangle = \frac{|P|^2}{\rho c} = \frac{P_o^2}{2\rho c} = \frac{P_o^2}{2z_c} \tag{A17}$$

Also, the average energy densities are equivalent for plane wave propagation.

Spherical waves are of great importance in scattering and, consequently, some of their properties will be mentioned. A spherical outgoing pressure wave will be defined as $P(r,t) = \frac{P_o}{r} e^{i(Kr-\omega t)}$. Note that the constant amplitude P_o has units of pressure × distance. The wave particle velocity defined by

$$\bar{u} = \frac{1}{i\omega\rho} \nabla P = \bar{u} = \frac{P_o \hat{r}}{\rho c r} e^{i(Kr-\omega t)} \times \left(1 - \frac{i}{Kr}\right)$$

is radial and has a term which is $\pi/2$ out-of-phase with respect to the pressure P. For $Kr >> 1$, $\bar{u}$ has the spherical wave representation and is in phase with P. The time-average intensity is also radial and of the form

$$I_r = \frac{P_o^2}{2\rho c r^2} = \frac{|P|^2}{\rho c}, \tag{A18}$$

identical to the intensity expression for plane waves.

Previously, the concept of acoustic impedance was introduced and was defined as a characteristic of the medium. It is convenient to introduce another impedance that is characteristic of any boundary interface. Define the acoustic impedance z (versus the characteristic impedance z_c) as the ratio of the pressure to the normal particle velocity at a point on a boundary interface. Thus,

$$P = z\,(u\cdot\hat{n}) \quad . \tag{A19}$$

This impedance, with dimensions of ρc, may be frequency dependent and complex, in which case the normal velocity component is not in phase with the pressure at the boundary. To normalize z, the specific acoustic impedance δ and admittance β are defined. Respectively, $\delta = \frac{z}{\rho c}$ and $\beta = \frac{\rho c}{z}$. Both are dimensionless. Note that δ and β, unlike z which by symmetry is the same regardless of the beam direction at the boundary interface, is dependent on the side of the boundary on which one is investigating the wave. For example, if the boundary in Fig. A1 is used, the admittance of a wave incident from the right would be $\frac{1}{\beta_2} = \frac{z_2}{\rho_2 c_2}$, from the left $\frac{1}{\beta_1} = \frac{z_1}{\rho_1 c_1}$. Since by symmetry $z_1 = z_2$, the admittances are then related by

$$\frac{\rho_2 c_2}{\beta_2} = \frac{\rho_1 c_1}{\beta_1} \quad . \tag{A20}$$

In order to determine z, one uses the definition of equation (A19). To determine β, one uses equation (A19) and (A5) for a time-harmonic wave, resulting in

$$\frac{\partial P}{\partial n} = iK\beta P, \qquad \text{(A21)}$$

where K is the wave number of the incident medium and $\frac{\partial P}{\partial n}$ is the directional derivative. The use of the specific acoustic impedance and admittance is in solving boundary value problems. For example, in acoustics, one obtains solutions for the wave equation on both sides of the medium, and then using the boundary conditions (A10) and (A11) and either of the equations of motion, solves for the unknown constants in the wave equation solutions. However, with knowledge of the acoustic impedance (not always easy to procure) one needs to only solve the wave equation on the side of the boundary of interest. Then using either equation of motion and the impedance relation (A20), the unknown constants in the wave equation solution is solved for. An example of this method for a scatter problem is given in Chapter 3. Other examples are in standard references (Morse and Ingard, 1968).

APPENDIX B

SCATTERING FROM A NONRIGID CYLINDER

This appendix discusses the scattering of acoustic waves by an infinite cylinder. The derivation is cursory and many steps are described, not derived. However, the method of derivation is the one commonly seen in the literature. The functional forms of the wave in various regions are presumed known by symmetry, and their constants are found by applying boundary conditions. All waves are assumed time harmonic of the form $e^{-i\omega t}$.

Initially, a plane wave $P_i = P_o e^{iKz}$ is incident on an infinite cylinder of radius a, of density ρ_e and acoustic speed c_e. From Fig. B1 and by symmetry, the scattered wave and the wave inside the cylinder are functions of r and θ and therefore may be expanded in cylindrical waves, which leads to the expressions

$$P_s = \sum_{\ell=0}^{\infty} A_\ell \, H_\ell(Kr)\cos(\ell\theta) \qquad \text{(B1)}$$

$$P_t = \sum_{\ell=0}^{\infty} B_\ell \, J_\ell(Kr)\cos(\ell\theta) \qquad \text{(B2)}$$

$$P_i = P_o\left[J_o(Kr) + \sum_{\ell=1}^{\infty} i^\ell \, J_\ell(Kr)\cos(\ell\theta)\right] \qquad \text{(B3)}$$

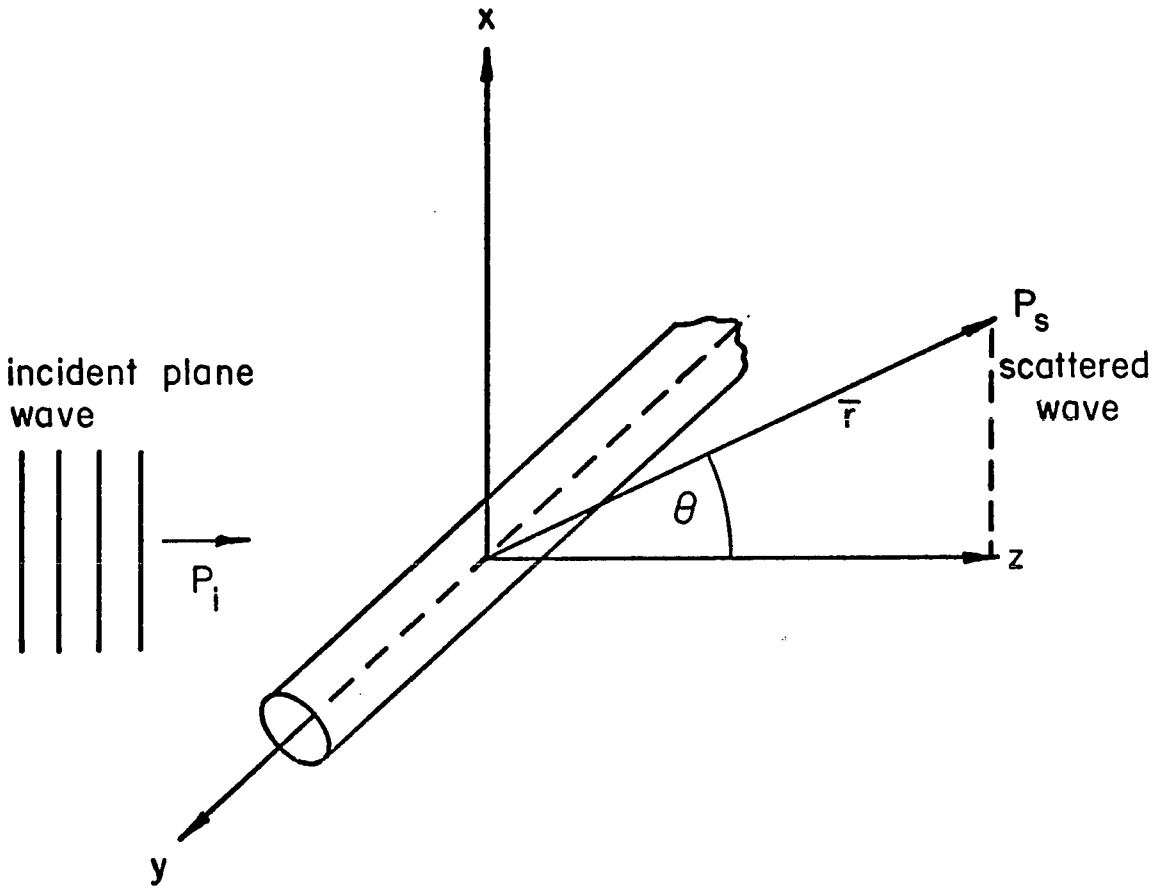

Fig. B1. Scattering of a plane wave from a cylinder.

where P_t is the wave inside the cylinder, and J_ℓ, N_ℓ, H_ℓ are respectively Bessel, Neumann, and Hankel functions of order ℓ. The wave inside the cylinder has a J and not a N, since it must be finite at the origin.

The boundary conditions are that at $r = a$

$$(P_i + P_s)\Big|_{r=a} = P_t\Big|_{r=a} \quad \text{and} \quad (\bar{u}_i + \bar{u}_s)\cdot\hat{n}\Big|_{r=a} = \hat{u}_r\cdot\hat{n}\Big|_{r=a}$$

where $\bar{u}$ is the particle velocity. From Appendix A and symmetry, $\bar{u}\cdot\hat{n} = u_r = \frac{1}{i\rho\omega}\frac{\partial P}{\partial r}$. If these boundary conditions are applied and respective terms are matched, one finds the coefficients A_ℓ are

$$A_o = -P_o \frac{J_o(x_e)J_o'(x) - \frac{z}{ze}J_o'(x_e)J_o(x)}{J_o(x_e)H_o'(x) - \frac{z}{ze}J_o'(x_e)H_o(x)} \tag{B4}$$

$$A_\ell = -2P_o\, i^\ell \frac{J_\ell(x_e)J_\ell'(x) - \frac{z}{ze}J_\ell'(x_e)J_\ell(x)}{J_\ell(x_e)H_\ell'(x) - \frac{z}{ze}J_\ell'(x_e)H_\ell(x)} \quad \ell>0 \tag{B5}$$

For the case $Kr >> 1$, the Hankel function may be approximated as

$$H_\ell(Kr) \sim \frac{2}{\pi Kr}\, e^{iKr}\, e^{-i\frac{\pi}{2}(\ell+\frac{1}{2})}. \tag{B6}$$

The scattered wave then has the form

$$P_s(r) = -P_o\, e^{-i\frac{\pi}{4}}\sqrt{\frac{\pi}{2Kr}}\left(e^{iKr}\,\Phi(\theta)\right) \tag{B7}$$

where

$$\Phi(\theta) = \sum_{\ell} \varepsilon_{\ell} R_{\ell} \cos(\ell\theta) \qquad \text{(B8)}$$

$$\varepsilon_{\ell} = \begin{cases} 1 & \ell=0 \\ 2 & \ell>0 \end{cases}$$

$$R_{\ell} = \frac{J_{\ell}(x_e)J'_{\ell}(x) - \frac{z}{ze} J'_{\ell}(x_e)J_{\ell}(x)}{J_{\ell}(x_e)H'_{\ell}(x) - \frac{z}{ze} J'_{\ell}(x_e)H_{\ell}(x)} \; . \qquad \text{(B9)}$$

Equation (B7) is the familiar form of a cylindrical wave with amplitude $P_o \Phi(\theta)$. The function $\Phi(\theta)$ is the scattering amplitude.

The total scattered power per unit length $\mathscr{P}_s$ is obtained from the integral

$$\mathscr{P}_s = \int_o^{2\pi} I_s r \, d\phi$$

$$= \frac{P_o^2}{2\rho c}\left(a \frac{\pi}{Ka} \sum_{\ell} \varepsilon_{\ell} |R_{\ell}|^2\right)$$

$$= I_o a \frac{\pi}{x}\left(\sum_{\ell} \varepsilon_{\ell} |R_{\ell}|^2\right). \qquad \text{(B10)}$$

To find resonances in $\mathscr{P}_s$, one must look for resonances in $|R_{\ell}|^2$. If the medium is nonabsorbing

$$|R_{\ell}|^2 = \frac{U_{\ell}^2}{U_{\ell}^2 + V_{\ell}^2} \qquad \text{(B11)}$$

where

$$U_\ell = J_\ell(x_e)J'_\ell(x) - \frac{z}{ze} J'_\ell(x_e)J_\ell(x) \qquad \text{(B12)}$$

$$V_\ell = J_\ell(x_e)N'_\ell(x) - \frac{z}{ze} J'_\ell(x_e)N_\ell(x) \ . \qquad \text{(B13)}$$

For a $\begin{Bmatrix}\text{maximum}\\ \text{minimum}\end{Bmatrix}$ in $|R_\ell|^2$; $\begin{Bmatrix}V_\ell\\ U_\ell\end{Bmatrix}$ approaches 0. Neither of equations (B12) or (B13) is readily solvable for this condition.

For large x, with the asymptotic expansions,

$$J_\ell(x) \to \frac{2}{\pi x} \cos\left(x - \frac{2\ell+1}{4}\pi\right)$$

$$N_\ell(x) \to \frac{2}{\pi x} \sin\left(x - \frac{2\ell+1}{4}\pi\right) ,$$

the expression V_ℓ becomes

$$V_\ell \sim -\cos\left(x_e - \frac{2\ell+1}{4}\pi\right)\cos\left(x - \frac{2\ell+1}{4}\pi\right)$$

$$+ \frac{z}{ze} \sin\left(x_e - \frac{2\ell+1}{4}\pi\right)\sin\left(x - \frac{2\ell+1}{4}\pi\right)$$

With trigometric identities, one has

$$V_\ell \sim \left(\frac{z}{ze} + 1\right)\cos\left(x-x_e\right) + \left(\frac{z}{ze} - 1\right)$$

$$\times \cos\left(x+x_e - (2\ell+1)\frac{\pi}{2}\right) \ .$$

The first term, independent of ℓ, will predict the minimum values of V_ℓ and thus of $\mathcal{P}_s$, if $x-x_e = (m+1)\frac{\pi}{2}$. This is the same phase condition derived for scattering from a sphere in Chapter 3. To find the separation between maxima in $\mathcal{P}_s$, let one maximum be associated with $(m+1)\frac{\pi}{2}$ and the other with $((m+1)+1)\frac{\pi}{2}$ (the next order), then

$$\Delta x = \frac{\pi}{1 - \frac{c}{c_e}} \qquad \text{where } x_e = \frac{c}{c_e} x$$

Thus, for large x, a sphere and cylinder give the same resonant structure.

For further reading in the scattering of cylinders, and a more thorough development than was represented here, one should consult the references, Morse and Ingard (1968), Bowman, Senior and Uslenghi (1969), and Rschevkin (1963).

REFERENCES

Anderson, V. C., "Sound Scattering from a Fluid Sphere," J. Acoust. Soc. Am. 22, 426 (1950).

Beyer, R. T. and S. V. Letcher, Physical Ultrasonics, Academic Press, New York (1969).

Billy, M. de and G. J. Quentin, "Methods of Analysis for Backscattering from Tissues," Ultrasonics 17, 85 (1979).

Bowman, J. J., T. B. A. Senior and P. L. E. Uslenghi, eds., Electromagnetic and Acoustic Scattering by Simple Shapes, North-Holland Publishing Co., Amsterdam (1969).

Dunn, F. and W. D. O'Brien, Jr., "Ultrasonic Absorption and Dispersion," in Ultrasound: It's Applications in Medicine and Biology, Part I, F. J. Fry, ed., Elsevier Scientific Publishing Co., New York, pp. 393-439 (1978).

Edmonds, P. D., "Ultrasonic Absorption of Hemoglobin Solutions," Biochim. Biophys. Acta 63, 216 (1962).

Edmonds, P. D., T. J. Baulk, III, J. F. Dyro and M. Hussey, "Ultrasonic Absorption of Aqueous Hemoglobin Solutions," Biochim. Biophys. Acta 200, 174 (1970).

Fry, F. J., ed., Ultrasound: It's Applications in Medicine and Biology, Parts I & II, Elsevier Scientific Publishing Co., New York (1978).

Goodman, J. W., Introduction to Fourier Optics, McGraw-Hill Book Co., New York (1968).

Goss, S. A., R. L. Johnston, and F. Dunn, "Comprehensive compilation of empirical ultrasonic properties of mammalian tissues," J. Acoust. Soc. Am. 64 (2), 423 (1978).

Hart, R. W. and E. W. Montroll, "On the Scattering of Plane Waves by Soft Obstacles. I. Spherical Obstacles," J. Appl. Phys. 22, 376 (1951).

Heuter, T. F. and R. H. Bolt, Sonics, John Wiley and Sons, Inc., New York (1966).

Hickling, R., "Analysis of Echoes from a Solid Elastic Sphere in Water," J. Acoust. Soc. Am. 34, 1582 (1962).

Hill, C. R., "Frequency and Angular Dependence of Ultrasonic Scattering from Tissue," in Ultrasonic Tissue Characterization, ed. M. Linzer, NBS Special Publication 453, Washington, pp. 197-206 (1976).

Hunt, F. V., "Propagation of Sound in Fluids," in American Institute of Physics Handbook, ed., D. E. Gray, McGraw Hill, Inc., New York (1972).

Hussey, M., Diagnostic Ultrasound, John Wiley and Sons, New York (1975).

Ishimaru, A., Wave Propagation and Scattering in Random Media, Academic Press, New York (1978).

Jackson, J. D., Classical Electrodynamics, Section Edition, John Wiley and Sons, New York (1975).

Jennings, W. D., E. Holasek, and E. W. Purnell, "Theoretical Analysis of Instantaneous Power Spectra as Applied to Spectra-Color Ultrasonography," in Ultrasonic Tissue Characterization II, ed. M. Linzer, NBS Special Publication 525, Washington, pp. 261-266 (1979).

Kessler, L. W. and D. E. Yuhas, "Acoustic Microscopy-1979," Proc. IEEE 67, 526 (1979).

Kinsler, L. E. and A. R. Frey, Fundamentals of Acoustics, Section Edition, John Wiley and Sons, New York (1962).

Landau, L. D. and E. M. Lifshitz, Fluid Mechanics, Addison-Wesley Publishing Co., Reading, Massachusetts (1959).

Lele, P. P., A. B. Mansfield, and A. I. Murphy, Tissue Characterization by Ultrasonic Frequency-dependent Attenuation and Scattering," in Ultrasonic Tissue Characterization, ed. M. Linzer, NBS Special Publication 453, Washington, pp. 167-196 (1976).

Lizzi, F. L. and M. E. Elbaum, "Clinical Spectrum Analysis Techniques for Tissue Characterization," in Ultrasonic Tissue Characterization II, ed. M. Linzer, NBS Special Publication 525, Wahington, pp. 111-124 (1979).

Morse, P. M. and H. Feshbach, Methods of Theoretical Physics, Parts I and II, McGraw-Hill Book Co., New York (1953).

Morse, P. M. and K. U. Ingard, Theoretical Acoustics, McGraw-Hill Book Co., New York (1968).

Nicholas, D., "An Introduction to the Theory of Acoustic Scattering by Biological Tissues," in Recent Advances in Ultrasound in Biomedicine, Vol. I, D. N. White, ed., Research Studies Press, Forest Grove, Oregon, pp. 1-28 (1977).

O'Brien, Jr., W. D., C. L. Christman, and F. Dunn, "Ultrasonic Investigation of Aqueous Solutions of Deoxyribose Nucleic Acid," J. Acoust. Soc. Am. 52, 1251 (1972).

O'Donnell, M. and J. G. Miller, "Mechanisms of Ultrasonic Attenuation in Soft Tissue," in Ultrasonic Tissue Characterization II, ed. M. Linzer, NBS Special Publication 525, Washington, pp. 37-40 (1979).

Quate, C. F., A. Atalar, and H. K. Wickramasinghe, "Acoustic Microscopy with Mechanical Scanning," Proc. IEEE 67, 1092 (1979).

Rhyne, T. L., "An Ultrasonic Tissue Signature for the Lung Surface," in Ultrasonic Tissue Characterization II, ed. M. Linzer, NBS Special Publication 525, Washington, pp. 135-141 (1979).

Rschevkin, S. N., The Theory of Sound, The MacMillan Co., New York (1963).

Seki, H., A. Granato and R. Truell, "Diffraction Effects in the Ultrasonic Field of a Piston Source and Their Importance in the Accurate Measurement of Attenuation," J. Acoust. Soc. Am. 28, 230 (1956).

Waag, R. C., P. P. K. Lee, R. M. Hunter, R. Gramiak, and E. A. Schenk, "Angle Scan and Frequency-Swept Ultrasonic Scattering Characterization of Tissue," in Ultrasonic Tissue Characterization II, ed. M. Linzer, NBS Special Publication 525, Washington, pp. 143-152 (1979).

Waag, R. C., R. M. Lerner, and R. Gramiak, "Swept-frequency Ultrasonic Determination of Tissue Microstructure," in Ultrasonic Tissue Characterization, ed. M. Linzer, NBS Special Publication 453, Washington, pp. 213-228 (1976).

Wells, P. N. T., Biomedical Ultrasonics, Academic Press, New York (1977).